Published for SISSA by Springer

Received: *November 26, 2025*
Accepted: *March 14, 2026*
Published: *June 8, 2026*

Search for higgsinos in compressed mass spectra using low-momentum tracks in pp collisions at $\sqrt{s} = 13$ TeV with the ATLAS detector

The ATLAS collaboration

Full author list at the end of the paper

E-mail: atlas.publications@cern.ch

Abstract: This paper presents two searches for the electroweak production of higgsinos with compressed mass spectra using $140\,\text{fb}^{-1}$ of $\sqrt{s} = 13$ TeV proton-proton collision data collected by the ATLAS experiment at the Large Hadron Collider. Events are required to feature an energetic jet, large missing transverse momentum, and at least one low-momentum charged particle that serves as a candidate higgsino decay product. In the first search, targeting higgsino mass splittings in the range of 0.3–1 GeV, the higgsinos are expected to predominantly decay into pions that are identified as low-momentum charged particles with large transverse impact parameters due to the long higgsino lifetime ($c\tau \approx \mathcal{O}(0.1\text{–}10\,\text{mm})$), and neural networks are used to discriminate between signal and background processes. The second search targets larger mass splittings in the range of 1–3 GeV, where the higgsinos are expected to decay promptly into low-momentum leptons, one of which is identified by dedicated low-momentum electron or muon taggers based on neural networks utilising tracking and calorimeter information. No significant excess above the Standard Model prediction is observed in either search and the results are interpreted within simplified models, to set lower limits on the masses of the higgsino-like charginos and neutralinos. Together, these searches exclude chargino masses below 126 GeV at 95% confidence level for mass splittings between the chargino and lightest neutralino in the range of 0.3–2 GeV. This represents the first ATLAS constraints in a portion of this parameter space and surpasses the limits previously set by other experiments.

Keywords: Hadron-Hadron Scattering

ArXiv ePrint: 2511.20042

https://doi.org/10.1007/JHEP06(2026)094

JHEP06(2026)094

Contents

1 Introduction

Supersymmetry (SUSY) [1–6] proposes a symmetry between bosons and fermions, thus predicting new particles that have identical quantum numbers as their Standard Model (SM) partners except for their spin. Specifically, SUSY introduces bosonic superpartners of the SM fermions and fermionic superpartners of the SM bosons. In SUSY models with R-parity conservation [7], the lightest SUSY particle (LSP) must be stable and, if electrically neutral and weakly interacting, can be a viable dark matter candidate [8, 9]. In addition, SUSY can provide a necessary condition gauge coupling unification [10–13] and a solution to the fine-tuning problem of the Higgs boson mass [14, 15], making it a leading candidate for physics beyond the SM.

In the minimal supersymmetric extension of the SM (MSSM) [16, 17], the bino, wino, and higgsino fields are the fermionic partners of the $SU(2) \times U(1)$ gauge fields in the SM and the two complex scalar Higgs doublets, respectively. The bino, wino, and higgsino fields are collectively referred to as 'electroweakinos,' which mix to form mass eigenstates known as neutralinos $\tilde{\chi}_i^0$ ($i = 1, 2, 3, 4$) and charginos $\tilde{\chi}_j^\pm$ ($j = 1, 2$) with the subscripts indicating increasing mass. The masses of the bino, wino, and higgsino fields are parameterised in terms of M_1, M_2, and μ, respectively. For large values of $\tan\beta$, representing the ratio between the vacuum expectation values of the two Higgs doublets, the phenomenology of the electroweakinos is driven by these three mass parameters.

This paper presents searches targeting SUSY scenarios in which the masses of the higgsino states are much smaller compared with the masses of the bino and wino states (i.e. $|\mu| \ll M_1, M_2$). Such scenarios are motivated by the role of μ in naturalness arguments [14, 15], which favour values of $|\mu|$ near the weak scale [18–21]. In these scenarios, the lightest SUSY particles are a triplet of higgsino-like states ($\tilde{\chi}_1^0, \tilde{\chi}_1^\pm, \tilde{\chi}_2^0$) having 'compressed mass spectra', with minimal mass splittings of about 300 MeV due to radiative corrections. Larger mass splitting values of a few GeV can be generated depending on the values of M_1 and M_2 relative to μ. Throughout this paper, the LSP is assumed to be the lightest neutralino ($\tilde{\chi}_1^0$) and the higgsino-like mass eigenstates are referred to as 'higgsinos' for simplicity.

Various ATLAS and CMS searches were conducted to explore this regime of compressed mass spectra, primarily with the use of 'tracks' that represent the reconstructed trajectories of charged particles in the inner detector. Highly compressed scenarios with $\Delta m(\tilde{\chi}_1^\pm, \tilde{\chi}_1^0) \lesssim$ 300–400 MeV were searched for using the 'disappearing track' signature that targets the long-lived ($c\tau > \mathcal{O}(10\text{ mm})$) $\tilde{\chi}_1^\pm$. In these scenarios, a significant fraction of the produced $\tilde{\chi}_1^\pm$ particles can traverse several silicon layers of the inner detector before decaying into an invisible $\tilde{\chi}_1^0$ and a low-momentum ('soft') charged pion (i.e. $\tilde{\chi}_1^\pm \to \tilde{\chi}_1^0 \pi^\pm$) that is not reconstructed, leading to the distinct signature of a charged particle track disappearing within the inner detector [22–25]. Scenarios with $\Delta m(\tilde{\chi}_1^\pm, \tilde{\chi}_1^0) \approx$ 300–900 MeV, and thus shorter $\tilde{\chi}_1^\pm$ lifetimes ($c\tau \approx \mathcal{O}(0.1\text{–}10\text{ mm})$), were searched for using a 'mildly displaced track' signature [26], in which the $\tilde{\chi}_1^\pm$ decay occurs before reaching the tracking detector and instead, the charged pion is reconstructed as a soft track with a large transverse impact parameter [27], denoted by d_0 and defined as the shortest distance between the track and the beam line in the transverse plane. Scenarios with mass splittings larger than approximately 1.5 GeV, corresponding to $c\tau < \mathcal{O}(0.1\text{ mm})$, were explored by searches targeting low-momentum prompt lepton[1] signatures from $\tilde{\chi}_2^0 \to \tilde{\chi}_1^0 Z^* \to \tilde{\chi}_1^0 \ell^+ \ell^-$ [28–32]. Despite these efforts, the strongest constraints on scenarios with $\Delta m(\tilde{\chi}_1^\pm, \tilde{\chi}_1^0) \approx$ 0.9–1.2 GeV are still set by the LEP experiments [33]. Additionally, ATLAS has performed a scan of the electroweak sector of the phenomenological MSSM [34, 35] that highlights the continued viability of higgsinos in this mass regime after accounting for constraints from previous Run-2 searches, flavour physics observables, precision electroweak measurements, and the observed dark matter relic density [36].

[1]The term 'lepton' in this paper refers to electrons or muons and does not include neutrinos and τ-leptons unless otherwise specified.

JHEP06(2026)094

The searches in this paper use 140 fb^{-1} of proton-proton (pp) collision data at a centre-of-mass energy $\sqrt{s} = 13$ TeV, collected by the ATLAS experiment [37] from 2015 to 2018 at the CERN Large Hadron Collider (LHC). The pair production of higgsinos via electroweak interactions is assumed, with subsequent decays into a stable $\tilde{\chi}_1^0$, the LSP, and SM particles. Simplified SUSY models [38–40] are used to optimise the searches and interpret the results.

Two searches are designed to identify at least one of the higgsino decay products as a low-momentum track using machine learning techniques, which are adopted to search a range of mass splitting scenarios of the higgsinos. The first search targets smaller mass splittings ($\Delta m(\tilde{\chi}_1^{\pm}, \tilde{\chi}_1^0) \approx 0.3$–$1$ GeV) using event signatures similar to the one employed in ref. [27], where soft pion tracks with large d_0 are identified as the long-lived higgsino decay product candidates. This signature is also relevant for SUSY models where $M_2 \ll M_1, |\mu|$, such that the lightest particles are the wino-like $\tilde{\chi}_1^{\pm}$ and $\tilde{\chi}_1^0$ with $\Delta m(\tilde{\chi}_1^{\pm}, \tilde{\chi}_1^0)$ being on the order of a few hundred MeV [41]. In contrast to this previous search, the sensitivity is enhanced using two dedicated neural-network (NN) classifiers: one exploiting the kinematic information of individual tracks (referred to as the 'track-level' NN) and the other exploiting global kinematic observables of the event (referred to as the 'event-level' NN) to provide discrimination between signal and SM background processes. The second search targets slightly larger mass splittings ($\Delta m(\tilde{\chi}_1^{\pm}, \tilde{\chi}_1^0) \approx 1$–$3$ GeV) by using NN-based soft-electron and -muon identification algorithms, or 'taggers', to identify the leptons from the $\tilde{\chi}_2^0 \to Z^*(\to \ell^+\ell^-)\tilde{\chi}_1^0$ decays. These advanced soft-lepton taggers extend the identification of electrons and muons to lower transverse momenta than what is achievable with the existing ATLAS algorithms, granting the ability to search for such new physics in this regime of mass splittings.

The paper is structured as follows: Section 2 highlights the analysis strategies of the two searches in further detail. Section 3 provides a brief overview of the ATLAS detector. Details of the data and simulated event samples used in the analyses are given in section 4. The object reconstruction and identification methods are presented in section 5. The event selection strategies and signal region definitions are outlined in section 6. The background estimation methods are discussed in section 7, followed by a summary of the systematic uncertainty in section 8. Finally, the search results and their statistical interpretations are presented in section 9, followed by the conclusion in section 10.

2 Analysis strategy

Two search strategies are employed in this paper to search for the direct production of higgsinos that feature small mass splittings between the $\tilde{\chi}_1^0$ LSP and the slightly heavier $\tilde{\chi}_2^0$ and $\tilde{\chi}_1^{\pm}$ particles. They are referred to as the 'displaced track' and the 'one-lepton and one-track ($1\ell1$T)' searches. In this regime, the transverse momenta (p_{T}) of the SM particles arising from the $\tilde{\chi}_2^0$ and $\tilde{\chi}_1^{\pm}$ decays are well below the ATLAS trigger thresholds. Additionally, the signal processes are expected to result in two undetected $\tilde{\chi}_1^0$ particles that are typically back-to-back in the transverse plane, therefore producing only a small amount of missing transverse momentum $\mathbf{p}_{\mathrm{T}}^{\mathrm{miss}}$ (with magnitude denoted by $E_{\mathrm{T}}^{\mathrm{miss}}$), defined as the negative vector sum of the transverse momenta of all reconstructed particles in the event. In such cases, the missing transverse momentum triggers remain inefficient. Both of the searches therefore target events in which the higgsinos are produced in association with a high-p_{T} jet

JHEP06(2026)094

from initial-state radiation (ISR), which provides a boost to the higgsinos in the direction opposite to that of the ISR jet in the transverse plane. While reducing the signal acceptance, the boost from the ISR jet serves to increase the p_{T} of the two $\tilde{\chi}_1^0$ particles and align their directions in the transverse plane, thereby increasing the $E_{\mathrm{T}}^{\mathrm{miss}}$ in the event. The large $E_{\mathrm{T}}^{\mathrm{miss}}$ then allows the $E_{\mathrm{T}}^{\mathrm{miss}}$ trigger to be highly efficient and provides important discrimination between the signal and SM background processes.

In addition to this common selection, each search attempts to reconstruct the soft SM particles from the $\tilde{\chi}_2^0$ and $\tilde{\chi}_1^{\pm}$ decays to further reduce the large SM backgrounds. In contrast to previous ATLAS searches for higgsino-like LSPs with compressed mass spectra, the identification of these soft decay products, and the discrimination between signal and SM background processes, are performed using several NN classifiers.

The first, 'displaced track' search, targets models in which $\Delta m(\tilde{\chi}_1^{\pm}, \tilde{\chi}_1^0) \approx 0.3$–$1$ GeV, where the dominant decay mode of the charged higgsino is expected to be $\tilde{\chi}_1^{\pm} \to \pi^{\pm}\tilde{\chi}_1^0$ [42] and the decay length of this particle is $\mathcal{O}(0.1$–10 mm), i.e. well before reaching the ATLAS tracking detector. The charged pions from these decays can be identified as low-transverse-momentum tracks, typically having $p_{\mathrm{T}} < 5$ GeV, with moderately large $|d_0|$ relative to the beam line. An example diagram showing $\tilde{\chi}_1^{\pm}\tilde{\chi}_1^0$ production in association with an ISR jet is shown in figure 1(a), where the $\tilde{\chi}_1^{\pm}$ decays into a charged pion and the $\tilde{\chi}_1^0$ LSP. The displaced track search leverages two fully connected NNs to discriminate between the signal and SM background processes. The first network uses event-level information such as the jet kinematics and missing transverse momentum, while the second network uses tracking information to identify tracks that are consistent with arising from the decay of a moderately long-lived $\tilde{\chi}_1^{\pm}$, providing additional discriminating power. The output scores of these networks are used to define the analysis regions, as described in section 6.1. The estimate of the SM backgrounds, which are largely represented by $Z(\to \nu\bar{\nu}) +$ jets and $W^{\pm}(\to \tau^{\pm}\nu_{\tau}) +$ jets processes, is performed using simulation, with the normalisations of the dominant backgrounds being constrained in control regions, as described in section 7.1.

The second, '$1\ell 1$T' search, is designed to have sensitivity to models with larger mass splittings where 1 GeV $\lesssim \Delta m(\tilde{\chi}_1^{\pm}, \tilde{\chi}_1^0) \lesssim 3$ GeV, under the assumption that $\Delta m(\tilde{\chi}_2^0, \tilde{\chi}_1^0) = 2\Delta m(\tilde{\chi}_1^{\pm}, \tilde{\chi}_1^0)$. Here, the $\tilde{\chi}_1^{\pm}$ and $\tilde{\chi}_2^0$ are assumed to decay promptly into off-shell SM gauge bosons and the $\tilde{\chi}_1^0$ LSP: $\tilde{\chi}_1^{\pm} \to W^{\pm *}\tilde{\chi}_1^0$ and $\tilde{\chi}_2^0 \to Z^*\tilde{\chi}_1^0$. The search targets events featuring two electrons or muons with opposite electric charges from the Z^* decay, where one of the leptons is identified using the standard ATLAS identification algorithms, defined in section 5, and the other is identified using dedicated soft-electron and soft-muon taggers based on NNs that are developed for this search. These taggers use charged particle tracks and energy deposits in the electromagnetic calorimeter to significantly increase the identification efficiency for electrons and muons with $p_{\mathrm{T}} \in [0.5, 5]$ GeV relative to standard identification methods, as described in section 5.1. Figure 1(b) shows an example diagram of $\tilde{\chi}_1^{\pm}\tilde{\chi}_2^0$ production in association with an ISR jet where the heavier higgsinos decay into an off-shell W/Z boson and the $\tilde{\chi}_1^0$ LSP. To further enhance the sensitivity to higgsino production, the search employs a parameterised NN (pNN) [43] to provide discrimination between the signal and SM background processes. The parameterisation is performed relative to $\Delta m(\tilde{\chi}_2^0, \tilde{\chi}_1^0)$, the parameter of the benchmark scenarios that has a significant impact on the signal event kinematics. The details

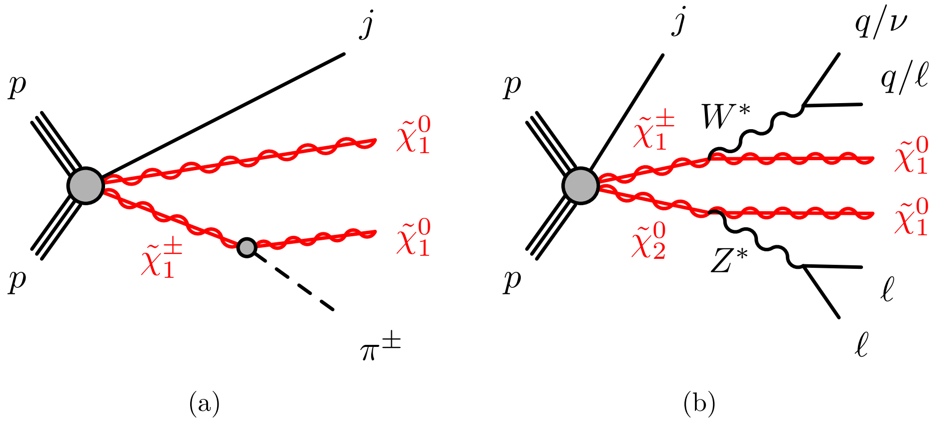

Figure 1. Example diagrams for the targeted signal processes featuring a jet (j) from initial-state radiation for (a) the displaced track search and (b) the $1\ell 1T$ search. While only the $\tilde{\chi}_1^0\tilde{\chi}_1^\pm$ ($\tilde{\chi}_2^0\tilde{\chi}_1^\pm$) diagram is shown for the displaced track ($1\ell 1T$) search, the additional production processes described in section 4 are considered as well.

of the event selection are given in section 6.2. The dominant SM backgrounds in which the lepton-tagged track is not a real lepton, dominated by $W^\pm$ + jets processes, are determined by data-driven methods, while the residual SM backgrounds featuring a real lepton-tagged track are estimated by using simulation, as described in section 7.2.

3 ATLAS detector

The ATLAS detector [37] at the LHC covers nearly the entire solid angle around the collision point.[2] It consists of an inner tracking detector surrounded by a thin superconducting solenoid, electromagnetic and hadronic calorimeters, and a muon spectrometer incorporating three large superconducting air-core toroidal magnets.

The inner-detector system is immersed in a 2 T axial magnetic field and provides charged-particle tracking in the range of $|\eta| < 2.5$. It consists of a high-granularity silicon pixel detector, a silicon microstrip detector (SCT), and a transition radiation straw-tube tracker (TRT), each spanning a sensitive radial distance from the interaction point of 33–150 mm, 299–560 mm, and 563–1066 mm, respectively [44]. The barrel (each endcap) consists of four (three) pixel layers, four (nine) double-layers of single-sided silicon microstrips, and 73 (160) layers of TRT straws. The pixel detector covers the vertex region and typically provides four measurements per track, the first hit generally being in the insertable B-layer (IBL) installed before Run 2 [45, 46]. The smaller radius and the reduced pixel size of IBL results in improvements of both the transverse and longitudinal impact parameter resolutions. The d_0 resolution reaches ~ 0.09 mm for tracks with $p_{\mathrm{T}} = 1$ GeV [47]. The SCT usually provides

[2] ATLAS uses a right-handed coordinate system with its origin at the nominal interaction point (IP) in the centre of the detector and the z-axis along the beam pipe. The x-axis points from the IP to the centre of the LHC ring, and the y-axis points upwards. Polar coordinates (r, ϕ) are used in the transverse plane, ϕ being the azimuthal angle around the z-axis. The pseudorapidity is defined in terms of the polar angle θ as $\eta = -\ln\tan(\theta/2)$ and is equal to the rapidity $y = \frac{1}{2}\ln\left(\frac{E+p_z}{E-p_z}\right)$ in the relativistic limit. Angular distance is measured in units of $\Delta R \equiv \sqrt{(\Delta y)^2 + (\Delta\phi)^2}$.

JHEP06(2026)094

eight measurements, each corresponding to a single side of the double-layered strips, per track. The TRT enables radially extended track reconstruction up to $|\eta| = 2.0$. As electrons tend to have higher relativistic gamma factors and thus higher probabilities of inducing transition radiation compared with other particles, the TRT is also capable of providing electron identification information based on the fraction of hits (typically 30 in total) above a higher energy-deposit threshold.

The calorimeter system covers the pseudorapidity range $|\eta| < 4.9$. Within the region $|\eta| < 3.2$, electromagnetic calorimetry is provided by barrel and endcap high-granularity lead/liquid-argon (LAr) calorimeters, with an additional thin LAr presampler covering $|\eta| < 1.8$ to correct for energy loss in material upstream of the calorimeters. Hadronic calorimetry is provided by the steel/scintillator-tile calorimeter, segmented into three barrel structures within $|\eta| < 1.7$, and two copper/LAr hadronic endcap calorimeters. The solid angle coverage is completed with forward copper/LAr and tungsten/LAr calorimeter modules optimised for electromagnetic and hadronic energy measurements, respectively. The electromagnetic calorimeters consist of three main layers and the presampler layer. The hadronic calorimeters consist of three (four) layers in the barrel (endcap) regions, providing sufficient containment of hadronic showers.

The muon spectrometer comprises separate trigger and high-precision tracking chambers measuring the deflection of muons in a magnetic field generated by the superconducting air-core toroidal magnets. The field integral of the toroids ranges between 2.0 and 6.0 T m across most of the detector. Three layers of precision chambers, each consisting of layers of drift tubes, cover the region $|\eta| < 2.7$, complemented by cathode-strip chambers in the forward region, where the background is highest. The muon trigger system covers the range $|\eta| < 2.4$ with resistive-plate chambers in the barrel, and thin-gap chambers in the endcap regions.

The luminosity is measured mainly by the LUCID–2 [48] detector that records Cherenkov light produced in the quartz windows of photomultipliers located close to the beampipe.

Events are selected by the first-level trigger system implemented in custom hardware, followed by selections made by algorithms implemented in software in the high-level trigger [49]. The first-level trigger accepts events from the 40 MHz bunch crossings at a rate below 100 kHz, which the high-level trigger further reduces to record complete events to disk at about 1.25 kHz.

A software suite [50] is used in the trigger and data acquisition systems of the experiment, in detector operations, in data simulation, and in the reconstruction and analysis of real and simulated data.

4 Data and simulated event samples

The considered data sample amounts to 140 fb^{-1} of $\sqrt{s} = 13$ TeV pp collision data recorded by the ATLAS detector from 2015–2018 with an uncertainty of 0.83% in the integrated luminosity [51]. The average number of interactions per bunch-crossing in the data sample is 33.7 [52]. The data are selected using missing transverse momentum triggers [53] that use different trigger thresholds depending on the data-taking periods, resulting in an efficiency of more than 95% for events with offline-calibrated $E_{\mathrm{T}}^{\mathrm{miss}}$ greater than 200 GeV. Additionally, single-electron and single-muon triggers [54, 55] are employed to collect a sample of events that are used to constrain SM backgrounds involving the production of $W^{\pm}$ or Z bosons, as described in section 7.1.

Monte Carlo (MC) simulation samples are produced for the signal and SM background processes to estimate their event yields and associated systematic uncertainty. The SM backgrounds in the searches are determined from both the data-driven methods and the MC simulation, as described in section 7. While the details of the signal and SM background MC simulation are given below, both of the sets of samples undergo the same procedure to include the effects of multiple pp interactions in the same and neighbouring bunch crossings (pile-up). In each case, the simulated hard-scattering events are overlaid with inelastic pp collision events generated with PYTHIA 8.186 [56] using the NNPDF2.3LO set of parton distribution functions (PDF) [57] and the A3 set of tuned parameters [58]. Weights are then applied to the simulated events to match the pile-up distribution observed in the data and the detector response is simulated using the ATLAS simulation framework [59] based on GEANT4 [60]. The full detector simulation is used for the SM background samples, while the signal samples use either this full detector simulation or the ATLAS fast simulation that relies on a parameterisation of the calorimeters, as detailed below.

Signal MC samples consisting of direct higgsino production are simulated for the displaced track and $1\ell 1T$ searches to optimise the event selections and interpret the results in the context of the simplified models under study. Since the $1\ell 1T$ search targets the soft leptons from the $\tilde{\chi}_2^0 \to Z^*(\to \ell^+\ell^-)\tilde{\chi}_1^0$ decays, the $\tilde{\chi}_2^0\tilde{\chi}_1^{\pm}$ and $\tilde{\chi}_2^0\tilde{\chi}_1^0$ production modes are simulated, while the samples used for the displaced track search also include the $\tilde{\chi}_1^0\tilde{\chi}_1^{\pm}$ and $\tilde{\chi}_1^+\tilde{\chi}_1^-$ processes. In each case, the $\tilde{\chi}_1^0\tilde{\chi}_1^0$ and $\tilde{\chi}_2^0\tilde{\chi}_2^0$ production modes are ignored due to their negligible production cross-sections when the $\tilde{\chi}_1^0$ and $\tilde{\chi}_2^0$ are higgsino-like states. In the simplified model considered here, the $\tilde{\chi}_1^{\pm}$ mass is set to be halfway between the neutralino masses, such that $\Delta m(\tilde{\chi}_2^0, \tilde{\chi}_1^0) = 2\Delta m(\tilde{\chi}_1^{\pm}, \tilde{\chi}_1^0)$. The MC samples are generated at leading-order (LO) with MADGRAPH5_AMC@NLO 2.9.5 [61] for the displaced track search and version 2.9.3 for the $1\ell 1T$ search using the NNPDF2.3LO [57] PDF set and including up to two additional partons in the matrix element calculation. The simulated events for the displaced track search and the $1\ell 1T$ search are then interfaced with PYTHIA 8.306 [62] and PYTHIA 8.245 [63], respectively, to model the parton shower, hadronisation, and underlying event using the A14 set of tuned parameters [64]. Matching between the matrix element and parton shower jets is performed using the CKKW-L scheme [65] with the matching scale set to 15 GeV. At least one parton in the final state is required to have a transverse momentum greater than 50 GeV to enforce the ISR topology targeted by both of the searches. The decays of b- and c-hadrons are modelled by EVTGEN 1.7.0 [66].

For the signal samples used by the $1\ell 1T$ search, the branching fractions for the $\tilde{\chi}_2^0 \to Z^*\tilde{\chi}_1^0$ and $\tilde{\chi}_1^{\pm} \to W^{\pm *}\tilde{\chi}_1^0$ are set to 100% and the higgsinos are decayed with MADSPIN [67] to account for spin correlations effects. The leptonic branching fractions of the $\tilde{\chi}_2^0 \to Z^*\tilde{\chi}_1^0$, typically 5% each for $\tilde{\chi}_2^0 \to e^+e^-\tilde{\chi}_1^0$ and $\tilde{\chi}_2^0 \to \mu^+\mu^-\tilde{\chi}_1^0$, are calculated with SUSY-HIT [68] for different $\Delta m(\tilde{\chi}_2^0, \tilde{\chi}_1^0)$ values and incorporated in the signal yield calculation. The higgsino branching fractions in the samples used by the displaced track search are calculated following the prescription in ref. [42], which accounts for the mass splitting between the heavier $\tilde{\chi}_2^0/\tilde{\chi}_1^{\pm}$ and the $\tilde{\chi}_1^0$. For $\Delta m(\tilde{\chi}_1^{\pm}, \tilde{\chi}_1^0) = 0.5$ GeV, the branching fraction for $\tilde{\chi}_1^{\pm} \to \pi^{\pm}\tilde{\chi}_1^0$ is approximately 80%, with the remaining 20% corresponding to $\tilde{\chi}_1^\pm \to e^\pm/\mu^\pm\nu\tilde{\chi}_1^0$. In the simplified model, this corresponds to $\Delta m(\tilde{\chi}_2^0, \tilde{\chi}_1^0) = 1$ GeV, for which the dominant branching fractions are approximately 30% for each of the $\tilde{\chi}_2^0 \to \pi^0\tilde{\chi}_1^0$, $\tilde{\chi}_2^0 \to \pi^+\pi^-\tilde{\chi}_1^0$, and $\tilde{\chi}_2^0 \to \nu\bar{\nu}\tilde{\chi}_1^0$ processes. In addition to the branching fractions, the mass splitting between the higgsinos determines the $\tilde{\chi}_1^\pm$ and $\tilde{\chi}_2^0$ lifetimes, where smaller mass splittings result in longer lifetimes and flight lengths. The higgsino decays for these samples are performed using PYTHIA and the higgsino lifetimes are determined by the mass splitting according to the prescription in ref. [42].

The higgsino production cross-sections and associated uncertainty are calculated using RESUMMINO 2.0.1 at NLO+NLL precision [69–77] using an envelope of the CTEQ6.6 [78] and MSTW2008nlo90cl [79] PDF sets. The uncertainty originates primarily from QCD renormalisation and factorisation scales. Taking an example with $m(\tilde{\chi}_2^0) = 102$ GeV, $m(\tilde{\chi}_1^\pm) = 101$ GeV, and $m(\tilde{\chi}_1^0) = 100$ GeV, the cross-section values are 5.3 ± 0.2 pb, 3.2 ± 0.1 pb, 5.5 ± 0.2 pb and 2.9 ± 0.1 pb for $\tilde{\chi}_2^0\tilde{\chi}_1^\pm$, $\tilde{\chi}_2^0\tilde{\chi}_1^0$, $\tilde{\chi}_1^0\tilde{\chi}_1^\pm$ and $\tilde{\chi}_1^+\tilde{\chi}_1^-$ production, respectively. The samples used for the 1ℓ1T search use the full detector simulation, while those used for the displaced track search use the ATLAS fast simulation as its analysis signature is less dependent to calorimeter responses.

The SM background processes are simulated using a variety of MC generators, with table 1 providing a summary of the matrix element and parton shower configurations as well as the accuracy of the cross-section calculation used for each of the background samples. The dominant sources of SM backgrounds for both the displaced track and the 1ℓ1T searches arise from vector boson production with subsequent leptonic decays, in association with at least one high-p_{T} jet. These processes are simulated using SHERPA 2.2.11 with the NNPDF3.0NNLO PDF set [80], where the matrix element calculation includes up to two additional partons at NLO accuracy and up to five additional partons at LO accuracy. The $Z^{(*)}/\gamma^*$+jets samples provide coverage of the dilepton invariant mass down to 10 GeV. Minor backgrounds arise from the production of diboson pairs ($VV = WW, ZZ, WZ$), top quarks ($t\bar{t}$, single-t in the s, t, and tW channels), multijets, and $\gamma +$ jets. The diboson samples are modelled with either SHERPA version 2.2.1 or 2.2.2, depending on the specific process, at NLO accuracy with the NNPDF3.0NNLO PDF set. The $t\bar{t}$, single-t and tW backgrounds are simulated using POWHEG BOX v2 for the matrix element and PYTHIA 8.230 for the parton shower, using the NNPDF3.0NLO and NNPDF2.3LO PDF sets, respectively. The diagram removal scheme [81] is used to account for interference effects between the $t\bar{t}$ and tW processes. Multijet samples are modelled at LO using PYTHIA 8.230 and the NNPDF2.3LO PDF set for both the matrix element and the parton shower. Finally, the $\gamma +$ jets processes are modelled using SHERPA 2.2.2 at NLO accuracy with the NNPDF3.0NNLO PDF set. Backgrounds that are simulated using SHERPA model the decays of b- and c-hadrons internally, while the other samples make use of EVTGEN 1.6.0 or 1.2.0 [66]. Backgrounds such as triboson production and other rare processes involving top quarks or Higgs bosons are found to be negligible in the searches.

5 Event reconstruction

The trajectories of charged particles are reconstructed from the inner detector hits as tracks using clusterisation and combinatorial track finding algorithms [105]. The kinematic variables of the track such as p_{T}, η and ϕ are defined at the perigee, the point of closest approach of

JHEP06(2026)094

Physics process	Matrix element	Parton shower	Cross-section	Tune	PDF (ME)	PDF (PS)
$V+\text{jets}$	SHERPA 2.2.11 [82]	SHERPA 2.2.11	NLO [83–86]	Default [87]	NNPDF3.0NNLO [80]	NNPDF3.0NNLO
Diboson (VV)	SHERPA 2.2.1, 2.2.2	SHERPA 2.2.1, 2.2.2 [88, 89]	NLO	Default	NNPDF3.0NNLO	NNPDF3.0NNLO
$t\bar{t}$	POWHEG BOX v2 [90–93]	PYTHIA 8.230 [63]	NNLO+NNLL [94–100]	A14 [64]	NNPDF3.0NLO [80]	NNPDF2.3LO [57]
Single-top	POWHEG BOX v2 [91–93, 101, 102]	PYTHIA 8.230	NLO+NNLL [103, 104]	A14	NNPDF3.0NLO	NNPDF2.3LO
Multijets	PYTHIA 8.230	PYTHIA 8.230	LO	A14	NNPDF2.3LO	NNPDF2.3LO
$\gamma+\text{jets}$	SHERPA 2.2.2	SHERPA 2.2.2	NLO	Default	NNPDF3.0NNLO	NNPDF3.0NNLO

Table 1. A summary of the configurations used to generate the MC samples for the SM background processes. Starting from the second column, the table provides the generators used for the matrix element (ME), the generators used for the parton shower (PS), the order in α_s used to determine the production cross-section, the tune for the underlying event, the PDF set used for the matrix element calculation, and the PDF set used for the parton shower. The symbol V is used to denote the W and Z vector bosons.

the track to the beam line. Tracks with p_T down to 500 MeV are reconstructed. All events are required to have at least one reconstructed pp interaction vertex with a minimum of two associated tracks. In events with multiple vertices, the primary vertex is defined as the vertex having the highest $\sum p_\mathrm{T}^2$ of associated tracks. A set of basic quality criteria [106] is applied to reject events with detector noise or non-collision backgrounds.

Leptons, jets, and tracks are 'preselected' using loose identification criteria and must satisfy more restrictive 'tight' identification requirements to be selected for the search regions described in section 6. Preselected leptons and jets are primarily used to resolve ambiguities between tracks and energy clusters associated with multiple lepton and jet candidates.

Isolation criteria are used in the definition of tight leptons and are based on tracking information, calorimeter energy clusters, or both. Isolation energies are computed as a $\sum p_\mathrm{T}$ of nearby activity, excluding the contributions from nearby leptons. Requiring small isolation energies helps to reduce contributions from semileptonic heavy-flavour hadron decays and jets misidentified as prompt leptons. The isolation requirements are based on those described in refs. [107] and [108]. The isolation variable $p_\mathrm{T}^{\mathrm{cone}X}$ is defined as the $\sum p_\mathrm{T}$ of all tracks satisfying $\Delta R < X/100$ and $p_\mathrm{T} > 1$ GeV. For the $1\ell 1\mathrm{T}$ search, this variable is adjusted by subtracting the p_T of the paired lepton or track as described later.

Electrons are required to have $p_\mathrm{T} > 4.5$ GeV and $|\eta| < 2.47$. Preselected electrons are further required to satisfy the calorimeter- and tracking-based *Loose* likelihood identification [107] and to have a longitudinal impact parameter z_0 relative to the primary vertex satisfying $|z_0 \sin\theta| < 0.5$ mm. Tight electrons must satisfy the *Medium* identification criterion [107], having typical selection efficiency of over 80% for $p_\mathrm{T} > 10$ GeV and 70–80% for $p_\mathrm{T} = 4.5$–10 GeV, and be associated with the primary vertex, with the significance of the transverse impact parameter relative to the beam position satisfying $S(d_0) \equiv |d_0|/\sigma(d_0) < 5$, where $\sigma(d_0)$ is the uncertainty in d_0. For the displaced track search, tight electrons are further selected using the *Loose_VarRad* isolation working point [107], whereas for the $1\ell 1\mathrm{T}$ search, the *TightTrackOnly_VarRad* isolation working point [107] is required with an adjustment to subtract the contribution of the signal candidate track. This adjustment is performed to avoid vetoing signal processes in which the two leptons originating from the $\tilde{\chi}_2^0$ are nearby.

Muons are required to satisfy $p_\mathrm{T} > 3$ GeV and $|\eta| < 2.5$. Preselected muons are identified using the *Medium* criterion [108], having typical selection efficiency of over 90% for $p_\mathrm{T} > 5$ GeV and 50–90% for $p_{\mathrm{T}} = 3$–5 GeV, and are required to satisfy $|z_0 \sin\theta| < 0.5$ mm. Tight muons must satisfy the promptness requirement of $|d_0|/\sigma(d_0) < 3$. For the displaced track search, tight muons are further selected using the *Pflow_Loose* isolation working point [108], whereas for the $1\ell1$T search, the *TightTrackOnly* isolation working point [108] is required with an adjustment to subtract the contribution of the signal candidate track, similar to the electrons.

Jets are reconstructed from particle flow objects [109] using the anti-k_t algorithm [110, 111] with radius parameter $R = 0.4$. Preselected jets are required to have $p_{\mathrm{T}} > 20$ GeV and $|\eta| < 4.5$ after being calibrated according to the procedure in ref. [112]. For suppressing jets originating from pile-up, jets with $p_{\mathrm{T}} < 60$ GeV and $|\eta| < 2.5$ are required to satisfy the *Tight* working point of the jet vertex tagger [113], using information from the tracks associated with the jet. From the sample of preselected jets, tight jets are further selected when they satisfy $|\eta| < 2.8$, which ensures that the jets are within the acceptance of the high-granularity endcap calorimeters.

Jets originating from the hadronisation of b-quarks, referred to as b-tagged jets, are identified from preselected jets within $|\eta| < 2.5$ using the *DL1r* algorithm [114]. The $p_{\mathrm{T}} > 20$ GeV requirement is maintained to maximise the rejection of the $t\bar{t}$ background in analysis regions that veto events containing b-tagged jets. The b-tagging algorithm working point is chosen so that b-jets from simulated $t\bar{t}$ events are identified with an 85% efficiency, with corresponding rejection factors of approximately 2.9 and 40 for jets containing c-hadrons and jets arising from light-flavour quarks and gluons, respectively [115, 116].

To resolve ambiguities between nearby reconstructed leptons and jets, the following procedures are performed. First, preselected muons that share an inner detector track with a preselected electron candidate are rejected. Next, non-b-tagged preselected jets within $\Delta R < 0.2$ of a preselected electron are discarded. Preselected electrons satisfying $\Delta R < \min(0.4, 0.04 + 10\ \mathrm{GeV}/p_{\mathrm{T}}(e))$ relative to a preselected jet are then removed. Non-b-tagged preselected jets within $\Delta R < 0.2$ of a preselected muon are then rejected. Finally, preselected muons satisfying $\Delta R < \min(0.4, 0.04{+}10\ \mathrm{GeV}/p_{\mathrm{T}}(\mu))$ with respect to a preselected jet are removed.

The missing transverse momentum is defined as the negative vector sum of the transverse momenta of all preselected objects (leptons, jets, and photons [107]) and an additional soft term that is constructed from all tracks that are not associated with any lepton or jet but are associated with the primary vertex. In this way, $E_{\mathrm{T}}^{\mathrm{miss}}$ is adjusted for the best calibration of leptons and jets, while maintaining pile-up independence in the soft term [117].

Scale factors are applied to the efficiencies of reconstructed electrons [107], muons [108] and b-tagged jets [118] in the simulated samples to match the reconstruction efficiencies in data. The scale factors for b-tagged jets account for the differences between data and simulated samples in the identification efficiencies for jets including b-hadron decays and for the misidentification rates of jets initiated from charm quarks, light-flavour quarks, or gluons. In addition, scale factors are used to reweight simulated samples to properly model the trigger efficiency observed in data.

JHEP06(2026)094

5.1 Low-p_T lepton-track identification

In the $1\ell 1$T search, low-p_T lepton-track identification (ID) methods are used to identify leptons eluding standard identification methods and to gain sensitivity to unexplored low-Δm regions. Tracks with $p_\mathrm{T} > 500$ MeV and $|\eta| < 2.5$ are preselected using the *Tight Primary* working point defined in ref. [119]. In low-p_T regimes with $p_\mathrm{T} < 5$ GeV, tracks are dominated by hadrons (mostly charged pions) and fake combinatorial tracks. The target of the low-p_T lepton-track ID is to distinguish lepton-tracks from such background tracks by exploiting information mainly from detectors situated closer to the interaction point, compared to those used in standard methods. A low-p_T electron-track ID and a low-p_T muon-track ID are developed separately with independent optimisations.

The low-p_T electron-track candidate is required to have $p_\mathrm{T} \in [0.5, 5]$ GeV and $|\eta| < 2.5$. Tracks are extrapolated to a matching calorimeter energy cluster based on its position and energy deposit when available, however, the existence of a matched cluster is not always required. The matching for low-p_T electron-tracks is performed assuming a constant magnetic field in the volume of the inner detector and using the perigee parameters of the track. A fully connected NN model with two 128-node hidden layers is trained using single particle MC events to separate low-p_T electron-tracks from dominant low-p_T hadronic tracks using silicon tracking information including track p_T and track η, along with optional TRT and electromagnetic calorimeter energy cluster information. Tracking fit errors, hit information in the TRT detector, and energy deposits in the inner layers of the electromagnetic calorimeter show notable differences between electron and hadronic tracks due to the effects of bremsstrahlung. An identification working point for the $1\ell 1$T search is dynamically defined by adopting another NN using track p_T, track $|\eta|$, and the score from the previous network as inputs. By setting a threshold on the output score of this network, a working point optimised within the 3D space of the inputs is chosen. The latter network is trained with signal higgsino and background $W^{\pm}$+jets MC events satisfying the event-selection criteria defined later in section 6.

The low-p_T muon-track candidate is required to have $p_\mathrm{T} \in [1, 5]$ GeV and $|\eta| < 1.6$. A large fraction of muons with p_T below 3 GeV make a full-stop in the calorimeters and do not reach the muon spectrometer. Thus, the low-p_T muon track is identified using information only from the inner detector and calorimeters. As opposed to the case of electron-tracks, muon candidate tracks are always required to have a matching calorimeter energy cluster. A fully connected NN model with six 64-node hidden layers is trained using $J/\psi \to \mu^+\mu^-$ MC events to separate low-p_T muon-tracks from dominant low-p_T hadronic tracks using track p_T, track η, and energy deposits in each calorimeter layer. Low-p_T muons tend to act as minimum ionising particles and deposit less energy in the calorimeters compared with low-p_T hadrons, allowing their identification without the use of muon detectors. Similarly to the electron-track case, a working point for the $1\ell 1$T search is dynamically defined with another NN using track p_T, track η, and the previous network score, with the training performed with signal higgsino and background $W^{\pm}$+jets MC events that satisfy the $1\ell 1$T event-selection criteria.

Figure 2 shows the signal and background track efficiencies of the low-p_T lepton-track ID methods as a function of track p_T. Both of the ID selections are optimised to maximise

JHEP06(2026)094

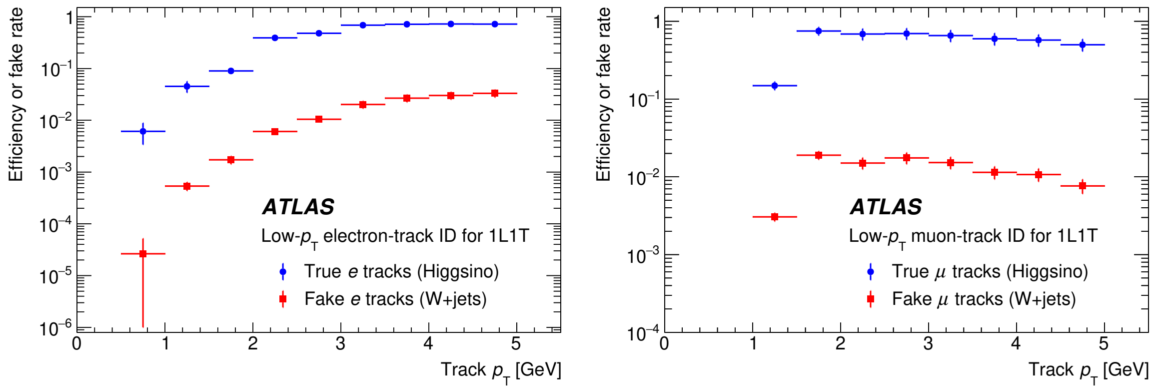

(a) (b)

Figure 2. Simulated true-track efficiency and fake-track rate as a function of track p_{T} for (a) the low-p_{T} electron-track ID and (b) the low-p_{T} muon-track ID. The scale factors obtained from the calibration methods are applied with their corresponding uncertainty. The total uncertainty including the statistical and systematic uncertainties are shown, where the former uncertainty is found to be negligible. The true track is defined as a track matched to a lepton originating from $\tilde{\chi}_2^0 \to \tilde{\chi}_1^0 \ell^+ \ell^-$ decay in signal events satisfying the event selections defined later in section 6. The fake track is defined as a track in $W^{\pm}$+jets events that satisfies the same selection, excluding the track associated with the lepton from the $W^{\pm}$ decay.

the final sensitivity to signal higgsino models. Both of the lepton-track ID methods have tighter criteria in very low-p_{T} regimes of $p_{\mathrm{T}} < 1.5$ GeV, where contributions from hadronic and fake tracks become significant. The electron-track ID method has tighter criteria in terms of efficiency to achieve sufficient background suppression in the target region. For the low-p_{T} electron-track ID, the signal efficiency ranges in 0.6–70%, while the fake rate is kept within 0.003–3%. For the low-p_{T} muon-track ID, the signal efficiency ranges in 15–75%, while the fake rate is kept within 0.3–2%.

The scale factors and their uncertainty for low-p_{T} lepton-tracks are obtained using individual calibration methods for the electron and muon channels. The low-p_{T} electron-track ID is calibrated using a 'tag-and-probe method' [107] focusing on the distribution of ΔR between the low-p_{T} electron-track and the photon in $Z \to e^+e^-\gamma$ processes, particularly in events where an electron and the photon take away most of the energy, leaving the other electron to have a low p_{T}. In such event topologies, real low-p_{T} electrons from $Z \to e^+e^-\gamma$ tend to be distributed close to the photon and have small ΔR, whereas fake misidentified electrons are randomly distributed and have broader ΔR distributions. This shape difference in ΔR between the low-p_{T} electron-track and the photon is used to obtain the identification efficiency in data. The low-p_{T} muon-track ID is calibrated using a tag-and-probe method using $J/\psi \to \mu^+\mu^-$ processes, similar to that used in the calibration of standard muon identification [108]. The invariant mass distribution of the dimuon system is fitted using crystal-ball and quadratic functions. In both cases, the scale factors are evaluated by taking the ratio between the measured efficiency in data and the simulated efficiency in MC. They are only applied to the signal MC samples and the minor SM backgrounds of the $1\ell 1$T search that are evaluated using MC samples.

JHEP06(2026)094

Variable	Requirement
Trigger	$E_{\mathrm{T}}^{\mathrm{miss}}$ or single-lepton
$E_{\mathrm{T}}^{\mathrm{miss}}$ [GeV]	> 275
Number of jets with $p_{\mathrm{T}} > 30$ GeV	$[1, 4]$
Leading jet p_{T} [GeV]	> 250
Leading jet $\lvert\eta\rvert$	< 2.4
$\min \Delta\phi(\mathbf{p}_{\mathrm{T}}^{\mathrm{miss}}, \mathbf{j})$	> 0.4
Number of preselected leptons ($N_{\text{pre-lep}}$)	$= 0$ (only for SR)
Number of tracks	≥ 1

Table 2. Event-level selections applied to all events used for the displaced track search. The single-lepton trigger is used only for events in control and validation regions. The $\Delta\phi$ variables are defined to be in the range of $[0, \pi)$. The requirement on the number of tracks refers to the tracks defined in section 5.

6 Event selection

This section describes the event selections for the displaced track and $1\ell 1$T searches, each focusing on different mass splitting regions, and thus relying on distinct strategies exploiting NN models. For both of the searches, signal regions are defined to isolate the signal processes. As later described in section 7, control regions are defined to normalise the background processes and validation regions adjacent to the signal regions are defined to validate the background estimate.

6.1 Displaced track event selection

The displaced track search targets scenarios where $\Delta m(\tilde{\chi}_1^{\pm}, \tilde{\chi}_1^0) \approx 0.3$–$1.0$ GeV and the SM decay products of the moderately long-lived ($\mathcal{O}(0.1$–10 mm)) $\tilde{\chi}_1^{\pm}$ and $\tilde{\chi}_2^0$ particles can be reconstructed as low-p_{T} tracks with significant d_0. Events are selected using an $E_{\mathrm{T}}^{\mathrm{miss}}$ trigger and are first required to satisfy the event-level selections listed in table 2. Although the $E_{\mathrm{T}}^{\mathrm{miss}}$ trigger is fully efficient above 200 GeV, the reconstructed $E_{\mathrm{T}}^{\mathrm{miss}}$ is required to be larger than 275 GeV to enhance signal sensitivity. For signal events in which the $\tilde{\chi}_1^0$-pair significantly contributes to the invisible momentum, the high $E_{\mathrm{T}}^{\mathrm{miss}}$ requirement indicates a phase space in which the higgsino system is recoiling against hadronic activity in the form of ISR jets. Thus, all events are required to have at least one central jet with $p_{\mathrm{T}} > 250$ GeV. Up to four jets are allowed in the event, each satisfying $\Delta\phi(\mathbf{p}_{\mathrm{T}}^{\mathrm{miss}}, \mathbf{j}) > 0.4$. For the signal region (SR), the number of preselected leptons in each event is required to be zero.

To exploit the available information and to maximise the signal sensitivity, a machine learning based approach using NNs is adopted for further event selection. In particular, two independent NNs are trained to discriminate between signal and background processes: one using event-level information and the other using track-level information. Both of the models are fully connected networks implemented in `PyTorch` [120] and are optimised using binary cross-entropy loss. They each adopt an optimised structure of three hidden layers with 50, 30,

JHEP06(2026)094

	Input variable	Description
Event-level NN	$E_{\mathrm{T}}^{\mathrm{miss}}$	Magnitude of the missing transverse momentum
	Leading jet p_{T}	Kinematics of the leading jet
	Leading jet η	
	N_{jet}^{30}	Number of jets with $p_{\mathrm{T}} > 30$ GeV
	$\min \Delta\phi(\mathbf{p}_{\mathrm{T}}^{\mathrm{miss}}, \mathbf{j})$	Minimum azimuthal angular difference between $\mathbf{p}_{\mathrm{T}}^{\mathrm{miss}}$ and all jets in the event
	m_{eff}	Scalar sum of p_{T} of all jets with $p_{\mathrm{T}} > 30$ GeV and $E_{\mathrm{T}}^{\mathrm{miss}}$
	H_{T}	Scalar sum of p_{T} of all jets $p_{\mathrm{T}} > 30$ GeV
Track-level NN	Track p_{T}	Kinematics of the track
	Track η	
	Track d_0	Transverse impact parameter
	Track $S(d_0)$	Significance of transverse impact parameter $\|d_0/\sigma(d_0)\|$
	Track $z_0 \sin\theta$	Longitudinal impact parameter
	Track $p_{\mathrm{T}}^{\mathrm{cone40}}$	Scalar sum of p_{T} of tracks within $\Delta R < 0.4$ (excluding itself)
	Track $p_{\mathrm{T}}^{\mathrm{cone100}}$	Scalar sum of p_{T} of tracks within $\Delta R < 1.0$ (excluding itself)
	$\Delta\phi(\mathbf{trk}, \mathbf{p}_{\mathrm{T}}^{\mathrm{miss}})$	Azimuthal angular difference between the track and $\mathbf{p}_{\mathrm{T}}^{\mathrm{miss}}$
	Tight Primary	Binary to indicate if the track satisfies the *Tight Primary* track quality working point
	Secondary vertex matching	Binary to indicate if the track is matched to a secondary vertex
	Secondary vertex mass	Mass of secondary vertex reconstructed by associated tracks, -1 GeV if unmatched

Table 3. Summary of input variables of (top) event-level NN and (bottom) track-level NN. Events may not contain more than four jets, following the requirement in table 2.

and 15 nodes, respectively, and rectified linear unit (ReLU) activation. Both of the output scores range from 0 to 1, with higher scores corresponding to more signal-like events or tracks. The use of two independent NNs is adopted for its high flexibility in designing and validating the background estimation method later mentioned in section 7.1.

The lists of input variables for both of the networks are given in table 3. The event-level NN uses the event topology information based on $E_{\mathrm{T}}^{\mathrm{miss}}$ and hadronic jets. The inputs that provide the strongest discrimination power between signal and background processes are $E_{\mathrm{T}}^{\mathrm{miss}}$ and the effective mass, m_{eff}, defined as the scalar sum of p_{T} of all jets with $p_{\mathrm{T}} > 30$ GeV and $E_{\mathrm{T}}^{\mathrm{miss}}$. The track-level NN exploits a variety of track information, such as the kinematics, impact parameters, isolation variables, and angular difference between the track and the missing transverse momentum. In addition, an inclusive secondary vertexing algorithm [121] is used to identify tracks with $p_{\mathrm{T}} > 500$ MeV that are consistent with being produced at vertices that are displaced from the primary vertex. The invariant mass of the reconstructed secondary vertex, calculated under the assumption that each track is a charged pion, is used to discriminate between background tracks originating from the decays of long-lived hadrons (e.g. K_S^0, Λ^0) and those due to $\tilde{\chi}_2^0 \to \pi^+\pi^-\tilde{\chi}_1^0$ decays. For reconstructed secondary vertices with exactly two associated tracks, at least one of the tracks is required to satisfy $|d_0| > 2.0$ mm. The track d_0, $S(d_0)$, and isolation variables have the highest importance as they contribute to the separation from low-p_{T} QCD tracks.

The event-level and track-level NNs for the displaced track search are trained using signal and background MC events satisfying the selection criteria in table 2. The signal samples used for the training of each NN span values of $m(\tilde{\chi}_1^{\pm})$ from 85 GeV to 225 GeV and $\Delta m(\tilde{\chi}_1^{\pm}, \tilde{\chi}_1^0)$ from 0.25 GeV to 1.5 GeV. The individual signal samples are weighted according to their

SR name	Event score	Track score	Additional requirement
SR-DT-1	> 0.712	> 0.788	—
SR-DT-2	> 0.645	> 0.799	$\notin$ SR-DT-1
SR-DT-3	> 0.645	> 0.716	$\notin$ (SR-DT-1 $\cup$ SR-DT-2)
SR-DT-4	> 0.582	> 0.705	$\notin$ (SR-DT-1 $\cup$ SR-DT-2 $\cup$ SR-DT-3)

Table 4. Definition of the displaced track SRs in the event score vs track score plane. Tighter SRs such as SR-DT-1 have higher sensitivity, while looser SRs such as SR-DT-4 capture additional signal with lower purity that did not fall in the SRs with lower index.

production cross-sections during the training. The simulated signal and background events are split into five batches, of which 60%, 20%, and 20% are allocated to training, validation, and testing sets, respectively. The training is performed using a five-fold cross-validation configuration with early stopping to minimise overfitting. A total of approximately 2.0×10^5 and 1.0×10^5 events are used for signal and background samples, respectively. The training configurations of the event-level and track-level NNs are summarised in table 15 in appendix A.

Events satisfying the selection criteria in table 2 are assigned an event score by the event-level NN. A track score is also assigned by calculating the output of the track-level NN for each track and selecting the track with the highest track-level NN score in the event. As listed in table 4, a set of four mutually exclusive SRs are then defined in the event score vs track score 2D plane. No veto on the presence of b-tagged jets is applied in the SRs, as such a requirement is not found to significantly reduce the SM background or increase the expected sensitivity. The score requirements that define the four SRs are the result of an optimisation procedure that maximises the average expected significance among all signal MC samples that were used to train the NNs. The significance metric used for the optimisation is based on the profile likelihood method and described in ref. [122]. As a result of the NN training and score optimisation procedures, the SRs provide good coverage across a range of mass splitting scenarios, though no individual SR is tuned to provide sensitivity to a specific mass splitting.

6.2 $1\ell 1$T event selection

All events used for the $1\ell 1$T search are selected by an $E_{\mathrm{T}}^{\mathrm{miss}}$ trigger and are first required to satisfy the kinematic event selections listed in table 5. The reconstructed $E_{\mathrm{T}}^{\mathrm{miss}}$ is required to be larger than 200 GeV, corresponding to the lowest value at which the $E_{\mathrm{T}}^{\mathrm{miss}}$ trigger is fully efficient and chosen to ensure sufficient data statistics. For signal events satisfying this high-$E_{\mathrm{T}}^{\mathrm{miss}}$ requirement, the higgsino system typically recoils against hadronic activity, namely ISR jets. To explicitly select events with this topology, events are required to have at least one jet with $p_{\mathrm{T}} > 100$ GeV. Moreover, events with one or more b-tagged jets with $p_{\mathrm{T}} > 20$ GeV are vetoed to suppress background contributions from $t\bar{t}$ production.

Events are required to have exactly one tight lepton and are further categorised into two channels depending on the lepton flavour. The tight lepton requirement ensures that there is no overlap between the $1\ell 1$T analysis regions and the SRs of the displaced track search. The p_{T} of the lepton is required to be below 10 GeV and above the lower bound of lepton

Variable	Electron channel	Muon channel
Trigger	$E_{\mathrm{T}}^{\mathrm{miss}}$	
$E_{\mathrm{T}}^{\mathrm{miss}}$ [GeV]	> 200	
Number of jets with $p_{\mathrm{T}} > 20$ GeV	≥ 1	
Leading jet p_{T} [GeV]	> 100	
Number of b-tagged jets ($N_{b\text{-jet}}^{20}$)	$= 0$	
Number of tight leptons ($N_{\text{tight-lep}}$)	$= 1$ (electron)	$= 1$ (muon)
Lepton p_{T} [GeV]	[4.5, 10]	[3, 10]
Lepton $\lvert z_0 \sin\theta \rvert$ [mm]	< 0.5	
Lepton $\lvert d_0/\sigma(d_0) \rvert$	< 5	< 3
Number of tracks	≥ 1	

Table 5. Kinematic event selections applied to all events used for the $1\ell1\mathrm{T}$ search. The requirement on the number of tracks refers to the preselected tracks defined in section 5.1.

identification methods, which are 4.5 GeV and 3 GeV for electrons and muons, respectively. As the decay length of $\tilde{\chi}_2^0$ is $\mathcal{O}(0.01\text{–}0.1$ mm) for the targeted region, the leptons emerging from the $\tilde{\chi}_2^0 \to \tilde{\chi}_1^0 \ell^+\ell^-$ decay are expected to be prompt. Thus, requirements on z_0 and d_0 are also imposed for the lepton. Finally, at least one additional track satisfying the criteria in section 5.1 other than the reconstructed lepton is required in each event, which correspond to lepton-track candidates also originating from $\tilde{\chi}_2^0$ for signal higgsino events.

After the kinematic event selections are applied, preselection criteria listed in table 6 are applied to tracks to identify the candidates for the lepton-track. The charge of the track is required to be the opposite of that of the lepton, as they are expected to originate from Z^* decay. The p_{T} and $|\eta|$ requirements on the track follow the requirements of the low-p_{T} lepton-track identification methods described in section 5.1. The tracks are also required to be prompt with upper bounds on $|z_0 \sin\theta|$ and $|d_0|$. The upper bound on $p_{\mathrm{T}}^{\mathrm{cone30}}$ requires there to be little activity surrounding the track, where the tight lepton is excluded from the determination of this variable in order to retain signal efficiency. The invariant mass $m(Z^*)$ reconstructed from the lepton and the candidate lepton-track is required to be smaller than 5 GeV and outside the range 3.0–3.2 GeV, where the latter requirement vetoes J/ψ mass resonances. Contributions from other SM resonances are found to be negligible in the selected range of $m(Z^*)$. As the SUSY system is boosted, the lepton and the lepton-track have trajectories that are increasingly collinear. Thus, $\Delta R(\boldsymbol{\ell}, \mathbf{trk})$ in $[0.1, 1.4]$ is required; the upper bound is set to 1.4 to veto most background tracks, while the lower bound is set to 0.1 to veto tracks from photon conversions nearby the lepton. Upper thresholds on the impact parameter differences between the lepton and the lepton-track are optimised to further suppress background tracks, as specified in table 6, where the requirements are looser for the electron channel to accommodate effects from bremsstrahlung.

As the event topology of signal higgsino events depends sensitively on the mass splitting $\Delta m(\tilde{\chi}_2^0, \tilde{\chi}_1^0)$, the main event selection of the $1\ell1\mathrm{T}$ search is performed using a pNN. For very

JHEP06(2026)094

Variable	Electron channel	Muon channel
Track charge	Opposite of lepton charge	
Track p_{T} [GeV]	$[0.5, 5]$	$[1, 5]$
Track $\|\eta\|$	< 2.5	< 1.6
Track $\|z_0 \sin\theta\|$ [mm]	< 0.5	
Track $\|d_0\|$ [mm]	< 0.5	
Track $p_{\mathrm{T}}^{\mathrm{cone30}}/p_{\mathrm{T}}$	< 0.06	
$m(Z^*)$ [GeV]	< 3 or $[3.2,\ 5]$	
$\Delta R(\boldsymbol{\ell}, \mathbf{trk})$	$[0.1, 1.4]$	
$\Delta d_0(\ell, \mathrm{trk})$ [mm]	< 0.25	< 0.10
$\Delta z_0(\ell, \mathrm{trk})$ [mm]	< 0.30	< 0.26

Table 6. Track preselections applied to candidates of low-p_{T} lepton-tracks for the $1\ell1$T search.

small $\Delta m(\tilde{\chi}^0_2, \tilde{\chi}^0_1)$, the leptons emitted from the $\tilde{\chi}^0_2 \to \tilde{\chi}^0_1 Z^*$ decay have very low p_{T}, and the two $\tilde{\chi}^0_1$ tend to become more collimated, leading to higher $E_{\mathrm{T}}^{\mathrm{miss}}$ values. In this case, variables such as $\Delta R(\boldsymbol{\ell}, \mathbf{trk})$ and $\Delta\phi(\mathbf{p}_{\mathrm{T}}^{\mathrm{miss}}, \mathbf{Z}^*)$ have very small values. For larger $\Delta m(\tilde{\chi}^0_2, \tilde{\chi}^0_1)$, the leptons have higher p_{T}, leading to lower $E_{\mathrm{T}}^{\mathrm{miss}}$, larger $\Delta R(\boldsymbol{\ell}, \mathbf{trk})$, and larger $\Delta\phi(\mathbf{p}_{\mathrm{T}}^{\mathrm{miss}}, \mathbf{Z}^*)$. The pNN is introduced to consider these dependencies and to classify signal and background events in a dynamic manner. By choosing $\Delta m(\tilde{\chi}^0_2, \tilde{\chi}^0_1)$ as the physics parameter θ (referred to as pNN-θ), it is possible to realise $\Delta m(\tilde{\chi}^0_2, \tilde{\chi}^0_1)$-dependent event selection with a single network model. This also simplifies the training procedure, as the pNN has the ability to smoothly interpolate between different $\Delta m(\tilde{\chi}^0_2, \tilde{\chi}^0_1)$ values used for training, thus giving the possibility to explore various mass splitting scenarios with a limited number of training samples. Regions of the $1\ell1$T search for a specific pNN-θ value are labelled with suffixes of '-dM{pNN-θ}'.

Figure 3 shows the overall structure of the pNN model developed for the event selection used for both the electron and muon channels. It is implemented with `TensorFlow` [123], using the `Keras` [124] frontend. Based on $\Delta m(\tilde{\chi}^0_2, \tilde{\chi}^0_1)$ corresponding to the pNN-θ and 16 kinematic variables, the algorithm outputs a score characterizing how signal-like a given event is (referred to as pNN score) ranging from 0 to 1. The 16 kinematic variables are listed in table 7. Besides pNN-θ, input variables such as lepton p_{T}, track p_{T}, $E_{\mathrm{T}}^{\mathrm{miss}}$, leading jet p_{T}, $m(Z^*)$, $\Delta R(\boldsymbol{\ell}, \mathbf{trk})$, $H(\ell, \mathrm{trk})/E_{\mathrm{T}}^{\mathrm{miss}}$, $m_{\mathrm{T}}(\boldsymbol{\ell}, \mathbf{p}_{\mathrm{T}}^{\mathrm{miss}})$, $\Delta\phi(\mathbf{p}_{\mathrm{T}}^{\mathrm{miss}}, \mathbf{Z}^*)$, and $\Delta\phi(\mathbf{j}_1, \mathbf{Z}^*)$ have significant dependence on $\Delta m(\tilde{\chi}^0_2, \tilde{\chi}^0_1)$, thus having high importance.[3] The topology differences between signal and background events tend to become more significant for smaller $\Delta m(\tilde{\chi}^0_2, \tilde{\chi}^0_1)$ as the lepton, track, and $E_{\mathrm{T}}^{\mathrm{miss}}$ are more likely to be in close proximity in the transverse plane for signal processes compared with the dominant $W^{\pm}$+jets background processes. For improved signal

[3] $H(\ell, \mathrm{trk})$ represents the scalar p_{T} sum of the lepton and the track. $m_{\mathrm{T}}(\boldsymbol{\ell}, \mathbf{p}_{\mathrm{T}}^{\mathrm{miss}})$ represents the transverse mass reconstructed from the lepton and the missing transverse momentum and is defined as $\sqrt{2p_{\mathrm{T}}^{\ell} E_{\mathrm{T}}^{\mathrm{miss}}\left\{1 - \Delta\phi(\boldsymbol{\ell}, \mathbf{p}_{\mathrm{T}}^{\mathrm{miss}})\right\}}$, where p_{T}^{ℓ} is the p_{T} of the lepton, and $\Delta\phi(\boldsymbol{\ell}, \mathbf{p}_{\mathrm{T}}^{\mathrm{miss}})$ is the azimuthal angular difference between the lepton and the missing transverse momentum.

JHEP06(2026)094

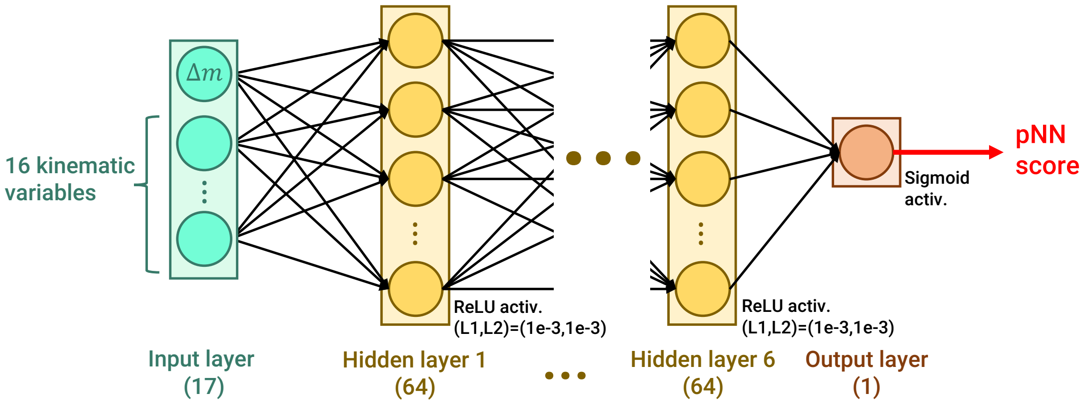

Figure 3. Overall structure of the pNN model used for event selection. The $\Delta m(\tilde{\chi}_2^0, \tilde{\chi}_1^0)$ and 16 kinematic variables are used as inputs, and there are six hidden layers with 64 nodes each. The nodes are fully connected. L1 and L2 regularisations are applied to each layer for increased signal sensitivity. The output pNN score ranges from 0 to 1, with 1 meaning that the input event is signal event-like.

Input variable	Description
$\Delta m(\tilde{\chi}_2^0, \tilde{\chi}_1^0)$	pNN-θ, mass difference between $\tilde{\chi}_2^0$ and $\tilde{\chi}_1^0$
Lepton p_{T}, η, ϕ	Kinematics of the standard lepton
Track p_{T}, η, ϕ	Kinematics of the track
$E_{\mathrm{T}}^{\mathrm{miss}}$, $\phi(\mathbf{p}_{\mathrm{T}}^{\mathrm{miss}})$	Kinematics of the missing transverse momentum
Leading jet p_{T}, ϕ	Kinematics of the leading jet
$m(Z^*)$	Mass of Z^* reconstructed from the lepton and the track
$\Delta R(\boldsymbol{\ell}, \mathbf{trk})$	Distance between the lepton and the track
$H(\ell, \mathrm{trk})/E_{\mathrm{T}}^{\mathrm{miss}}$	Ratio of scalar sum of lepton p_{T} and track p_{T} to $E_{\mathrm{T}}^{\mathrm{miss}}$
$m_{\mathrm{T}}(\boldsymbol{\ell}, \mathbf{p}_{\mathrm{T}}^{\mathrm{miss}})$	Transverse mass reconstructed from the lepton and the missing transverse momentum
$\Delta\phi(\mathbf{p}_{\mathrm{T}}^{\mathrm{miss}}, \mathbf{Z}^*)$	Azimuthal angular difference between the missing transverse momentum and Z^*
$\Delta\phi(\mathbf{j}_1, \mathbf{Z}^*)$	Azimuthal angular difference between the leading jet and Z^*

Table 7. Summary of input variables of the pNN. The same set of variables is used for the electron and muon channels.

sensitivity, L1 and L2 regularisations [125] are applied to each hidden layer to suppress the contributions of background events in high pNN-score regions.

Since the kinematic requirements for leptons and tracks differ for the electron and muon channels, the training of the pNN is done separately for each channel using the same pNN model structure. To train the pNN, each of the inputs are standardised into a Gaussian distribution. Higgsino production and $W^{\pm}$+jets MC events are used as signal and background training samples, respectively. To ensure enough statistics, higgsino production MC events are used inclusively in terms of mass points and production channels. The pNN is trained with pNN-θ = 1, 1.5, 2, 3, 4, and 5 GeV and the same values are used to obtain six non-orthogonal search results for each of the lepton flavours. The pNN-θ of background training samples are assigned randomly so that their distribution matches that of the signal training samples.

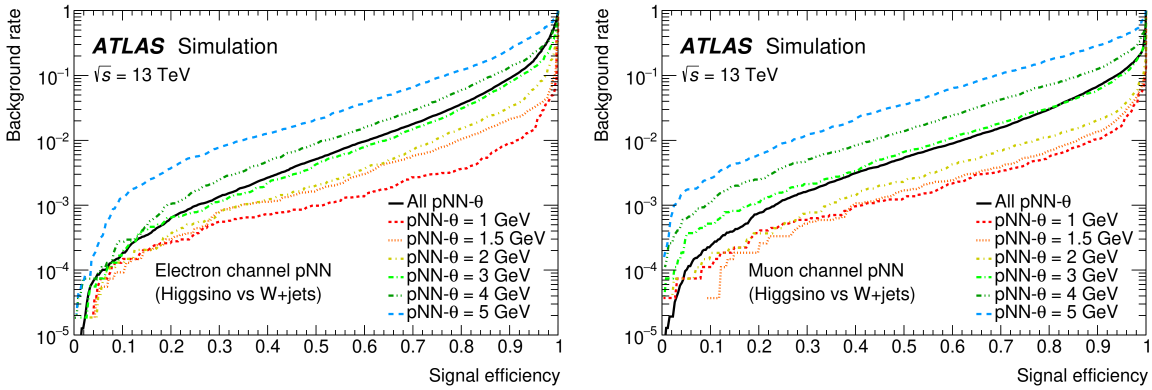

(a) (b)

Figure 4. ROC curves of pNN of each pNN-θ for (a) the electron channel and (b) the muon channel. For each curve, only signal events with $\Delta m(\tilde{\chi}_2^0, \tilde{\chi}_1^0)$ matching the pNN-θ are considered. The performance is better for smaller $\Delta m(\tilde{\chi}_2^0, \tilde{\chi}_1^0)$ values for both channels. The steps in the curves are due to the limited statistical precision of the MC samples used.

70% of the simulated signal and background events are used for training and validation of the network, and the remaining 30% are used for testing. All training samples are required to satisfy the event and track preselections described in table 5 and table 6. For the electron channel, about 2.2×10^4 signal events and 6.3×10^5 background events are used for the training and its validation, where 20% are assigned as validation samples. For the muon channel, about 5.1×10^4 signal events and 3.8×10^5 background events are used for the training and its validation, where 20% are assigned as validation samples. The training configurations of the pNN, common to both electron and muon channels, are summarised in table 15 in appendix A. Figure 4 shows the performance of the pNN for each pNN-θ as a receiver operating characteristic (ROC) curve. The separation of signal and background events is stronger for smaller $\Delta m(\tilde{\chi}_2^0, \tilde{\chi}_1^0)$ values due to the mentioned topology differences.

After the application of the lepton-track preselection in table 6, the pNN score is calculated for each candidate track. The track with the highest pNN score is then selected for each event and its score is assigned as the pNN score of the event. Subsequently, selection criteria in table 8 are applied to select signal-like events with a same-flavour opposite-charge lepton and lepton-track pair to define the SR. As the pNN and low-p_{T} lepton-track ID are not directly dependent on one another, the application of the low-p_{T} lepton-track ID on top of the pNN score requirement significantly reduces the background contribution. The first requirement of high pNN score vetoes background events having non-signal-like event topology. Then by selecting events having a track with a large value of the low-p_{T} lepton-track ID score, further significant background suppression is achieved through rejection of hadronic and fake tracks, which are the main background track components in the targeted regime.

JHEP06(2026)094

Variable	SR-1e1T	SR-1μ1T
$\Delta\phi(\mathbf{p}_{\mathrm{T}}^{\mathrm{miss}}, \mathbf{Z}^{*})$	< 1.0	
pNN score	> 0.95	
Low-p_{T} lepton-track ID score	> 0.8	> 0.6

Table 8. Summary of the selection criteria of the SR.

7 Background estimation

Following the event selection criteria, SM backgrounds for the displaced track and 1ℓ1T searches consist of events with a high-p_{T} jet, high $E_{\mathrm{T}}^{\mathrm{miss}}$, and low-$p_{\mathrm{T}}$ tracks. This section presents the background estimate methods for both searches, each exploiting semi-data-driven methods to estimate contributions from low-p_{T} tracks for such events. The control and validation regions used in these methods are found to have negligible contributions from potential signal processes.

For the background estimation and the interpretation of final results, three configurations of fits to the data are used. The first configuration, referred to as the background-only fit, does not include any contributions from the signal models and uses only the control regions to extract the necessary normalisation and reweighting factors. Its results are then extrapolated to the validation and signal regions to compare the post-fit SM predictions with the observed data without allowing the observed data in those regions to bias the fitted background event yields. The second configuration, referred to as the discovery fit, includes the control regions and one target signal region to derive a p-value representing the compatibility of the observed data with the background-only hypothesis. The third configuration uses both the control and signal regions to determine the compatibility of the observed data with the target signal model. In cases where there is no significant excess in data, this configuration is often referred to as the exclusion fit.

7.1 Displaced track background estimation

The leading SM background contributions in the SRs for the displaced track search originate from processes that result in high $E_{\mathrm{T}}^{\mathrm{miss}}$ from neutrinos, such as $Z(\rightarrow \nu\bar{\nu})$+jets and $W^{\pm}(\rightarrow \tau^{\pm}\nu_{\tau})$+jets. Subleading contributions arise from diboson production and $W^{\pm}(\rightarrow \ell^{\pm}\nu_{\ell})$+jets. Studies using the background MC samples show that approximately 40% of the signal candidate tracks selected by the track-level NN in the SRs arise from pile-up interactions. These backgrounds are estimated by using a semi-data-driven approach that combines simulation-based predictions with reweighting corrections derived in control regions (CRs). Validation regions (VRs) orthogonal to the SRs are used to validate these corrections. Other processes such as top quark production and multijet processes are found to have negligible impact in the SRs and are estimated directly from MC simulation.

Each process of the leading and subleading background contributions is normalised by a corresponding normalisation factor obtained by simultaneously fitting kinematic distributions in the mutually orthogonal CRs listed in table 9, defined to enhance each of the processes. No requirement is made on the track-level NN score in these CRs. Normalisation factors

CR name	Trigger	$N_{\text{tight-lep}}$	$N^{20}_{b\text{-jet}}$	$E_{\text{T}}^{\text{miss}}$ [GeV]	$E_{\text{T}}^{\text{miss, no-}\ell}$ [GeV]
CR-DT-1ℓ	Single-lepton	$1e/1\mu$	$=0$	—	>200
CR-DT-2ℓ	Single-lepton	$2e/2\mu$	$=0$	—	>200
CR-DT-1e1μ	Single-lepton	$1e{+}1\mu$	$=0$	—	>200
CR-DT-lowMET	$E_{\text{T}}^{\text{miss}}$	$=0$	—	[275, 325]	—

Table 9. Requirements of the CRs used in the displaced track search that are mutually orthogonal due to the lepton requirements. There are no overlapping events between the CRs and the SRs of the displaced track search. $E_{\text{T}}^{\text{miss, no-}\ell}$ denotes $E_{\text{T}}^{\text{miss}}$ with the leptons treated as invisible.

for $W^{\pm}(\to \ell^{\pm}\nu_{\ell})$+jets and $W^{\pm}(\to \tau^{\pm}_{\text{lep}}\nu_{\tau})$+jets in which the τ-lepton decays leptonically are constrained by fitting the distribution of the transverse mass m_{T} in CRs requiring exactly one tight lepton, defined as CR-DT-1ℓ ($\ell = e, \mu$). As m_{T} tends to be smaller for $W^{\pm}(\to \tau^{\pm}_{\text{lep}}\nu_{\tau})$+jets processes, CR-DT-1$\ell$ regions are separated into two bins with m_{T} in $[20, 40)$ and $[40, 120)$ GeV to simultaneously constrain the corresponding factors. The normalisation factors obtained for $W^{\pm}(\to \ell^{\pm}\nu_{\ell})$+jets and $W^{\pm}(\to \tau^{\pm}_{\text{lep}}\nu_{\tau})$+jets are 1.20 ± 0.01 and 1.2 ± 0.1, respectively.

Normalisation factors for $Z(\to \nu\bar{\nu})$+jets and $Z(\to \ell^{+}\ell^{-})$+jets processes are presumed to be the same and are constrained by fitting the dilepton mass in CRs with two same-flavour tight leptons, defined as CR-DT-2ℓ. While diboson processes make subleading contributions to CR-DT-2ℓ, they are primarily constrained by the simultaneous fit in a CR that requires two different-flavour tight leptons, defined as CR-DT-1e1μ. The leptonic CRs CR-DT-1ℓ, CR-DT-2ℓ, and CR-DT-1e1μ are triggered with single-lepton triggers and require high $E_{\text{T}}^{\text{miss}}$ with the leptons treated as invisible particles, denoted by $E_{\text{T}}^{\text{miss, no-}\ell}$, which helps in keeping the event topology similar to the targeted process. The p_{T} threshold of the single-electron (single-muon) triggers varied between 24 GeV and 26 GeV (20 GeV and 26 GeV) during the 2015–2018 data-taking period. The offline p_{T} of the electrons and muons are required to be above these trigger thresholds in CR-DT-1ℓ to ensure that the trigger efficiencies are in their plateau regions. This requirement also enforces orthogonality between CR-DT-1ℓ and the SRs of the 1ℓ1T search, which require the lepton p_{T} to be below 10 GeV. The number of b-jets is required to be zero to suppress contributions from top quark processes. The normalisation factors obtained for Z+jets and diboson processes are 1.29 ± 0.01 and 1.4 ± 0.2, respectively.

Finally, CR-DT-lowMET provides constraints on the normalisation factor for $W^{\pm}(\to \tau^{\pm}_{\text{had}}\nu_{\tau})$+jets processes in which the τ-lepton decays hadronically. In this region, $E_{\text{T}}^{\text{miss}}$ is required to be in $[275, 325]$ GeV and the distribution of $\min \Delta\phi(\mathbf{p}_{\text{T}}^{\text{miss}}, \mathbf{j})$, defined as the minimum azimuthal separation between the missing transverse momentum and any jet, is used for the fit. The normalisation factor obtained for $W^{\pm}(\to \tau^{\pm}_{\text{had}}\nu_{\tau})$+jets processes is 1.37 ± 0.04.

In addition to the event-level normalisation, track-level reweighting is applied to correct for any mismodelling in the kinematics of the tracks. The track-level reweighting consists of three sets of factors which are also obtained by a simultaneous fit later described in section 9.1. The first set of track reweighting factors is applied to consider the modelling differences between tracks originating from primary vertices and those that do not, dominantly tracks

JHEP06(2026)094

Variable	Requirement
Track p_{T} [GeV]	> 2.5
Track $\|\eta\|$	< 1.5
Track $\|d_0\|$ [mm]	< 10
Track $z_0 \sin\theta$ [mm]	< 1.5
Track $p_{\mathrm{T}}^{\mathrm{cone40}}$ [GeV]	< 1.0
$\Delta\phi(\mathbf{trk}, \mathbf{p}_{\mathrm{T}}^{\mathrm{miss,\ no\text{-}\ell}})$	≤ 1.0
Lepton veto	Not matched to a lepton-associated track

Table 10. Summary of the τ-track criteria applied to obtain the track reweighting factor in CR-DT-lowMET.

from pile-up. The reweighting factors are process-independent and are determined using CR-DT-1μ, having enough events. CR-DT-1μ is categorised into two regions by $|z_0 \sin\theta|$: a region with $|z_0 \sin\theta| < 0.1$ mm dominated by tracks associated with the primary collision and a region with $|z_0 \sin\theta| > 0.5$ mm dominated by pile-up tracks. The factors are binned in track p_{T} and are only applied to tracks with $p_{\mathrm{T}} < 3.2$ GeV, where such mismodelling is prominent. The obtained first set of reweighting factors ranges in 1–1.4 with a relative uncertainty below 4%. The validity of these factors for different processes is confirmed in other CRs, such as CR-DT-1e and CR-DT-lowMET.

The second set of reweighting factors corrects for the mismodelling of the track isolation variable, resulting in fewer isolated tracks in data. Similarly to the first set, this set of factors is obtained in CR-DT-1μ categorised into two regions using the same $|z_0 \sin\theta|$ requirements and is applied separately. The factors are binned in $p_{\mathrm{T}}^{\mathrm{cone40}}$ and their obtained values are in the range of 0.8–1.1 with a relative uncertainty below 3%. The validity of these factors has also been confirmed in other CRs to ensure process independence.

The third reweighting factor corrects for the mismodelling of leptonic or hadronic tracks originating from τ-lepton decays under the high-$E_{\mathrm{T}}^{\mathrm{miss}}$ preselection with a lower bound of 275 GeV, which is not applied in the first and second sets of factors. A single normalisation factor is obtained in CR-DT-lowMET with additional 'τ-track' criteria as defined in table 10 to enhance the contributions from the targeted $W^{\pm}(\rightarrow \tau_{\mathrm{had}}^{\pm}\nu_{\tau})$+jets processes. The obtained third reweighting factor is 0.64 with a relative uncertainty below 5%. This factor is applied only to simulated tracks originating from τ-leptons.

As shown in table 11, four VR categories are constructed to validate different aspects of the background estimation method for the displaced track search. Figure 5 illustrates how the different VRs map onto the event-level NN score vs track-level NN score plane. Each of the categories is further divided into three or four regions, depending on their event-level and track-level NN scores. VR-DT-μ uses the single-muon trigger and all other VRs use the $E_{\mathrm{T}}^{\mathrm{miss}}$ trigger. While some VRs may overlap with CRs by definition, they represent only a small fraction of the event yields in these CRs and therefore still provide a means of validating the background estimation strategy.

VR name	$N_{\text{pre-lep}}$	Event-level NN score	Track-level NN score	Additional requirement
VR-DT-Evt-1	$= 0$	$[0.712, 1]$	< 0.705	—
VR-DT-Evt-2	$= 0$	$[0.645, 0.712)$	< 0.705	—
VR-DT-Evt-3	$= 0$	$[0.582, 0.645)$	< 0.705	—
VR-DT-Trk-1	$= 0$	< 0.582	$[0.799, 1]$	$E_{\text{T}}^{\text{miss}} \in [325, 500]$ GeV
VR-DT-Trk-2	$= 0$	< 0.582	$[0.788, 0.799)$	$E_{\text{T}}^{\text{miss}} \in [325, 500]$ GeV
VR-DT-Trk-3	$= 0$	< 0.582	$[0.716, 0.788)$	$E_{\text{T}}^{\text{miss}} \in [325, 500]$ GeV
VR-DT-Trk-4	$= 0$	< 0.582	$[0.705, 0.716)$	$E_{\text{T}}^{\text{miss}} \in [325, 500]$ GeV
VR-DT-μ-1	$= 1$ (tight muon)	Same as SR-DT-1		Single-muon trigger, $E_{\text{T}}^{\text{miss, no-}\ell}$ used
VR-DT-μ-2	$= 1$ (tight muon)	Same as SR-DT-2		Single-muon trigger, $E_{\text{T}}^{\text{miss, no-}\ell}$ used
VR-DT-μ-3	$= 1$ (tight muon)	Same as SR-DT-3		Single-muon trigger, $E_{\text{T}}^{\text{miss, no-}\ell}$ used
VR-DT-μ-4	$= 1$ (tight muon)	Same as SR-DT-4		Single-muon trigger, $E_{\text{T}}^{\text{miss, no-}\ell}$ used
VR-DT-τ-1	$= 0$	$[0.712, 1]$	—	τ-track criteria with track p_{T} >8 GeV
VR-DT-τ-2	$= 0$	$[0.645, 0.712)$	—	τ-track criteria with track p_{T} >8 GeV
VR-DT-τ-3	$= 0$	$[0.582, 0.645)$	—	τ-track criteria with track p_{T} >8 GeV

Table 11. Definitions of the four VR categories used in the displaced track search.

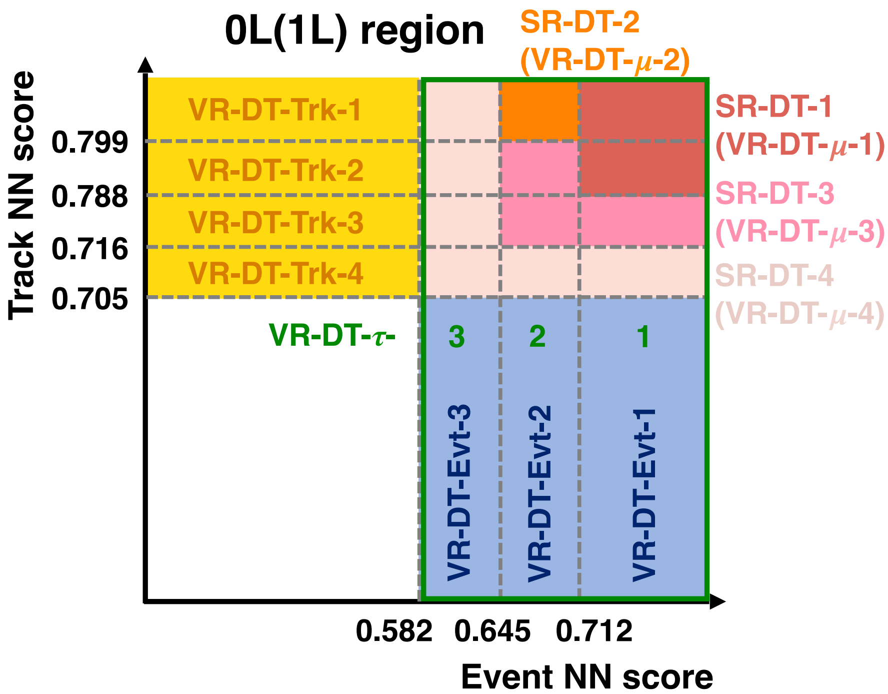

Figure 5. Illustration of the four validation region categories defined in the event- vs. track-level NN score plane. Each VR is further divided into three or four slices defined by the event and track NN scores. VR-DT-μ regions have the same score requirements as the SR-DT regions but with the 1L requirement and are denoted in parentheses.

VR-DT-Evt is defined to have high event-level NN scores, but vetoes events having tracks with high track-level NN scores; it verifies the validity of the event-level NN model and the event-level normalisation factor for each background process. On the other hand, VR-DT-Trk is defined to have a high track-level NN score, but vetoes events with high event-level NN score. It is further required to have moderate $E_{\mathrm{T}}^{\mathrm{miss}}$ in the range of 325–500 GeV to ensure sufficiently low signal contamination and retain orthogonality with CR-DT-lowMET. VR-DT-Trk helps in verifying the validity of track-level NN model and the track-level corrections using reweighting factors.

To validate the estimation method in a region where the event-level and track-level networks both yield high scores, VR-DT-μ is defined by requiring one tight muon. For this region, the single-muon trigger set is used and $E_{\mathrm{T}}^{\mathrm{miss}}$ is substituted by $E_{\mathrm{T}}^{\mathrm{miss,\ no\text{-}\ell}}$ to mimic the kinematics in the SRs excluding leptons. All of the event-level and track-level selections for this region are performed with this substitution. Furthermore, VR-DT-τ is defined to validate the modelling of $W^{\pm}(\to \tau^{\pm}\nu_{\tau})$+jets processes in regions with high event-level NN scores. In VR-DT-τ, tracks are required to satisfy the τ-track criteria used for CR-DT-lowMET but with track $p_{\mathrm{T}} > 8$ GeV. Compared to the signal processes of interest, the track p_{T} tends to be larger in $W^{\pm}(\to \tau^{\pm}\nu_{\tau})$+jets events and this track p_{T} requirement is found to suppress signal contamination while retaining sufficient statistics for validating the modelling of the $W^{\pm}(\to \tau^{\pm}\nu_{\tau})$+jets background.

7.2 1ℓ1T background estimation

SM background processes with a high-p_{T} jet and a boosted system with neutrinos in the final state could satisfy the leading jet and $E_{\mathrm{T}}^{\mathrm{miss}}$ selection of the 1ℓ1T search. The identified lepton is usually a real lepton, whereas the tracks identified with the low-p_{T} lepton-track identification methods have significant contributions from fake leptons. Since these tracks are required to be prompt, most of them are expected to correspond to low-p_{T} hadrons originating from the underlying event. From these object-based considerations, the most dominant SM background process is $W^{\pm}$+jets with a leptonic $W^{\pm}$ decay. In addition to these dominant backgrounds, there are small contributions from events in which the low-p_{T} lepton-track corresponds to a real lepton. Such backgrounds are contributions from processes that feature two or more leptons in their final states, including $Z^{(*)}$+jets and diboson. Thus, the SM backgrounds for the 1ℓ1T search are categorised into two components: 'fake lepton-track' backgrounds from events in which the low-p_{T} lepton-track corresponds to a fake lepton, and 'true lepton-track' backgrounds in which the low-p_{T} lepton-track corresponds to a real lepton. The dominant fake lepton-track backgrounds are estimated by a data-driven method described below, whereas the small true lepton-track backgrounds are estimated directly using MC simulation.

As MC simulation is not expected to accurately model processes with fake lepton-tracks, a data-driven method is used to estimate the contributions of fake lepton-track backgrounds. The method is performed by defining control regions, subtracting the true lepton-track contributions from each, and obtaining the ratio of yields of the fake lepton-track contributions between those regions. Regions are defined by applying the event and object criteria in tables 5 and 6 and imposing requirements on the pNN score and $\Delta\phi(\mathbf{p}_{\mathrm{T}}^{\mathrm{miss}}, \mathbf{Z}^{*})$ as illustrated

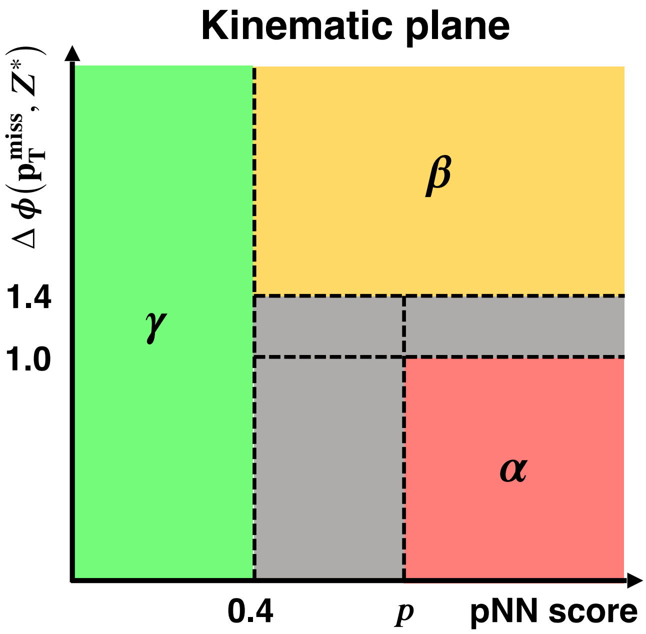

Figure 6. Kinematic plane diagram used for region definitions of the $1\ell1$T search. In terms of kinematic variables, the SRs, CRs, and VRs are defined by imposing requirements on the pNN score and $\Delta\phi(\mathbf{p}_{\mathrm{T}}^{\mathrm{miss}}, \mathbf{Z}^{*})$. The value p is either 0.95 for the SRs and their corresponding CRs or 0.4 for the VRs and their corresponding CRs.

in figure 6. The α-region is defined by pNN score > 0.95 and $\Delta\phi(\mathbf{p}_{\mathrm{T}}^{\mathrm{miss}}, \mathbf{Z}^{*}) < 1.0$, and the γ-region is defined by pNN score < 0.4. Both of these are further categorised into 'pass' and 'fail' regions following figure 7, based on whether the low-p_{T} lepton candidate track passes or fails the ID-score requirements in table 8. Therefore, the pass region within the α-region corresponds to the SR. Within the γ-region, dominated by SM backgrounds, the pass and fail regions are denoted by CR-$1\ell1$T-A and CR-$1\ell1$T-B, respectively. 'Transfer factors (TFs)' are measured by taking the ratio of the number of events belonging to CR-$1\ell1$T-A and that of CR-$1\ell1$T-B, separately for each of the track p_{T} bins in [0.5, 1.0), [1.0, 1.5), [1.5, 2.0), [2.0, 3.0), and [3.0, 5.0] GeV for the electron channel and [1.0, 1.5), [1.5, 2.0), [2.0, 3.0), and [3.0, 5.0] GeV for the muon channel. The measured TFs are then applied to the number of events in the fail region within the α-region, defined as CR-$1\ell1$T-C. This p_{T}-binned method accounts for the effects of indirect correlations between the low-p_{T} lepton-track ID and the event selection pNN through the track kinematics and improves the estimate of the pNN-score distribution in the SR. The TF values range in $\mathcal{O}(10^{-4}$–$10^{-2})$, typically having larger values in higher track p_{T} bins.

Three VRs are defined to validate the background estimation method of the $1\ell1$T search. VR-$1\ell1$T-highLarge(hL) is defined as the low-p_{T} lepton-track ID pass region within the β-region in figure 6 with pNN score higher than 0.4 and $\Delta\phi(\mathbf{p}_{\mathrm{T}}^{\mathrm{miss}}, \mathbf{Z}^{*})$ larger than 1.4, to test the validity of applying the TFs measured in low pNN-score regions to high pNN-score regions. The TFs used to estimate the background in the SR are applied to the fail region within β-region, labelled as CR-$1\ell1$T-hL, to estimate the yield in VR-$1\ell1$T-hL.

JHEP06(2026)094

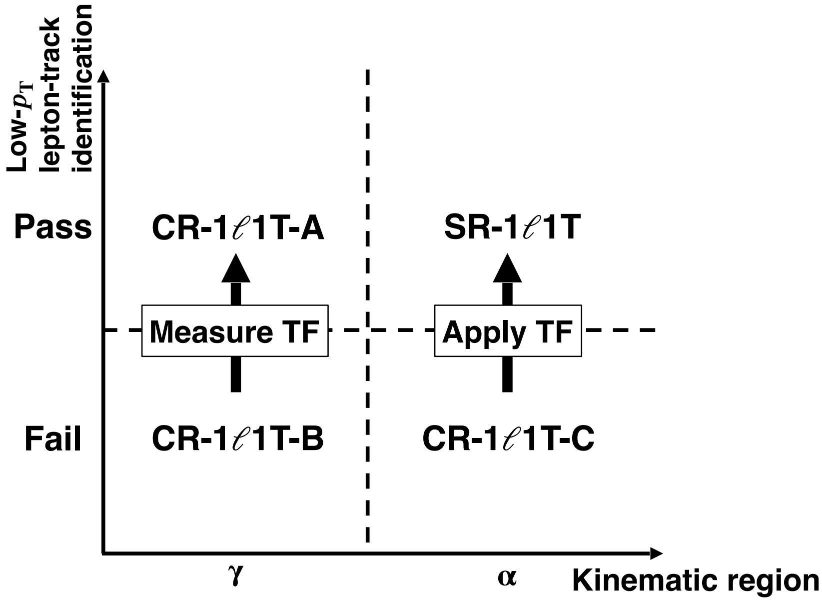

Figure 7. Schematic diagram of the background estimation method for the 1ℓ1T search. CR-1ℓ1T-A and CR-1ℓ1T-B are used to measure the transfer factors (pass-to-fail ratio) of the low-p_{T} lepton-track identification. The transfer factors are binned in track p_{T} to correctly estimate the pNN-score shape in the SR. The measured transfer factors are then applied to CR-1ℓ1T-C to estimate the background in SR-1ℓ1T.

VR-1ℓ1T-DF and VR-1ℓ1T-SS are used to validate the overall estimation method. VR-1ℓ1T-DF is defined by inverting the flavour requirement of the tight lepton (e.g. a muon and a low-p_{T} electron track are required for VR-1e1T-DF). To avoid possible overlaps with the SRs, the track is explicitly required to fail the 'other' low-p_{T} lepton-track ID criterion indicated in table 8 (e.g. the track in VR-1e1T-DF is required to have low-p_{T} muon-track ID score below 0.6). VR-1ℓ1T-SS is defined by requiring the same charge between the lepton and the low-p_{T} lepton-track. Except for the loosened pNN-score requirement of > 0.4 to ensure sufficient statistics, kinematic requirements are the same as those for the SR. For these two VRs, the yields are obtained with dedicated CRs and TFs, similar to the method illustrated in figure 7. All of the SR, CRs, and VRs used in the 1ℓ1T search are listed in table 12.

8 Systematic uncertainty

Systematic uncertainty is evaluated for all signal samples and background processes. The sources of uncertainty are common to both the displaced track and 1ℓ1T searches unless noted.

Figure 8 shows the relative systematic uncertainty in the predicted SM background yields in the SRs derived from background-only fits to the CRs. Sources of experimental uncertainty include those related to the reconstruction and selection of objects relevant to the analysis. As both the displaced track and 1ℓ1T searches target boosted topologies with a high-p_{T} leading jet and high $E_{\mathrm{T}}^{\mathrm{miss}}$, sources of uncertainty related to these objects are found to be dominant experimental uncertainty. Sources of uncertainty related to jets, which mainly involve the jet energy scale (JES) and jet energy resolution (JER), are evaluated as a function of jet p_{T} and

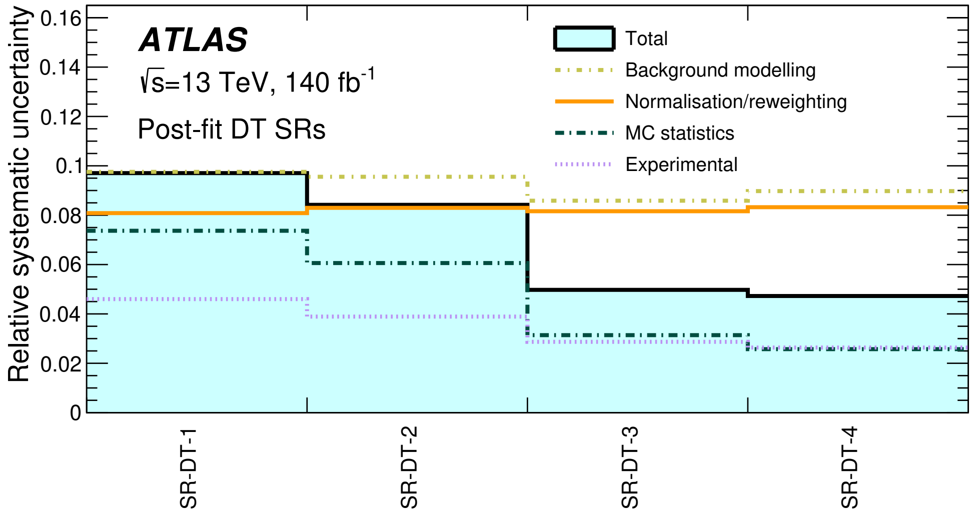

(a)

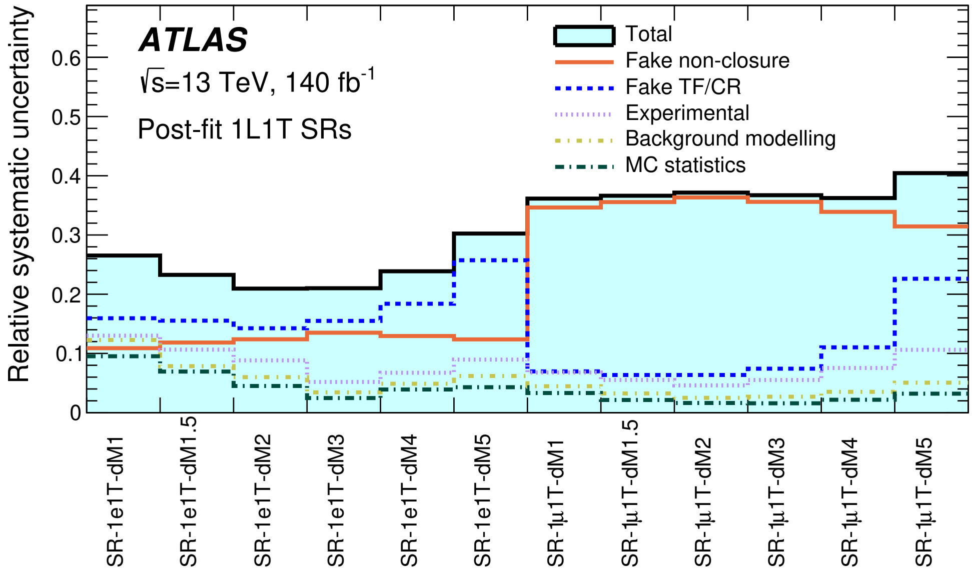

(b)

Figure 8. The relative systematic uncertainty (post-fit) in the fitted SM background event yields in the SRs obtained from a background-only fit to the CRs for (a) the displaced track search and (b) the $1\ell1$T search. The 'Normalisation/reweighting' category for the displaced track search includes all sources of uncertainty relevant to the normalisation and reweighting factors used in the background estimation. The 'Fake non-closure' category for the $1\ell1$T search denotes the non-closure uncertainty assigned to the fake lepton-track background component. The 'Fake TF/CR' category for the $1\ell1$T search includes all sources of uncertainty related to the transfer factors and statistical uncertainty in the CRs for the data-driven estimate of the fake lepton-track component. Sources of uncertainty related to the reconstruction and identification of jets, $E_{\mathrm{T}}^{\mathrm{miss}}$, leptons, and lepton-tracks are included in the 'Experimental' category. The 'Background modelling' category includes the theory uncertainty in the background processes. The 'MC Statistics' uncertainty originates from the limited size of the MC samples. The individual sources of uncertainty can be correlated and therefore do not necessarily sum in quadrature to the total uncertainty.

JHEP06(2026)094

Region name	Sign	Flavour	pNN score	$\Delta\phi(\mathbf{p}_{\mathrm{T}}^{\mathrm{miss}}, \mathbf{Z}^{*})$	Region type	Low-p_{T} lepton-track ID	Description
SR-1ℓ1T	OS	SF	> 0.95	< 1.0	α	Pass	SR with OS-SF
CR-1ℓ1T-A	OS	SF	< 0.4	—	γ	Pass	TF measurement numerator
CR-1ℓ1T-B	OS	SF	< 0.4	—	γ	Fail	TF measurement denominator
CR-1ℓ1T-C	OS	SF	> 0.95	< 1.0	α	Fail	TF application CR for SR
CR-1ℓ1T-hL	OS	SF	> 0.4	> 1.4	β	Fail	TF application CR for VR-1ℓ1T-hL
CR-1ℓ1T-SS-A	SS	SF	< 0.4	—	γ	Pass	TF-SS measurement numerator
CR-1ℓ1T-SS-B	SS	SF	< 0.4	—	γ	Fail	TF-SS measurement denominator
CR-1ℓ1T-SS-C	SS	SF	> 0.4	< 1.0	α	Fail	TF-SS application CR for VR-SS
CR-1ℓ1T-DF-A	OS	DF	< 0.4	—	γ	Pass	TF-DF measurement numerator
CR-1ℓ1T-DF-B	OS	DF	< 0.4	—	γ	Fail	TF-DF measurement denominator
CR-1ℓ1T-DF-C	OS	DF	> 0.4	< 1.0	α	Fail	TF-DF application CR for VR-DF
VR-1ℓ1T-hL	OS	SF	> 0.4	> 1.4	β	Pass	VR within OS-SF with large $\Delta\phi(\mathbf{p}_{\mathrm{T}}^{\mathrm{miss}}, \mathbf{Z}^{*})$
VR-1ℓ1T-SS	SS	SF	> 0.4	< 1.0	α	Pass	VR with SS-SF
VR-1ℓ1T-DF	OS	DF	> 0.4	< 1.0	α	Pass	VR with OS-DF

Table 12. List of SR, CRs, and VRs used in the 1ℓ1T search. OS/SS stands for opposite/same sign, and SF/DF stands for same/different flavour, of the lepton and the lepton-track. The pNN-score thresholds for α-regions for SS-SF and OS-DF are lowered to 0.4 to increase event yields. For DF regions, as described in the text, there are additional requirements on the low-p_{T} lepton-track ID scores to avoid possible region overlaps with the SR in the other channel with different lepton flavour.

η. This uncertainty is determined from data and MC studies such as the measurement of jet-p_{T} balance in dijet and Z/γ+jets processes [112]. Sources of uncertainty related to b-jet identification and vertex tagging are also considered. Uncertainty in the modelling of $E_{\mathrm{T}}^{\mathrm{miss}}$ in the MC simulation is estimated by propagating the energy and momentum scale of the objects entering the calculation of $E_{\mathrm{T}}^{\mathrm{miss}}$ and the variations of the resolution and scale of the soft-term. Sources of systematic uncertainty for leptons include those in the reconstruction, identification and isolation efficiencies, and those in the momentum/energy resolution and scale [108, 126]. Other sources of experimental uncertainty originate from pile-up modelling, tracking efficiency, and track impact parameter resolution. For the background MC samples of the 1ℓ1T search, the experimental uncertainty only affects the subdominant true lepton-track component, hence to avoid fit instabilities, a single 50% envelope uncertainty is assigned, which is found to cover all of the individual sources of experimental uncertainty, the largest of which is 40%. Moreover, the 1ℓ1T search considers sources of uncertainty in low-p_{T} lepton-track identification performance, such as those originating from the calibration.

For the displaced track search, uncertainty in the semi-data driven background estimation is considered. Uncertainty in the event-level normalisation factors for each background processes and track-level reweighting factors, originating from the data and MC statistics in the CRs, is taken into account by performing a simultaneous fit with all sources of uncertainty included. The relative uncertainty values of these factors are typically below 10%.

For the 1ℓ1T search, uncertainty in the transfer factors and statistical uncertainty in the corresponding CRs is incorporated into a simultaneous fit. Moreover, a non-closure uncertainty is applied to the fake lepton-track component to consider sources of uncertainty originating from the data-driven estimation method itself, such as the choice of variables used to define the CRs. The non-closure uncertainty is defined in such a way as to ensure

JHEP06(2026)094

compatibility between the total background prediction and the observed data in all VRs of the $1\ell1$T search, taking into account the statistical uncertainty in the data. A non-closure uncertainty of 15% and 40% is assigned to the fake lepton-track components of the $1e1$T and $1\mu1$T channels, respectively.

Theory modelling uncertainty is also considered for MC samples of dominant background processes. For the displaced track search, these sources of uncertainty are considered for all background processes. For the $1\ell1$T search, the fake lepton-track background is estimated using data-driven methods and therefore no theory uncertainty is assigned to this component. The remaining 10–20% of the total background in this search arises from processes that produce true lepton-tracks and is estimated using MC samples. Theory uncertainty is therefore considered for the V+jets and diboson processes that dominate the true lepton-track background.

Common to both of the searches, uncertainty originating from the choice of QCD renormalisation and factorisation scales is evaluated by varying the corresponding MC generator parameters up and down by a factor of two around their nominal values. Uncertainty associated with the choice of PDF set [57, 80] and the strong coupling constant α_{s} is also considered. Furthermore for the displaced track search, uncertainty in the resummation and matching scale between matrix elements and parton showers is considered for V+jets samples by varying up and down the corresponding parameters in Sherpa.

For signal samples, uncertainty originating from multi-parton interactions and parton showers is considered on top of the theory uncertainty mentioned above. This uncertainty is evaluated from the change of yields with different tune variations using a few of the samples. Five types of variations are considered according to the A14 tune of Pythia [64]: one for underlying event effects, one for jet structure effects, and three for different aspects of extra jet production. The sum in quadrature of the five variations is used as the overall uncertainty. As this uncertainty is found to have little dependence on the SUSY particle masses, uncertainties of 6.4% and 15% are assigned to all signal samples for the displaced track and $1\ell1$T searches, respectively.

As shown in figure 8, the systematic uncertainty of the displaced track search is dominated by the uncertainty related to the normalisation and track reweighting factors, and the background modelling uncertainty. The impact of a given category of uncertainty is estimated by taking the results from the nominal background-only likelihood fit to the CRs, fixing the parameters associated with the other sources of uncertainty to their best-fit values, and propagating the variations of the remaining floating parameters to the background prediction in the SRs using the covariance matrix from the nominal fit [127]. The profile likelihood method used for the fits is described in more detail in section 9. Since the individual sources of uncertainty in different categories can be correlated, the uncertainties from each category do not necessarily sum in quadrature to the total systematic uncertainty using this decomposition method, and can even be larger than the total in the case of the displaced track SRs. This feature arises mainly from anti-correlations between the theoretical uncertainties and those related to the normalisation and reweighting factors for the dominant $Z(\to \nu\bar{\nu})$+jets and $W^{\pm}(\to \tau^{\pm}\nu_{\tau})$+jets backgrounds, leading to a partial cancellation when they are included simultaneously in the likelihood fit. For the $1\ell1$T search, the non-closure uncertainty in

JHEP06(2026)094

the fake lepton-track contribution is the most significant, especially for $1\mu1\mathrm{T}$. For $1e1\mathrm{T}$, uncertainty in the transfer factors and CR statistical uncertainty become more dominant, due to limited data.

9 Results

Data in the CRs, VRs, and SRs are compared with SM predictions using a profile likelihood method [128]. The sources of systematic uncertainty are treated as nuisance parameters with Gaussian-distributed constraints in the likelihood. The correlations among the sources of uncertainty are considered in this method. Following the comparisons in the control and validation regions in section 9.1, results in the signal regions are shown in section 9.2. Section 9.3 and section 9.4 show the results of model-independent and model-dependent interpretations, respectively.

9.1 Control and validation regions

Background-only fits of the CRs are performed using only the CRs to constrain the fit parameters. For the displaced track search, a simultaneous fit is performed using all CRs to constrain all event normalisation and track reweighting factors. For the $1\ell1\mathrm{T}$ search, data in CR-$1\ell1\mathrm{T}$-A, CR-$1\ell1\mathrm{T}$-B, and CR-$1\ell1\mathrm{T}$-C are fitted simultaneously to constrain the TFs and to obtain the background contribution in the SRs. The same procedure is performed to estimate the SM background yields in the VRs, using the CRs defined in section 7.2.

The SM background prediction obtained from the background-only fit is first compared with data in the VRs to verify the validity and accuracy of the background estimation method. Figure 9 shows a comparison between the data and estimated background event yields in the VRs, where all differences are below the 2σ level. The non-closure uncertainty in the fake lepton-track components mentioned in section 8 is applied to the $1\ell1\mathrm{T}$ search. Figures 10 and 11 show examples of kinematic distributions in the VRs after a background-only fit using the CRs.

9.2 Event yields in signal regions

The data and the SM background prediction obtained from the background-only fit are then compared in the SRs. Such comparisons are shown in figure 12 and table 13. Deviations in all regions are within 2σ. The largest deviations for the displaced track and $1\ell1\mathrm{T}$ searches are found to be -1.3σ in SR-DT-4 and 1.5σ in SR-$1\mu1\mathrm{T}$-dM5, respectively. Figures 13 and 14 show examples of kinematic distributions in the SRs after a background-only fit using the CRs. For the $1\ell1\mathrm{T}$ search, the $m(Z^*)$ distributions for the signal and background processes in figure 14 demonstrate that the pNN is successfully learning to select events based on the reconstructed Z^* mass, which is expected to have a kinematic cutoff at $\Delta m(\tilde{\chi}^0_2, \tilde{\chi}^0_1)$ for signal processes.

JHEP06(2026)094

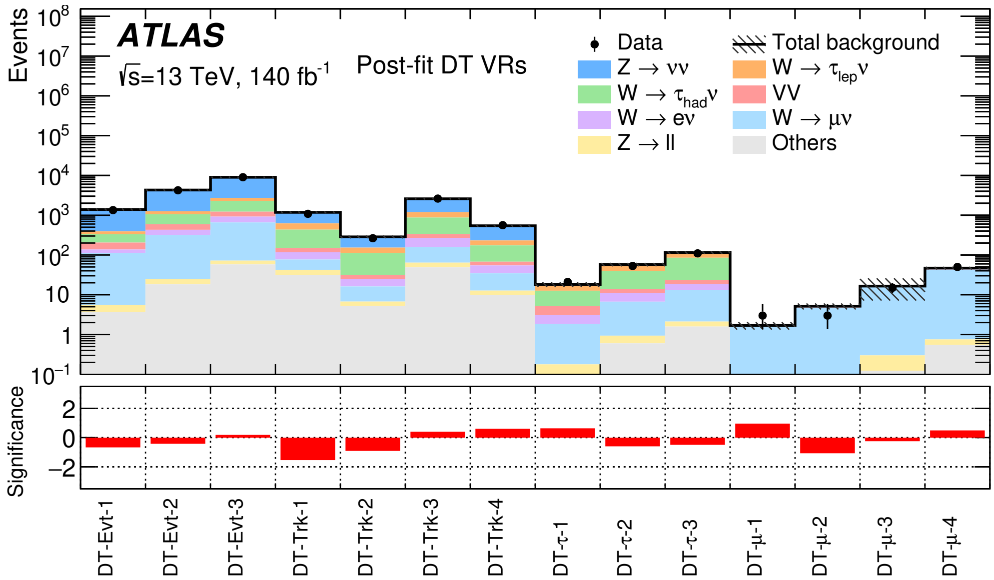

(a)

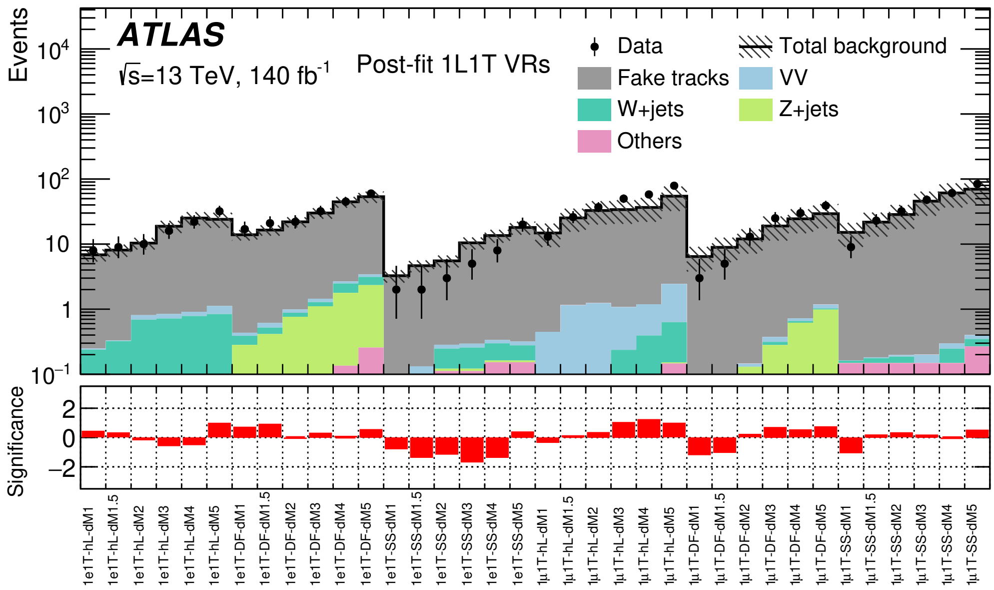

(b)

Figure 9. Comparison of the observed and expected event yields in all VRs of (a) the displaced track search and (b) the $1\ell 1$T search. The bottom panel in each plot shows the significance of the difference between the observed and the predicted yields, following the profile likelihood method of ref. [129] in the case where the observed yield exceeds the prediction and using the same expression with an overall minus sign when the observed yield is below the prediction. (a) All slices are shown for each of the four VR categories: VR-DT-Evt, VR-DT-Trk, VR-DT-τ, and VR-DT-μ. (b) On the left of the plot are VRs for $1e1$T and on the right are VRs for $1\mu 1$T. All six pNN-θ =1, 1.5, 2, 3, 4, and 5 GeV slices are shown for each of the three VRs: VR-hL, VR-DF, and VR-SS. The category 'Others' contains background processes including top quarks, multijets and γ+jets. Uncertainty in the estimated background includes both the statistical and systematic uncertainties.

JHEP06(2026)094

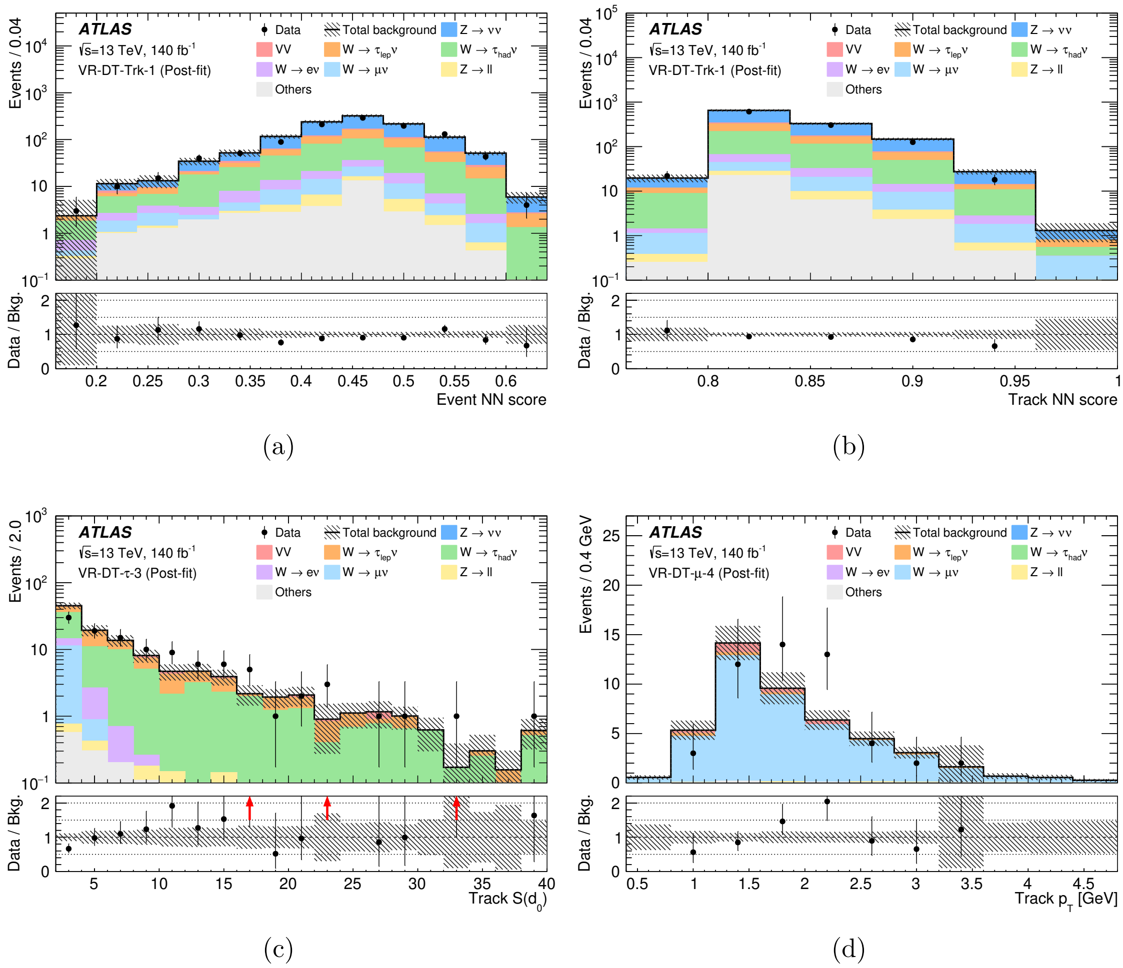

Figure 10. Examples of kinematic distributions in the VRs of the displaced track search after the background-only fit using the CRs. (a) and (b) show distributions of event-level and track-level NN scores in VR-DT-Trk-1, respectively. (c) shows the distribution of transverse impact parameter significance, $S(d_0)$, of the track in VR-DT-τ-3. (d) shows the distribution of track p_{T} in VR-DT-μ-4. The category 'Others' contains background processes including top quarks, multijets and γ+jets. The uncertainty bands on the expected background include all statistical and systematic uncertainties. Upper arrows in the lower panel indicate data points outside the vertical range shown.

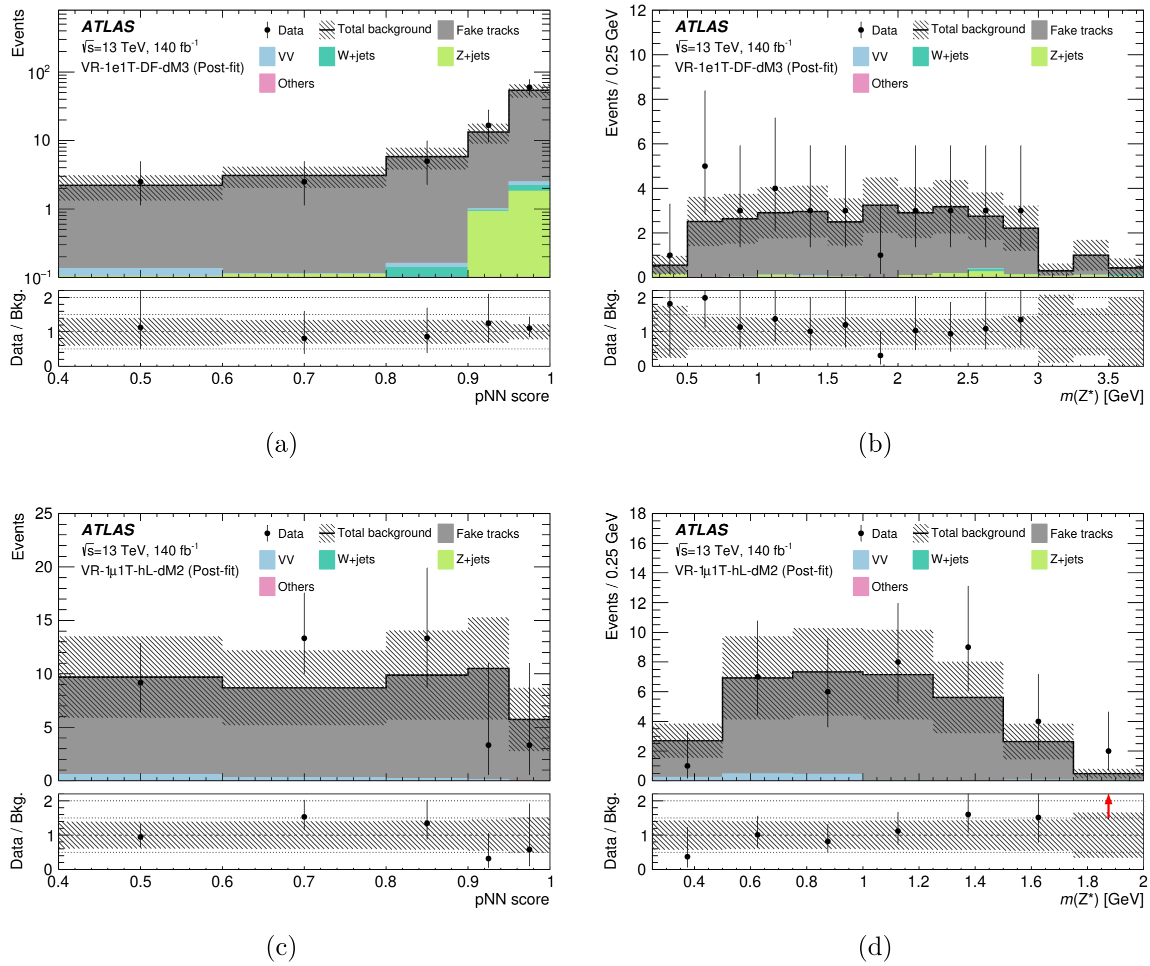

Figure 11. Examples of kinematic distributions in the VRs of the $1\ell1$T search after the background-only fit using the CRs. (a) and (b) show distributions of pNN score and $m(Z^*)$ in VR-1e1T-DF-dM3, respectively. (c) and (d) show distributions of pNN score and $m(Z^*)$ in VR-1μ1T-hL-dM2. The category 'Others' contains background processes including top quarks, multijets and γ+jets. The uncertainty bands on the expected background include all statistical and systematic uncertainties. Upper arrows in the lower panel indicate data points outside the vertical range shown.

JHEP06(2026)094

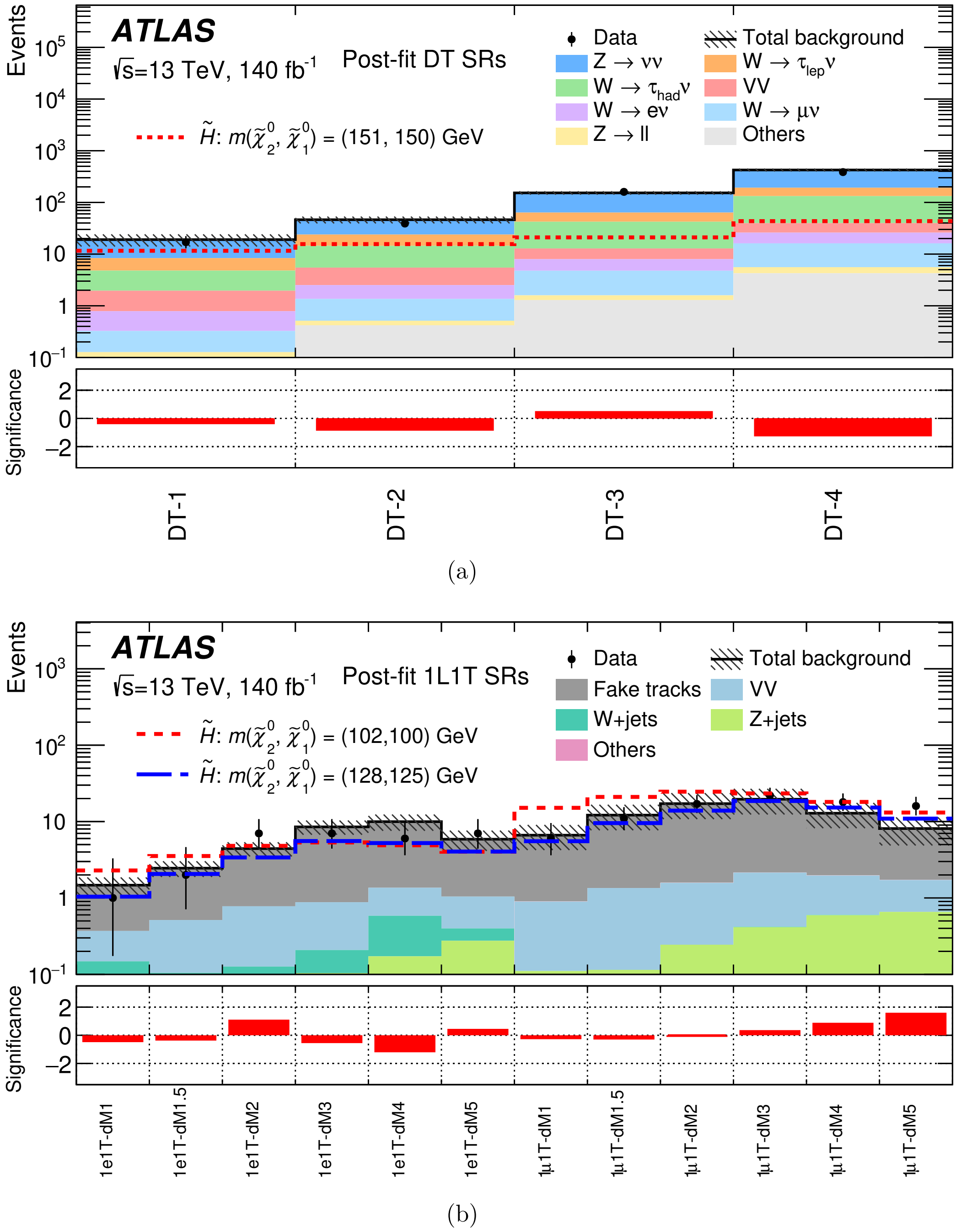

Figure 12. Comparison of the observed and expected event yields in all SRs of (a) the displaced track search and (b) the $1\ell 1$T search. The bottom panel in each plot shows the significance of the difference between the observed and the predicted yields, following the profile likelihood method of ref. [129] in the case where the observed yield exceeds the prediction and using the same expression with an overall minus sign when the observed yield is below the prediction. (a) All four SRs are shown for the displaced track search. (b) On the left of the plot are the SRs for $1e1$T and on the right are the SRs for $1\mu 1$T. All six pNN-θ =1, 1.5, 2, 3, 4, and 5 GeV slices are shown. The category 'Others' contains background processes including top quarks, multijets and γ+jets. Uncertainty in the estimated background includes both statistical and systematic uncertainties. Predicted yields for some signal mass points are overlaid for reference.

JHEP06(2026)094

SR name	SR-DT-1	SR-DT-2	SR-DT-3	SR-DT-4
Observed	17	39	160	386
Fitted SM events	19.0 ± 1.9	46.2 ± 3.9	152.9 ± 7.6	424 ± 20
$Z \to \nu\bar{\nu}$	10.5 ± 1.5	21.9 ± 3.2	87 ± 10	226 ± 29
$W^{\pm} \to \tau^{\pm}_{\text{had}}\nu_{\tau}$	3.0 ± 0.7	9.6 ± 3.0	31.6 ± 6.0	99 ± 23
$W^{\pm} \to \tau^{\pm}_{\text{lep}}\nu_{\tau}$	3.6 ± 1.1	9.5 ± 2.0	21.4 ± 5.6	60 ± 12
VV	1.2 ± 0.4	2.9 ± 0.5	4.8 ± 1.0	13.4 ± 2.5
$W^{\pm} \to e^{\pm}\nu_{e}$	0.5 ± 0.2	1.1 ± 0.5	3.2 ± 1.7	9.8 ± 4.1
$W^{\pm} \to \mu^{\pm}\nu_{\mu}$	0.20 ± 0.05	0.84 ± 0.08	3.2 ± 0.3	10.5 ± 1.0
$Z \to \ell^{+}\ell^{-}$	0.04 ± 0.02	0.1 ± 0.1	0.30 ± 0.10	1.3 ± 0.4
Others	0.1 ± 0.1	0.4 ± 0.2	1.3 ± 0.4	4.3 ± 1.5

	SR pNN-θ [GeV]	1	1.5	2	3	4	5
SR-1e1T	Observed	1	2	7	7	6	7
	Fitted SM events	1.5 ± 0.4	2.5 ± 0.6	4.4 ± 0.9	8.5 ± 1.8	10.0 ± 2.4	5.8 ± 1.8
	Fake tracks	1.1 ± 0.4	1.9 ± 0.6	3.7 ± 1.1	7.6 ± 2.2	8.6 ± 2.5	4.8 ± 1.8
	VV	0.22 ± 0.17	0.41 ± 0.29	0.66 ± 0.43	0.67 ± 0.43	0.78 ± 0.53	0.64 ± 0.44
	$W^{\pm}$+jets	$0.10^{+0.13}_{-0.10}$	$0.10^{+0.13}_{-0.10}$	$0.10^{+0.13}_{-0.10}$	$0.10^{+0.13}_{-0.10}$	$0.41^{+0.43}_{-0.41}$	$0.12^{+0.14}_{-0.12}$
	Z+jets	$0.04^{+0.09}_{-0.04}$	< 0.01	$0.02^{+0.09}_{-0.02}$	$0.10^{+0.16}_{-0.10}$	$0.17^{+0.20}_{-0.17}$	$0.27^{+0.28}_{-0.27}$
	Others	< 0.01	< 0.01	< 0.01	< 0.01	< 0.01	< 0.01
SR-1μ1T	Observed	6	11	17	22	18	16
	Fitted SM events	6.6 ± 2.2	12.2 ± 4.5	17.2 ± 6.4	19.6 ± 7.2	12.9 ± 4.7	8.1 ± 3.3
	Fake tracks	5.7 ± 2.5	10.8 ± 4.6	15.6 ± 6.6	17.5 ± 7.5	10.9 ± 4.9	6.4 ± 3.5
	VV	0.79 ± 0.52	1.2 ± 0.8	1.3 ± 0.8	1.7 ± 1.0	1.4 ± 0.8	1.1 ± 0.7
	$W^{\pm}$+jets	< 0.01	< 0.01	< 0.01	< 0.01	< 0.01	< 0.01
	Z+jets	0.11 ± 0.09	0.11 ± 0.09	0.24 ± 0.18	0.41 ± 0.28	0.59 ± 0.36	0.66 ± 0.41
	Others	< 0.01	< 0.01	< 0.01	< 0.01	< 0.01	< 0.01

Table 13. Observed and predicted event yields in the SRs from a background-only fit using the CRs for (top) the displaced track search and (bottom) the $1\ell1$T search. The category 'Others' contains background processes including top quarks, multijets and γ+jets. Uncertainty in the predicted background yields includes statistical and systematic uncertainties.

JHEP06(2026)094

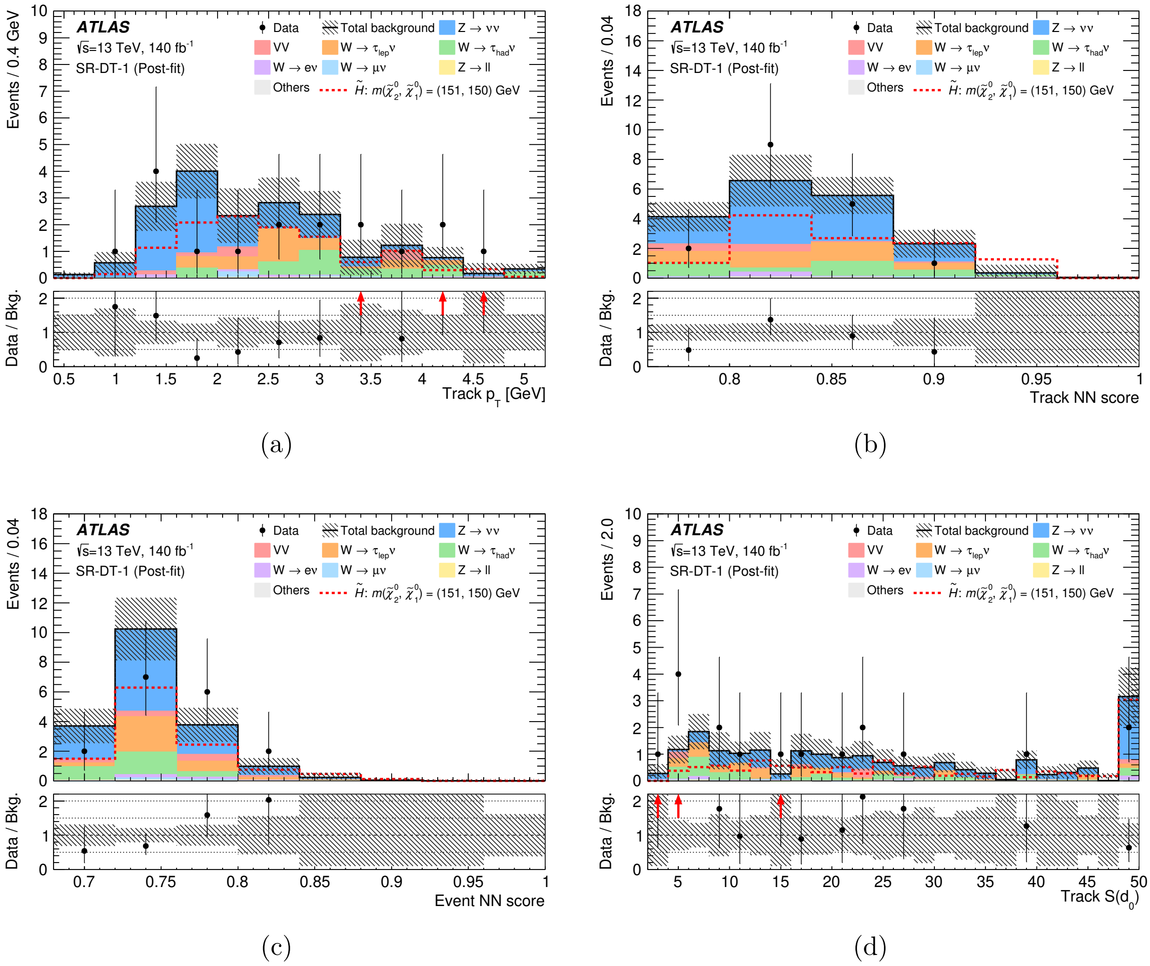

Figure 13. Examples of kinematic distributions in the SRs of the displaced track search after the background-only fit using the CRs. Overflow events are included in the last bin of the track $S(d_0)$ distribution.The category 'Others' contains background processes including top quarks, multijets and γ+jets. The uncertainty bands on the expected background include all statistical and systematic uncertainties. Upper arrows in the lower panel indicate data points outside the vertical range shown. Predicted yields for a signal mass point of $m(\tilde{\chi}^0_2, \tilde{\chi}^\pm_1, \tilde{\chi}^0_1) = (151, 150.5, 150)$ GeV are overlaid for reference.

9.3 Model-independent interpretation

For the $1\ell 1$T search, given the similarity of the phase space relevant to each of the SRs, SR-$1\ell 1$T-dM1, SR-$1\ell 1$T-dM3, and SR-$1\ell 1$T-dM5 are selected to test the excesses of events in the SRs and to set upper limits on the visible cross-sections of physics beyond the SM. For this purpose, each SR is constructed by combining the corresponding electron and muon channel SRs into a single bin. A discovery fit configuration mentioned in section 7 is applied, where a generic signal model with an unconstrained normalisation parameter is included to estimate the contributions from any phenomena beyond the SM. The probability under the SM-only hypothesis is quantified by calculating the p-value and the corresponding significance for each SR. For the final state targeted by the displaced track search, analogous results are reported in

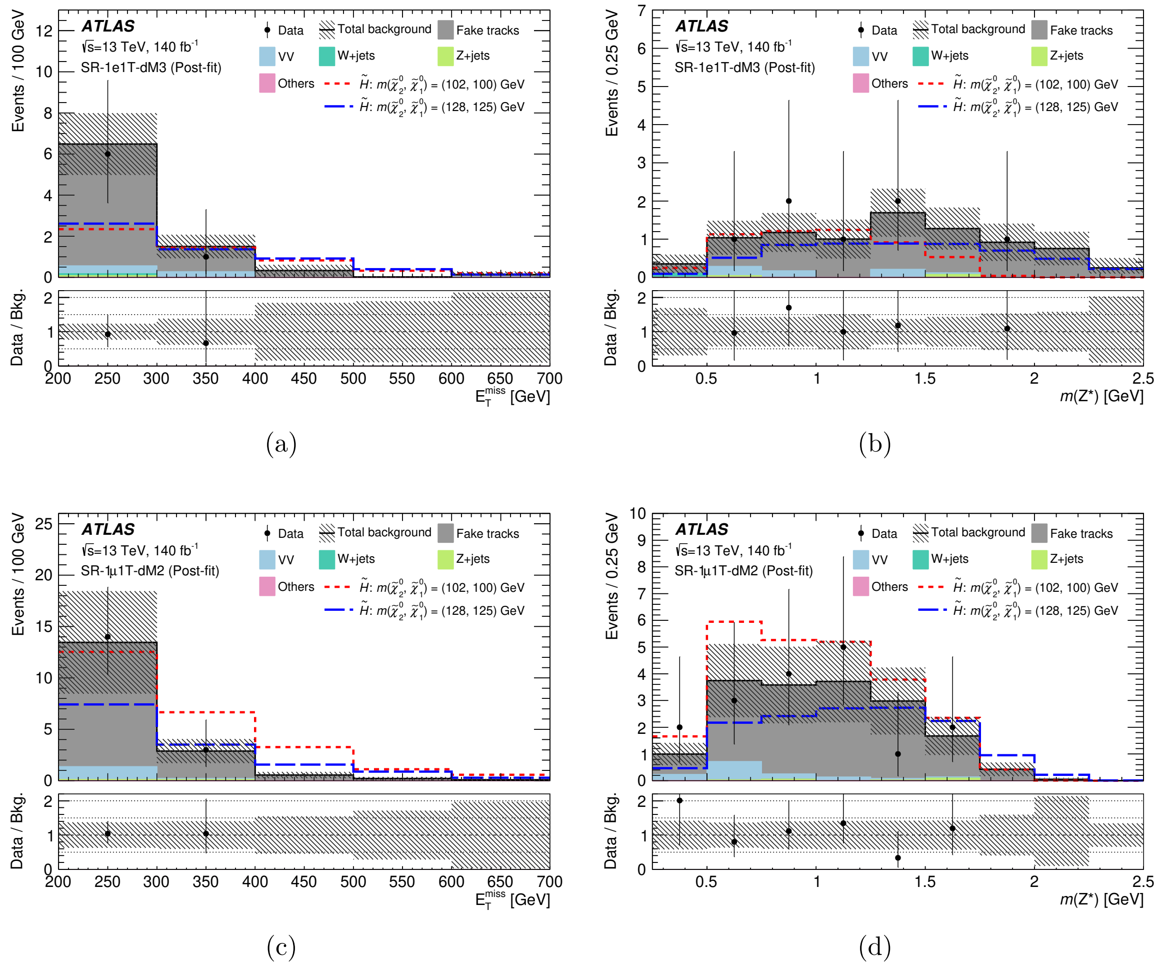

Figure 14. Examples of kinematic distributions in the SRs of the $1\ell 1$T search after the background-only fit using the CRs. (a) and (b) show distributions of $E_{\mathrm{T}}^{\mathrm{miss}}$ and $m(Z^*)$ in SR-1e1T-dM3, respectively. (c) and (d) show distributions for $E_{\mathrm{T}}^{\mathrm{miss}}$ and $m(Z^*)$ in SR-1μ1T-dM2, respectively. The category 'Others' contains background processes including top quarks, multijets and γ+jets. The uncertainty bands on the expected background include all statistical and systematic uncertainties. Predicted yields for signal mass points of $m(\tilde{\chi}_2^0, \tilde{\chi}_1^0) = (102, 100)$ and $(128, 125)$ GeV are overlaid for reference.

ref. [27], where the single-bin SRs are defined by a fixed set of kinematic requirements without the use of machine learning classifiers, thus enabling more straightforward reinterpretations of the results in the context of some generic beyond the SM physics process.

Table 14 shows the results of the model-independent interpretation for the $1\ell 1$T search. Data and predicted SM yields agree well in SR-$1\ell 1$T-dM1 and SR-$1\ell 1$T-dM3, resulting in 95% confidence level (CL) upper limits of 0.05 fb and 0.13 fb on the visible cross-section of physics beyond the SM. Consistent with the deviation observed in SR-1μ1T-dM5, a deviation of 1.5σ is observed between data and the SM predictions in SR-$1\ell 1$T-dM5, resulting in a looser upper limit of 0.14 fb.

SR name	N_{obs}	N_{exp}	$\langle\epsilon\sigma\rangle^{95}_{\text{obs}}$[fb]	S^{95}_{obs}	S^{95}_{exp}	$p(S=0)$	σ
SR-1ℓ1T-dM1	7	8.1 ± 2.4	0.05	7.4	$8.1^{+3.7}_{-2.2}$	—	—
SR-1ℓ1T-dM3	29	28.1 ± 7.4	0.13	18.5	$18.1^{+6.5}_{-4.7}$	0.47	0.07
SR-1ℓ1T-dM5	23	13.9 ± 3.7	0.14	20.1	$12.7^{+5.3}_{-3.5}$	0.07	1.48

Table 14. Results of the model-independent interpretation of the 1ℓ1T search. For each SR indicated in the first column, the observed N_{obs} number of events and predicted N_{exp} number of SM events are shown in the second and third columns. The following columns show the observed 95% CL upper limits on the visible cross-section, $\langle\epsilon\sigma\rangle^{95}_{\text{obs}}$, and on the observed and expected number of signal events corresponding to physics beyond the SM, denoted by S^{95}_{obs} and S^{95}_{exp}, respectively. The $\pm 1\sigma$ variations are also shown for S^{95}_{exp}. The final columns show the p-value for the SM-only hypothesis $p(S=0)$ and the corresponding Gaussian-equivalent statistical significance σ, where p-values are capped at 0.5. For cases in which the data yield is smaller than expected, the p-value and the significance are not shown.

9.4 Model-dependent interpretation

Exclusion fits are performed to set limits on the higgsino model under study. For the displaced track search, all CRs and SRs are fitted simultaneously with a parameter of interest corresponding to the signal strength, which scales the signal yields in all regions. For the 1ℓ1T search, the same procedure is performed for each pNN-θ. The CL$_s$ prescription [130] is used to perform hypothesis tests on the target higgsino model. Exclusion limits at 95% CL are presented in a two-dimensional plane with the horizontal axis given by the mass of $\tilde{\chi}^{\pm}_1$ and the vertical axis given by the mass difference between $\tilde{\chi}^{\pm}_1$ and $\tilde{\chi}^0_1$, where the simplified higgsino model assumes $\Delta m(\tilde{\chi}^0_2, \tilde{\chi}^0_1) = 2\Delta m(\tilde{\chi}^{\pm}_1, \tilde{\chi}^0_1)$.

Figure 15 shows the exclusion contours for the displaced track and 1ℓ1T searches overlaid on other search results. For the displaced track search, as slight deficits are observed in SR-DT-1, 2, and 4, the observed limit extends beyond the expected, reaching up to about $m(\tilde{\chi}^{\pm}_1) = 200$ GeV for $\Delta m(\tilde{\chi}^{\pm}_1, \tilde{\chi}^0_1) = 0.6$ GeV. Excluded $\Delta m(\tilde{\chi}^{\pm}_1, \tilde{\chi}^0_1)$ ranges from 0.3 to 1.2 GeV.

The exclusion contours of the 1ℓ1T search are drawn by taking an envelope of the six contours obtained from the six pNN-θ configurations. This procedure is performed by selecting the pNN-θ with the best expected CL$_s$ for each mass of the signal samples. The expected sensitivity of the 1ℓ1T search originates largely from 1μ1T, as the muon-identification efficiency is higher compared with that of electrons in the very low-p_T regime. The effects of a slight deficit in data observed in SR-1e1T-dM4 and slight excess observed in SR-1μ1T-dM5 cancel out to yield an observed limit close to the expected limit. The observed limit extends up to $m(\tilde{\chi}^{\pm}_1) = 130$ GeV at $\Delta m(\tilde{\chi}^{\pm}_1, \tilde{\chi}^0_1) = 2$ GeV.

The two searches complementarily explore simplified higgsino models in $\Delta m(\tilde{\chi}^{\pm}_1, \tilde{\chi}^0_1) =$ 0.3–3 GeV, surpassing existing limits set by the LEP experiment [33] and ATLAS searches [27, 29, 131].

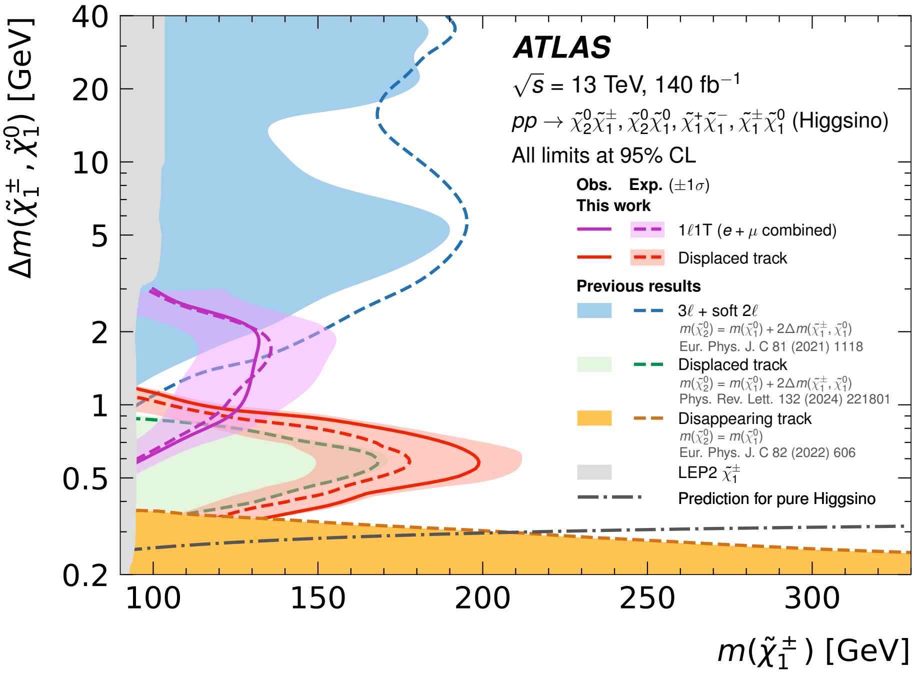

Figure 15. Observed (solid line) and expected (dashed line) limits at 95% CL for simplified higgsino models for $1\ell 1T$ (purple) and displaced track (red) searches. The limits are drawn in the $\Delta m(\tilde{\chi}_1^{\pm}, \tilde{\chi}_1^0)$ vs $m(\tilde{\chi}_1^{\pm})$ plane, with the assumption of $\Delta m(\tilde{\chi}_2^0, \tilde{\chi}_1^0) = 2\Delta m(\tilde{\chi}_1^{\pm}, \tilde{\chi}_1^0)$. The grey region denotes the mass exclusion limits from the LEP experiment [33]. The blue, light green, and yellow regions indicate the limits from ATLAS soft lepton [29, 30], displaced track [27], and disappearing track [23] searches.

10 Conclusion

Two searches for the direct production of higgsinos with compressed mass spectra are presented, based on 140 fb^{-1} of $\sqrt{s} = 13$ TeV pp collision data collected by the ATLAS experiment at the LHC. Events are required to contain missing transverse momentum, a high-p_{T} jet, and at least one soft charged particle consistent with the decay of a higgsino-like $\tilde{\chi}_2^0$ or $\tilde{\chi}_1^{\pm}$ into a nearly mass-degenerate higgsino-like $\tilde{\chi}_1^0$. For models with $\Delta m(\tilde{\chi}_1^{\pm}, \tilde{\chi}_1^0) \lesssim 1$ GeV, the charginos are expected to have non-negligible lifetimes and low-p_{T}, and displaced tracks from their potential decays are identified to reduce contributions from SM background processes. For models with larger mass splittings where the higgsino decays are expected to be prompt, events are selected that feature two low-p_{T} electrons or muons with opposite charge, where one of the leptons is identified using novel soft-lepton taggers. Both of the searches use NNs to provide discrimination between signal and SM background processes.

In each search, the data are found to be consistent with the SM predictions and the results are used to set lower limits on the higgsino masses at 95% CL in a simplified model where $\Delta m(\tilde{\chi}_2^0, \tilde{\chi}_1^0) = 2\Delta m(\tilde{\chi}_1^{\pm}, \tilde{\chi}_1^0)$. The $1\ell 1T$ search is able to further constrain the region where 0.8 GeV $\lesssim \Delta m(\tilde{\chi}_1^{\pm}, \tilde{\chi}_1^0) \lesssim 2.0$ GeV, extending the limits established by other experiments up to a maximum of $m(\tilde{\chi}_1^{\pm}) = 132$ GeV for $\Delta m(\tilde{\chi}_1^{\pm}, \tilde{\chi}_1^0) = 1.8$ GeV. Additionally, upper limits on the visible cross-section are set at 95% CL for generic beyond the SM physics processes in the $1\ell 1T$ SRs that are optimised for 1, 3, and 5 GeV mass splittings. The displaced track

JHEP06(2026)094

search is able to extend the limits on $m(\tilde{\chi}_1^{\pm})$ previously set by the ATLAS experiment in this final state by approximately 30 GeV, with a maximum exclusion set at $m(\tilde{\chi}_1^{\pm}) = 199$ GeV for $\Delta m(\tilde{\chi}_1^{\pm}, \tilde{\chi}_1^0) = 0.6$ GeV. Taken together, the searches presented here exclude $\tilde{\chi}_1^{\pm}$ masses below 126 GeV at 95% CL over the targeted range of $\Delta m(\tilde{\chi}_1^{\pm}, \tilde{\chi}_1^0)$ within the simplified higgsino model. The limits set by the LEP experiments are now superseded by ATLAS in all ranges of $\Delta m(\tilde{\chi}_1^{\pm}, \tilde{\chi}_1^0)$ by these searches, providing additional scrutiny on the existence of light higgsinos with compressed mass spectra.

Acknowledgments

We thank CERN for the very successful operation of the LHC and its injectors, as well as the support staff at CERN and at our institutions worldwide without whom ATLAS could not be operated efficiently.

The crucial computing support from all WLCG partners is acknowledged gratefully, in particular from CERN, the ATLAS Tier-1 facilities at TRIUMF/SFU (Canada), NDGF (Denmark, Norway, Sweden), CC-IN2P3 (France), KIT/GridKA (Germany), INFN-CNAF (Italy), NL-T1 (Netherlands), PIC (Spain), RAL (U.K.) and BNL (U.S.A.), the Tier-2 facilities worldwide and large non-WLCG resource providers. Major contributors of computing resources are listed in ref. [132].

We gratefully acknowledge the support of ANPCyT, Argentina; YerPhI, Armenia; ARC, Australia; BMWFW and FWF, Austria; ANAS, Azerbaijan; CNPq and FAPESP, Brazil; NSERC, NRC and CFI, Canada; CERN; ANID, Chile; CAS, MOST and NSFC, China; Minciencias, Colombia; MEYS CR, Czech Republic; DNRF and DNSRC, Denmark; IN2P3-CNRS and CEA-DRF/IRFU, France; SRNSFG, Georgia; BMFTR, HGF and MPG, Germany; GSRI, Greece; RGC and Hong Kong SAR, China; ICHEP and Academy of Sciences and Humanities, Israel; INFN, Italy; MEXT and JSPS, Japan; CNRST, Morocco; NWO, Netherlands; RCN, Norway; MNiSW, Poland; FCT, Portugal; MNE/IFA, Romania; MSTDI, Serbia; MSSR, Slovakia; ARIS and MVZI, Slovenia; DSI/NRF, South Africa; MICIU/AEI, Spain; SRC and Wallenberg Foundation, Sweden; SERI, SNSF and Cantons of Bern and Geneva, Switzerland; NSTC, Taipei; TENMAK, Türkiye; STFC/UKRI, United Kingdom; DOE and NSF, United States of America.

Individual groups and members have received support from BCKDF, CANARIE, CRC and DRAC, Canada; CERN-CZ, FORTE and PRIMUS, Czech Republic; COST, ERC, ERDF, Horizon 2020, ICSC-NextGenerationEU and Marie Skłodowska-Curie Actions, European Union; Investissements d'Avenir Labex, Investissements d'Avenir Idex and ANR, France; DFG and AvH Foundation, Germany; Herakleitos, Thales and Aristeia programmes co-financed by EU-ESF and the Greek NSRF, Greece; BSF-NSF and MINERVA, Israel; NCN and NAWA, Poland; La Caixa Banking Foundation, CERCA Programme Generalitat de Catalunya and PROMETEO and GenT Programmes Generalitat Valenciana, Spain; Göran Gustafssons Stiftelse, Sweden; The Royal Society and Leverhulme Trust, United Kingdom; Eric and Wendy Schmidt Fund for Strategic Innovation, United States of America.

In addition, individual members wish to acknowledge support from CERN: European Organization for Nuclear Research (CERN DOCT); Chile: Agencia Nacional de Investigación y Desarrollo (ANID FONDECYT reg. 1230987, FONDECYT 1230812, FONDE-

JHEP06(2026)094

CYT 1240864, Fondecyt 3240661, Fondecyt Regular 1240721); China: Chinese Ministry of Science and Technology (MOST-2023YFA1605700, MOST-2023YFA1609300), National Natural Science Foundation of China (NSFC – 12175119, NSFC 12275265); Czech Republic: Czech Science Foundation (GACR – 24-11373S), Ministry of Education Youth and Sports (ERC-CZ-LL2327, FORTE CZ.02.01.01/00/22_008/0004632), PRIMUS Research Programme (PRIMUS/21/SCI/017); EU: H2020 European Research Council (ERC – 101002463); European Union: European Research Council (BARD No. 101116429, ERC – 948254, ERC 101089007), European Regional Development Fund (HE COFUND GA No. 101081355, ERDF), Horizon 2020 Framework Programme (MUCCA – CHIST-ERA-19-XAI-00), European Union, Future Artificial Intelligence Research (FAIR-NextGenerationEU PE00000013), Italian Center for High Performance Computing, Big Data and Quantum Computing (ICSC, NextGenerationEU); France: Agence Nationale de la Recherche (ANR-21-CE31-0013, ANR-21-CE31-0022, ANR-22-EDIR-0002, ANR-24-CE31-0504-01); Germany: Baden-Württemberg Stiftung (BW Stiftung-Postdoc Eliteprogramme), Deutsche Forschungsgemeinschaft (DFG – 469666862, DFG – CR 312/5-2); China: Research Grants Council (GRF); Italy: Istituto Nazionale di Fisica Nucleare (ICSC, NextGenerationEU), Ministero dell'Università e della Ricerca (NextGenEU 153D23001490006 M4C2.1.1, NextGenEU I53D23000820006 M4C2.1.1, NextGenEU I53D23001490006 M4C2.1.1, SOE2024_0000023); Japan: Japan Society for the Promotion of Science (JSPS KAKENHI JP22H01227, JSPS KAKENHI JP22H04944, JSPS KAKENHI JP22KK0227, JSPS KAKENHI JP24K23939, JSPS KAKENHI JP25H00650, JSPS KAKENHI JP25H01291, JSPS KAKENHI JP25K01023); Norway: Research Council of Norway (RCN-314472); Poland: Ministry of Science and Higher Education (IDUB AGH, POB8, D4 no 9722), Polish National Science Centre (NCN 2021/42/E/ST2/00350, NCN OPUS 2023/51/B/ST2/02507, NCN OPUS nr 2022/47/B/ST2/03059, NCN UMO-2019/34/E/ST2/00393, UMO-2022/47/O/ST2/00148, UMO-2023/49/B/ST2/04085, UMO-2023/51/B/ST2/00920, UMO-2024/53/N/ST2/00869); Portugal: Foundation for Science and Technology (FCT); Spain: Agencia de Gestión de Ayudas Universitarias y de Investigación (AGAUR – 2023 BP 00141), Generalitat Valenciana (ASFAE/2022/008), Ministry of Science and Innovation (MCIN & NextGenEU PCI2022-135018-2, MICIN & FEDER PID2021-125273NB, RYC2019-028510-I, RYC2020-030254-I, RYC2021-031273-I, RYC2022-038164-I), Ministerio de Ciencia, Innovación y Universidades/Agencia Estatal de Investigación (PID2022-142604OB-C22); Sweden: Carl Trygger Foundation (Carl Trygger Foundation CTS 22:2312), Swedish Research Council (Swedish Research Council 2023-04654, VR 2021-03651, VR 2022-03845, VR 2022-04683, VR 2023-03403, VR 2024-05451), Knut and Alice Wallenberg Foundation (KAW 2018.0458, KAW 2022.0358, KAW 2023.0366); Switzerland: Swiss National Science Foundation (SNSF – PCEFP2_194658); United Kingdom: Leverhulme Trust (Leverhulme Trust RPG-2020-004), Royal Society (NIF-R1-231091); United States of America: U.S. Department of Energy (ECA DE-AC02-76SF00515), Neubauer Family Foundation.

JHEP06(2026)094

A NN training configurations

Table 15 shows the training configurations of the event-level and track-level NNs used in the displaced track search presented in section 6.1 and the pNN used in the $1\ell 1T$ search presented in section 6.2. The configuration of the pNN is common to both electron and muon channels.

Hyperparameter	Event-level (DT)	Track-level (DT)	pNN ($1\ell 1T$)
Number of learnable parameters	2411	2611	21957
EarlyStopping [120, 123, 124]	Enabled		
Initial learning rate	0.01		0.0001
Loss type	Binary cross-entropy		
Optimiser	Adam [133]		

Table 15. Summary of the training configurations of the event-level and track-level NNs for the displaced track (DT) search and the event selection pNN for the $1\ell 1T$ search.

Data Availability Statement. The public release of data supporting the findings of this article will follow the CERN Open Data Policy [134]. The values of relevant plots and tables associated with this article are stored in HEPData (`https://www.hepdata.net/record/ins3086532` for this article).

Code Availability Statement. The ATLAS Collaboration's Athena software, including the configuration of the event generators, is open source (`http://gitlab.cern.ch/atlas/athena`).

References

[1] Y.A. Golfand and E.P. Likhtman, *Extension of the Algebra of Poincare Group Generators and Violation of P Invariance*, *JETP Lett.* **13** (1971) 323 [INSPIRE].

[2] D.V. Volkov and V.P. Akulov, *Is the neutrino a goldstone particle?*, *Phys. Lett. B* **46** (1973) 109 [INSPIRE].

[3] J. Wess and B. Zumino, *Supergauge transformations in four dimensions*, *Nucl. Phys. B* **70** (1974) 39 [INSPIRE].

[4] J. Wess and B. Zumino, *Supergauge invariant extension of quantum electrodynamics*, *Nucl. Phys. B* **78** (1974) 1 [INSPIRE].

[5] S. Ferrara and B. Zumino, *Supergauge invariant Yang-Mills theories*, *Nucl. Phys. B* **79** (1974) 413 [INSPIRE].

[6] A. Salam and J.A. Strathdee, *Super-symmetry and non-Abelian gauges*, *Phys. Lett. B* **51** (1974) 353 [INSPIRE].

[7] G.R. Farrar and P. Fayet, *Phenomenology of the production, decay, and detection of new hadronic states associated with supersymmetry*, *Phys. Lett. B* **76** (1978) 575 [INSPIRE].

[8] H. Goldberg, *Constraint on the Photino Mass from Cosmology*, *Phys. Rev. Lett.* **50** (1983) 1419 [*Erratum ibid.* **103** (2009) 099905] [INSPIRE].

[9] J.R. Ellis et al., *Supersymmetric relics from the big bang*, *Nucl. Phys. B* **238** (1984) 453 [INSPIRE].

[10] N. Sakai, *Naturalness in supersymmetric GUTS*, *Z. Phys. C* **11** (1981) 153 [INSPIRE].

[11] S. Dimopoulos, S. Raby and F. Wilczek, *Supersymmetry and the scale of unification*, *Phys. Rev. D* **24** (1981) 1681 [INSPIRE].

[12] L.E. Ibáñez and G.G. Ross, *Low-energy predictions in supersymmetric grand unified theories*, *Phys. Lett. B* **105** (1981) 439 [INSPIRE].

[13] S. Dimopoulos and H. Georgi, *Softly broken supersymmetry and SU(5)*, *Nucl. Phys. B* **193** (1981) 150 [INSPIRE].

[14] R. Barbieri and G.F. Giudice, *Upper bounds on supersymmetric particle masses*, *Nucl. Phys. B* **306** (1988) 63 [INSPIRE].

[15] B. de Carlos and J.A. Casas, *One-loop analysis of the electroweak breaking in supersymmetric models and the fine-tuning problem*, *Phys. Lett. B* **309** (1993) 320 [hep-ph/9303291] [INSPIRE].

[16] P. Fayet, *Supersymmetry and weak, electromagnetic and strong interactions*, *Phys. Lett. B* **64** (1976) 159 [INSPIRE].

[17] P. Fayet, *Spontaneously broken supersymmetric theories of weak, electromagnetic and strong interactions*, *Phys. Lett. B* **69** (1977) 489 [INSPIRE].

[18] R. Barbieri and D. Pappadopulo, *S-particles at their naturalness limits*, *JHEP* **10** (2009) 061 [arXiv:0906.4546] [INSPIRE].

[19] H. Baer, V. Barger and P. Huang, *Hidden SUSY at the LHC: the light higgsino-world scenario and the role of a lepton collider*, *JHEP* **11** (2011) 031 [arXiv:1107.5581] [INSPIRE].

[20] M. Papucci, J.T. Ruderman and A. Weiler, *Natural SUSY endures*, *JHEP* **09** (2012) 035 [arXiv:1110.6926] [INSPIRE].

[21] H. Baer et al., *Radiative Natural Supersymmetry with a 125 GeV Higgs Boson*, *Phys. Rev. Lett.* **109** (2012) 161802 [arXiv:1207.3343] [INSPIRE].

[22] ATLAS collaboration, *Search for long-lived charginos based on a disappearing-track signature in pp collisions at $\sqrt{s} = 13$ TeV with the ATLAS detector*, *JHEP* **06** (2018) 022 [arXiv:1712.02118] [INSPIRE].

[23] ATLAS collaboration, *Search for long-lived charginos based on a disappearing-track signature using 136 fb^{-1} of pp collisions at $\sqrt{s} = 13$ TeV with the ATLAS detector*, *Eur. Phys. J. C* **82** (2022) 606 [arXiv:2201.02472] [INSPIRE].

[24] CMS collaboration, *Search for disappearing tracks as a signature of new long-lived particles in proton-proton collisions at $\sqrt{s} = 13$ TeV*, *JHEP* **08** (2018) 016 [arXiv:1804.07321] [INSPIRE].

[25] CMS collaboration, *Search for disappearing tracks in proton-proton collisions at $\sqrt{s} = 13$ TeV*, *Phys. Lett. B* **806** (2020) 135502 [arXiv:2004.05153] [INSPIRE].

[26] H. Fukuda et al., *Cornering Higgsinos Using Soft Displaced Tracks*, *Phys. Rev. Lett.* **124** (2020) 101801 [arXiv:1910.08065] [INSPIRE].

[27] ATLAS collaboration, *Search for Nearly Mass-Degenerate Higgsinos Using Low-Momentum Mildly Displaced Tracks in pp Collisions at $\sqrt{s} = 13$ TeV with the ATLAS Detector*, *Phys. Rev. Lett.* **132** (2024) 221801 [arXiv:2401.14046] [INSPIRE].

[28] ATLAS collaboration, *Search for electroweak production of supersymmetric states in scenarios with compressed mass spectra at $\sqrt{s} = 13$ TeV with the ATLAS detector*, *Phys. Rev. D* **97** (2018) 052010 [arXiv:1712.08119] [INSPIRE].

[29] ATLAS collaboration, *Searches for electroweak production of supersymmetric particles with compressed mass spectra in $\sqrt{s} = 13$ TeV pp collisions with the ATLAS detector*, *Phys. Rev. D* **101** (2020) 052005 [arXiv:1911.12606] [INSPIRE].

[30] ATLAS collaboration, *Search for chargino-neutralino pair production in final states with three leptons and missing transverse momentum in $\sqrt{s} = 13$ TeV pp collisions with the ATLAS detector*, *Eur. Phys. J. C* **81** (2021) 1118 [arXiv:2106.01676] [INSPIRE].

[31] CMS collaboration, *Search for electroweak production of charginos and neutralinos in proton-proton collisions at $\sqrt{s} = 13$ TeV*, *JHEP* **04** (2022) 147 [arXiv:2106.14246] [INSPIRE].

[32] CMS collaboration, *Search for Higgsinos in final states with low-momentum lepton-track pairs at 13 TeV*, arXiv:2511.16394 [INSPIRE].

[33] ALEPH, DELPHI, L3 and OPAL collaborations, *Combined LEP Chargino Results, up to 208 GeV for low DM*, LEPSUSYWG/02-04.1, (2002).

[34] MSSM Working Group collaboration, *The Minimal Supersymmetric Standard Model: Group Summary Report*, in the proceedings of the *GDR (Groupement De Recherche) — Supersymetrie*, Montpellier, France, April 15–17 (1998) [hep-ph/9901246] [INSPIRE].

[35] C.F. Berger, J.S. Gainer, J.A.L. Hewett and T.G. Rizzo, *Supersymmetry without prejudice*, *JHEP* **02** (2009) 023 [arXiv:0812.0980] [INSPIRE].

[36] ATLAS collaboration, *ATLAS Run 2 searches for electroweak production of supersymmetric particles interpreted within the pMSSM*, *JHEP* **05** (2024) 106 [arXiv:2402.01392] [INSPIRE].

[37] ATLAS collaboration, *The ATLAS Experiment at the CERN Large Hadron Collider*, 2008 *JINST* **3** S08003 [INSPIRE].

[38] J. Alwall, M.-P. Le, M. Lisanti and J.G. Wacker, *Searching for directly decaying gluinos at the Tevatron*, *Phys. Lett. B* **666** (2008) 34 [arXiv:0803.0019] [INSPIRE].

[39] J. Alwall, P. Schuster and N. Toro, *Simplified models for a first characterization of new physics at the LHC*, *Phys. Rev. D* **79** (2009) 075020 [arXiv:0810.3921] [INSPIRE].

[40] LHC New Physics Working Group collaboration, *Simplified models for LHC new physics searches*, *J. Phys. G* **39** (2012) 105005 [arXiv:1105.2838] [INSPIRE].

[41] M. Ibe, S. Matsumoto and R. Sato, *Mass Splitting between Charged and Neutral Winos at Two-Loop Level*, *Phys. Lett. B* **721** (2013) 252 [arXiv:1212.5989] [INSPIRE].

[42] V.A. Beylin, V.I. Kuksa, G.M. Vereshkov and R.S. Pasechnik, *Neutralino-nucleon interaction in the Split Higgsino scenario of the Dark Matter*, *Int. J. Mod. Phys. A* **24** (2009) 6051 [arXiv:0903.4201] [INSPIRE].

[43] P. Baldi et al., *Parameterized neural networks for high-energy physics*, *Eur. Phys. J. C* **76** (2016) 235 [arXiv:1601.07913] [INSPIRE].

[44] ATLAS collaboration, *Study of the material of the ATLAS inner detector for Run 2 of the LHC*, 2017 *JINST* **12** P12009 [arXiv:1707.02826] [INSPIRE].

[45] ATLAS collaboration, *ATLAS Insertable B-Layer: Technical Design Report*, (2010), ATLAS-TDR-19.

[46] ATLAS IBL collaboration, *Production and integration of the ATLAS Insertable B-Layer*, 2018 *JINST* **13** T05008 [arXiv:1803.00844] [INSPIRE].

[47] ATLAS collaboration, *Impact Parameter resolutions in di-jet events*, ATL-IDTR-2018-008, (2018).

[48] G. Avoni et al., *The new LUCID-2 detector for luminosity measurement and monitoring in ATLAS*, 2018 *JINST* **13** P07017 [INSPIRE].

[49] ATLAS collaboration, *Performance of the ATLAS trigger system in 2015*, *Eur. Phys. J. C* **77** (2017) 317 [arXiv:1611.09661] [INSPIRE].

[50] ATLAS collaboration, *Software and computing for Run 3 of the ATLAS experiment at the LHC*, *Eur. Phys. J. C* **85** (2025) 234 [arXiv:2404.06335] [INSPIRE].

[51] ATLAS collaboration, *Luminosity determination in pp collisions at $\sqrt{s} = 13$ TeV using the ATLAS detector at the LHC*, *Eur. Phys. J. C* **83** (2023) 982 [arXiv:2212.09379] [INSPIRE].

[52] ATLAS collaboration, *ATLAS data quality operations and performance for 2015–2018 data-taking*, 2020 *JINST* **15** P04003 [arXiv:1911.04632] [INSPIRE].

[53] ATLAS collaboration, *Performance of the missing transverse momentum triggers for the ATLAS detector during Run-2 data taking*, *JHEP* **08** (2020) 080 [arXiv:2005.09554] [INSPIRE].

[54] ATLAS collaboration, *Performance of electron and photon triggers in ATLAS during LHC Run 2*, *Eur. Phys. J. C* **80** (2020) 47 [arXiv:1909.00761] [INSPIRE].

[55] ATLAS collaboration, *Performance of the ATLAS muon triggers in Run 2*, 2020 *JINST* **15** P09015 [arXiv:2004.13447] [INSPIRE].

[56] T. Sjöstrand, S. Mrenna and P.Z. Skands, *A brief introduction to PYTHIA 8.1*, *Comput. Phys. Commun.* **178** (2008) 852 [arXiv:0710.3820] [INSPIRE].

[57] R.D. Ball et al., *Parton distributions with LHC data*, *Nucl. Phys. B* **867** (2013) 244 [arXiv:1207.1303] [INSPIRE].

[58] ATLAS collaboration, *The Pythia 8 A3 tune description of ATLAS minimum bias and inelastic measurements incorporating the Donnachie-Landshoff diffractive model*, ATL-PHYS-PUB-2016-017 (2016) [INSPIRE].

[59] ATLAS collaboration, *The ATLAS Simulation Infrastructure*, *Eur. Phys. J. C* **70** (2010) 823 [arXiv:1005.4568] [INSPIRE].

[60] GEANT4 collaboration, *Geant4 — a simulation toolkit*, *Nucl. Instrum. Meth. A* **506** (2003) 250 [INSPIRE].

[61] J. Alwall et al., *The automated computation of tree-level and next-to-leading order differential cross sections, and their matching to parton shower simulations*, *JHEP* **07** (2014) 079 [arXiv:1405.0301] [INSPIRE].

[62] C. Bierlich et al., *A comprehensive guide to the physics and usage of PYTHIA 8.3*, *SciPost Phys. Codeb.* (2022) 8 [arXiv:2203.11601] [INSPIRE].

[63] T. Sjöstrand et al., *An introduction to PYTHIA 8.2*, *Comput. Phys. Commun.* **191** (2015) 159 [arXiv:1410.3012] [INSPIRE].

[64] ATLAS collaboration, *ATLAS Pythia 8 tunes to 7 TeV data*, ATL-PHYS-PUB-2014-021 (2014) [INSPIRE].

JHEP06(2026)094

[65] L. Lönnblad and S. Prestel, *Matching tree-level matrix elements with interleaved showers*, *JHEP* **03** (2012) 019 [arXiv:1109.4829] [INSPIRE].

[66] D.J. Lange, *The EvtGen particle decay simulation package*, *Nucl. Instrum. Meth. A* **462** (2001) 152 [INSPIRE].

[67] P. Artoisenet, R. Frederix, O. Mattelaer and R. Rietkerk, *Automatic spin-entangled decays of heavy resonances in Monte Carlo simulations*, *JHEP* **03** (2013) 015 [arXiv:1212.3460] [INSPIRE].

[68] A. Djouadi, M.M. Mühlleitner and M. Spira, *Decays of Supersymmetric Particles: the Program SUSY-HIT (SUspect-SdecaY-Hdecay-InTerface)*, *Acta Phys. Polon. B* **38** (2007) 635 [hep-ph/0609292] [INSPIRE].

[69] W. Beenakker et al., *Production of Charginos, Neutralinos, and Sleptons at Hadron Colliders*, *Phys. Rev. Lett.* **83** (1999) 3780 [*Erratum ibid.* **100** (2008) 029901] [hep-ph/9906298] [INSPIRE].

[70] J. Debove, B. Fuks and M. Klasen, *Threshold resummation for gaugino pair production at hadron colliders*, *Nucl. Phys. B* **842** (2011) 51 [arXiv:1005.2909] [INSPIRE].

[71] B. Fuks, M. Klasen, D.R. Lamprea and M. Rothering, *Gaugino production in proton-proton collisions at a center-of-mass energy of* 8 TeV, *JHEP* **10** (2012) 081 [arXiv:1207.2159] [INSPIRE].

[72] B. Fuks, M. Klasen, D.R. Lamprea and M. Rothering, *Precision predictions for electroweak superpartner production at hadron colliders with resummino*, *Eur. Phys. J. C* **73** (2013) 2480 [arXiv:1304.0790] [INSPIRE].

[73] J. Fiaschi and M. Klasen, *Neutralino-chargino pair production at NLO+NLL with resummation-improved parton density functions for LHC Run II*, *Phys. Rev. D* **98** (2018) 055014 [arXiv:1805.11322] [INSPIRE].

[74] G. Bozzi, B. Fuks and M. Klasen, *Threshold resummation for slepton-pair production at hadron colliders*, *Nucl. Phys. B* **777** (2007) 157 [hep-ph/0701202] [INSPIRE].

[75] B. Fuks, M. Klasen, D.R. Lamprea and M. Rothering, *Revisiting slepton pair production at the Large Hadron Collider*, *JHEP* **01** (2014) 168 [arXiv:1310.2621] [INSPIRE].

[76] J. Fiaschi and M. Klasen, *Slepton pair production at the LHC in NLO+NLL with resummation-improved parton densities*, *JHEP* **03** (2018) 094 [arXiv:1801.10357] [INSPIRE].

[77] J. Fiaschi, B. Fuks, M. Klasen and A. Neuwirth, *Electroweak superpartner production at 13.6 Tev with Resummino*, *Eur. Phys. J. C* **83** (2023) 707 [arXiv:2304.11915] [INSPIRE].

[78] J. Pumplin et al., *New Generation of Parton Distributions with Uncertainties from Global QCD Analysis*, *JHEP* **07** (2002) 012 [hep-ph/0201195] [INSPIRE].

[79] A.D. Martin, W.J. Stirling, R.S. Thorne and G. Watt, *Parton distributions for the LHC*, *Eur. Phys. J. C* **63** (2009) 189 [arXiv:0901.0002] [INSPIRE].

[80] NNPDF collaboration, *Parton distributions for the LHC run II*, *JHEP* **04** (2015) 040 [arXiv:1410.8849] [INSPIRE].

[81] S. Frixione et al., *Single-top hadroproduction in association with a W boson*, *JHEP* **07** (2008) 029 [arXiv:0805.3067] [INSPIRE].

[82] SHERPA collaboration, *Event generation with Sherpa 2.2*, *SciPost Phys.* **7** (2019) 034 [arXiv:1905.09127] [INSPIRE].

[83] S. Hoeche, F. Krauss, M. Schönherr and F. Siegert, *A critical appraisal of NLO+PS matching methods*, *JHEP* **09** (2012) 049 [arXiv:1111.1220] [INSPIRE].

JHEP06(2026)094

[84] S. Hoeche, F. Krauss, M. Schönherr and F. Siegert, *QCD matrix elements + parton showers. The NLO case*, *JHEP* **04** (2013) 027 [arXiv:1207.5030] [INSPIRE].

[85] S. Catani, F. Krauss, R. Kuhn and B.R. Webber, *QCD Matrix Elements + Parton Showers*, *JHEP* **11** (2001) 063 [hep-ph/0109231] [INSPIRE].

[86] S. Hoeche, F. Krauss, S. Schumann and F. Siegert, *QCD matrix elements and truncated showers*, *JHEP* **05** (2009) 053 [arXiv:0903.1219] [INSPIRE].

[87] ATLAS collaboration, *Multi-Boson Simulation for* 13 *TeV ATLAS Analyses*, ATL-PHYS-PUB-2017-005 (2017) [INSPIRE].

[88] T. Gleisberg and S. Hoeche, *Comix, a new matrix element generator*, *JHEP* **12** (2008) 039 [arXiv:0808.3674] [INSPIRE].

[89] S. Schumann and F. Krauss, *A parton shower algorithm based on Catani-Seymour dipole factorisation*, *JHEP* **03** (2008) 038 [arXiv:0709.1027] [INSPIRE].

[90] S. Frixione, P. Nason and G. Ridolfi, *A positive-weight next-to-leading-order Monte Carlo for heavy flavour hadroproduction*, *JHEP* **09** (2007) 126 [arXiv:0707.3088] [INSPIRE].

[91] P. Nason, *A new method for combining NLO QCD with shower Monte Carlo algorithms*, *JHEP* **11** (2004) 040 [hep-ph/0409146] [INSPIRE].

[92] S. Frixione, P. Nason and C. Oleari, *Matching NLO QCD computations with parton shower simulations: the POWHEG method*, *JHEP* **11** (2007) 070 [arXiv:0709.2092] [INSPIRE].

[93] S. Alioli, P. Nason, C. Oleari and E. Re, *A general framework for implementing NLO calculations in shower Monte Carlo programs: the POWHEG BOX*, *JHEP* **06** (2010) 043 [arXiv:1002.2581] [INSPIRE].

[94] M. Beneke, P. Falgari, S. Klein and C. Schwinn, *Hadronic top-quark pair production with NNLL threshold resummation*, *Nucl. Phys. B* **855** (2012) 695 [arXiv:1109.1536] [INSPIRE].

[95] M. Cacciari et al., *Top-pair production at hadron colliders with next-to-next-to-leading logarithmic soft-gluon resummation*, *Phys. Lett. B* **710** (2012) 612 [arXiv:1111.5869] [INSPIRE].

[96] P. Bärnreuther, M. Czakon and A. Mitov, *Percent-Level-Precision Physics at the Tevatron: Next-to-Next-to-Leading Order QCD Corrections to $q\bar{q} \to t\bar{t} + X$*, *Phys. Rev. Lett.* **109** (2012) 132001 [arXiv:1204.5201] [INSPIRE].

[97] M. Czakon and A. Mitov, *NNLO corrections to top-pair production at hadron colliders: the all-fermionic scattering channels*, *JHEP* **12** (2012) 054 [arXiv:1207.0236] [INSPIRE].

[98] M. Czakon and A. Mitov, *NNLO corrections to top pair production at hadron colliders: the quark-gluon reaction*, *JHEP* **01** (2013) 080 [arXiv:1210.6832] [INSPIRE].

[99] M. Czakon, P. Fiedler and A. Mitov, *Total Top-Quark Pair-Production Cross Section at Hadron Colliders Through $\mathcal{O}(\alpha_S^4)$*, *Phys. Rev. Lett.* **110** (2013) 252004 [arXiv:1303.6254] [INSPIRE].

[100] M. Czakon and A. Mitov, *Top++: A program for the calculation of the top-pair cross-section at hadron colliders*, *Comput. Phys. Commun.* **185** (2014) 2930 [arXiv:1112.5675] [INSPIRE].

[101] S. Alioli, P. Nason, C. Oleari and E. Re, *NLO single-top production matched with shower in POWHEG: s- and t-channel contributions*, *JHEP* **09** (2009) 111 [*Erratum ibid.* **02** (2010) 011] [arXiv:0907.4076] [INSPIRE].

[102] E. Re, *Single-top Wt-channel production matched with parton showers using the POWHEG method*, *Eur. Phys. J. C* **71** (2011) 1547 [arXiv:1009.2450] [INSPIRE].

[103] N. Kidonakis, *Two-loop soft anomalous dimensions for single top quark associated production with a W^- or H^-*, *Phys. Rev. D* **82** (2010) 054018 [arXiv:1005.4451] [INSPIRE].

[104] N. Kidonakis, *Top Quark Production*, in the proceedings of the *Helmholtz International Summer School on Physics of Heavy Quarks and Hadrons*, Dubna, Russian Federation, July 15–28 (2013) [DOI:10.3204/DESY-PROC-2013-03/Kidonakis] [arXiv:1311.0283] [INSPIRE].

[105] ATLAS collaboration, *Performance of the ATLAS track reconstruction algorithms in dense environments in LHC Run 2*, *Eur. Phys. J. C* **77** (2017) 673 [arXiv:1704.07983] [INSPIRE].

[106] ATLAS collaboration, *Characterisation and mitigation of beam-induced backgrounds observed in the ATLAS detector during the 2011 proton-proton run*, 2013 *JINST* **8** P07004 [arXiv:1303.0223] [INSPIRE].

[107] ATLAS collaboration, *Electron and photon efficiencies in LHC Run 2 with the ATLAS experiment*, *JHEP* **05** (2024) 162 [arXiv:2308.13362] [INSPIRE].

[108] ATLAS collaboration, *Muon reconstruction and identification efficiency in ATLAS using the full Run 2 pp collision data set at $\sqrt{s} = 13$ TeV*, *Eur. Phys. J. C* **81** (2021) 578 [arXiv:2012.00578] [INSPIRE].

[109] ATLAS collaboration, *Jet reconstruction and performance using particle flow with the ATLAS Detector*, *Eur. Phys. J. C* **77** (2017) 466 [arXiv:1703.10485] [INSPIRE].

[110] M. Cacciari, G.P. Salam and G. Soyez, *The anti-k_t jet clustering algorithm*, *JHEP* **04** (2008) 063 [arXiv:0802.1189] [INSPIRE].

[111] M. Cacciari, G.P. Salam and G. Soyez, *FastJet user manual*, *Eur. Phys. J. C* **72** (2012) 1896 [arXiv:1111.6097] [INSPIRE].

[112] ATLAS collaboration, *Jet energy scale and resolution measured in proton-proton collisions at $\sqrt{s} = 13$ TeV with the ATLAS detector*, *Eur. Phys. J. C* **81** (2021) 689 [arXiv:2007.02645] [INSPIRE].

[113] ATLAS collaboration, *Performance of pile-up mitigation techniques for jets in pp collisions at $\sqrt{s} = 8$ TeV using the ATLAS detector*, *Eur. Phys. J. C* **76** (2016) 581 [arXiv:1510.03823] [INSPIRE].

[114] ATLAS collaboration, *ATLAS flavour-tagging algorithms for the LHC Run 2 pp collision dataset*, *Eur. Phys. J. C* **83** (2023) 681 [arXiv:2211.16345] [INSPIRE].

[115] ATLAS collaboration, *Measurement of the c-jet mistagging efficiency in $t\bar{t}$ events using pp collision data at $\sqrt{s} = 13$ TeV collected with the ATLAS detector*, *Eur. Phys. J. C* **82** (2022) 95 [arXiv:2109.10627] [INSPIRE].

[116] ATLAS collaboration, *Calibration of the light-flavour jet mistagging efficiency of the b-tagging algorithms with Z+jets events using 139 fb^{-1} of ATLAS proton-proton collision data at $\sqrt{s} = 13$ TeV*, *Eur. Phys. J. C* **83** (2023) 728 [arXiv:2301.06319] [INSPIRE].

[117] ATLAS collaboration, *The performance of missing transverse momentum reconstruction and its significance with the ATLAS detector using 140 fb^{-1} of $\sqrt{s} = 13$ TeV pp collisions*, *Eur. Phys. J. C* **85** (2025) 606 [arXiv:2402.05858] [INSPIRE].

[118] ATLAS collaboration, *ATLAS b-jet identification performance and efficiency measurement with $t\bar{t}$ events in pp collisions at $\sqrt{s} = 13$ TeV*, *Eur. Phys. J. C* **79** (2019) 970 [arXiv:1907.05120] [INSPIRE].

[119] ATLAS collaboration, *Early Inner Detector Tracking Performance in the 2015 Data at $\sqrt{s} = 13$ TeV*, ATL-PHYS-PUB-2015-051 (2015) [INSPIRE].

JHEP06(2026)094

[120] A. Paszke et al., *PyTorch: An Imperative Style, High-Performance Deep Learning Library*, in *Advances in Neural Information Processing Systems*, H. Wallach et al. eds., Curran Associates, Inc. (2019) [arXiv:1912.01703] [INSPIRE].

[121] ATLAS collaboration, *Performance of vertex reconstruction algorithms for detection of new long-lived particle decays within the ATLAS inner detector*, ATL-PHYS-PUB-2019-013 (2019) [INSPIRE].

[122] ATLAS collaboration, *Formulae for Estimating Significance*, ATL-PHYS-PUB-2020-025 (2020) [INSPIRE].

[123] M. Abadi et al., *TensorFlow: Large-Scale Machine Learning on Heterogeneous Systems*, (2015), https://www.tensorflow.org/.

[124] F. Chollet et al., *Keras*, (2015), https://keras.io.

[125] A.Y. Ng, *Feature selection, L_1 vs. L_2 regularization, and rotational invariance*, in the proceedings of the *Twenty-first international conference on Machine learning — ICML '04*, Banff, Alberta, Canada, July 04–08, (2004) [DOI:10.1145/1015330.1015435].

[126] ATLAS collaboration, *Electron and photon performance measurements with the ATLAS detector using the 2015–2017 LHC proton–proton collision data*, 2019 *JINST* **14** P12006 [arXiv:1908.00005] [INSPIRE].

[127] M. Baak et al., *HistFitter software framework for statistical data analysis*, *Eur. Phys. J. C* **75** (2015) 153 [arXiv:1410.1280] [INSPIRE].

[128] G. Cowan, K. Cranmer, E. Gross and O. Vitells, *Asymptotic formulae for likelihood-based tests of new physics*, *Eur. Phys. J. C* **71** (2011) 1554 [*Erratum ibid.* **73** (2013) 2501] [arXiv:1007.1727] [INSPIRE].

[129] R.D. Cousins, J.T. Linnemann and J. Tucker, *Evaluation of three methods for calculating statistical significance when incorporating a systematic uncertainty into a test of the background-only hypothesis for a Poisson process*, *Nucl. Instrum. Meth. A* **595** (2008) 480 [physics/0702156] [INSPIRE].

[130] A.L. Read, *Presentation of search results: the CL_s technique*, *J. Phys. G* **28** (2002) 2693 [INSPIRE].

[131] ATLAS collaboration, *Search for squarks and gluinos in final states with same-sign leptons and jets using* $139\,fb^{-1}$ *of data collected with the ATLAS detector*, *JHEP* **06** (2020) 046 [arXiv:1909.08457] [INSPIRE].

[132] ATLAS collaboration, *ATLAS Computing Acknowledgements*, ATL-SOFT-PUB-2025-001 (2025) [INSPIRE].

[133] D.P. Kingma and J. Ba, *Adam: A Method for Stochastic Optimization*, in the proceedings of the *International Conference on Learning Representations*, San Diego, U.S.A., May 07–09 (2015) [arXiv:1412.6980] [INSPIRE].

[134] *CERN Open Data Policy for the LHC Experiments*, CERN-OPEN-2020-013, (2020).

The ATLAS collaboration

G. Aad[104], E. Aakvaag[17], B. Abbott[123], S. Abdelhameed[119a], K. Abeling[55], N.J. Abicht[49], S.H. Abidi[30], M. Aboelela[45], A. Aboulhorma[36e], H. Abramowicz[157], Y. Abulaiti[120], B.S. Acharya[69a,69b,a], A. Ackermann[63a], C. Adam Bourdarios[4], L. Adamczyk[87a], S.V. Addepalli[149], M.J. Addison[103], J. Adelman[118], A. Adiguzel[22c], T. Adye[137], A.A. Affolder[139], Y. Afik[40], M.N. Agaras[13], A. Aggarwal[102], C. Agheorghiesei[28c], F. Ahmadov[39,b], S. Ahuja[97], X. Ai[143b], G. Aielli[76a,76b], A. Aikot[169], M. Ait Tamlihat[36e], B. Aitbenchikh[36a], M. Akbiyik[102], T.P.A. Åkesson[100], A.V. Akimov[151], D. Akiyama[174], N.N. Akolkar[25], S. Aktas[172], G.L. Alberghi[24b], J. Albert[171], U. Alberti[20], P. Albicocco[53], G.L. Albouy[60], S. Alderweireldt[52], Z.L. Alegria[124], M. Aleksa[37], I.N. Aleksandrov[39], C. Alexa[28b], T. Alexopoulos[10], F. Alfonsi[24b], M. Algren[56], M. Alhroob[173], B. Ali[135], H.M. J. Ali[93,c], S. Ali[32], S.W. Alibocus[94], M. Aliev[34c], G. Alimonti[71a], W. Alkakhi[55], C. Allaire[66], B.M.M. Allbrooke[152], J.S. Allen[103], J.F. Allen[52], P.P. Allport[21], A. Aloisio[72a,72b], F. Alonso[92], C. Alpigiani[142], Z.M.K. Alsolami[93], A. Alvarez Fernandez[102], M. Alves Cardoso[56], M.G. Alviggi[72a,72b], M. Aly[103], Y. Amaral Coutinho[83b], A. Ambler[106], C. Amelung[37], M. Amerl[103], C.G. Ames[111], T. Amezza[130], D. Amidei[108], B. Amini[54], K. Amirie[161], A. Amirkhanov[39], S.P. Amor Dos Santos[133a], K.R. Amos[169], D. Amperiadou[158], S. An[84], C. Anastopoulos[145], T. Andeen[11], J.K. Anders[94], A.C. Anderson[59], A. Andreazza[71a,71b], S. Angelidakis[9], A. Angerami[42], A.V. Anisenkov[39], A. Annovi[74a], C. Antel[37], E. Antipov[151], M. Antonelli[53], F. Anulli[75a], M. Aoki[84], T. Aoki[159], M.A. Aparo[152], L. Aperio Bella[48], M. Apicella[31], C. Appelt[157], A. Apyan[27], M. Arampatzi[10], S.J. Arbiol Val[88], C. Arcangeletti[53], A.T.H. Arce[51], J-F. Arguin[110], S. Argyropoulos[158], J.-H. Arling[48], O. Arnaez[4], H. Arnold[151], G. Artoni[75a,75b], H. Asada[113], K. Asai[121], S. Asatryan[179], N.A. Asbah[37], R.A. Ashby Pickering[173], A.M. Aslam[97], K. Assamagan[30], R. Astalos[29a], K.S. V. Astrand[100], S. Atashi[165], R.J. Atkin[34a], H. Atmani[36f], P.A. Atmasiddha[131], K. Augsten[135], A.D. Auriol[41], V.A. Austrup[103], G. Avolio[37], K. Axiotis[56], A. Azzam[13], D. Babal[29b], H. Bachacou[138], K. Bachas[158,d], A. Bachiu[35], E. Bachmann[50], M.J. Backes[63a], A. Badea[40], T.M. Baer[108], P. Bagnaia[75a,75b], M. Bahmani[19], D. Bahner[54], K. Bai[126], J.T. Baines[137], L. Baines[96], O.K. Baker[178], E. Bakos[16], D. Bakshi Gupta[8], L.E. Balabram Filho[83b], V. Balakrishnan[123], R. Balasubramanian[4], E.M. Baldin[38], P. Balek[87a], E. Ballabene[24b,24a], F. Balli[138], L.M. Baltes[63a], W.K. Balunas[33], J. Balz[102], I. Bamwidhi[119b], E. Banas[88], M. Bandieramonte[132], A. Bandyopadhyay[25], S. Bansal[25], L. Barak[157], M. Barakat[48], E.L. Barberio[107], D. Barberis[18b], M. Barbero[104], M.Z. Barel[117], T. Barillari[112], M-S. Barisits[37], T. Barklow[149], P. Baron[136], D.A. Baron Moreno[103], A. Baroncelli[62], A.J. Barr[129], J.D. Barr[98], F. Barreiro[101], J. Barreiro Guimarães da Costa[14], M.G. Barros Teixeira[133a], S. Barsov[38], F. Bartels[63a], R. Bartoldus[149], A.E. Barton[93], P. Bartos[29a], A. Basan[102], M. Baselga[49], S. Bashiri[88], A. Bassalat[66,e], M.J. Basso[162a], S. Bataju[45], R. Bate[170], R.L. Bates[59], S. Batlamous[101], M. Battaglia[139], D. Battulga[19], M. Bauce[75a,75b], M. Bauer[79], P. Bauer[25], L.T. Bayer[48], L.T. Bazzano Hurrell[31], J.B. Beacham[112], T. Beau[130], J.Y. Beaucamp[92], P.H. Beauchemin[164], P. Bechtle[25], H.P. Beck[20,f], K. Becker[173], A.J. Beddall[82], V.A. Bednyakov[39], C.P. Bee[151],

JHEP06(2026)094

L.J. Beemster[16], M. Begalli[83d], M. Begel[30], J.K. Behr[48], J.F. Beirer[37], F. Beisiegel[25], M. Belfkir[119b], G. Bella[157], L. Bellagamba[24b], A. Bellerive[35], C.D. Bellgraph[68], P. Bellos[21], K. Beloborodov[38], I. Benaoumeur[21], D. Benchekroun[36a], F. Bendebba[36a], Y. Benhammou[157], K.C. Benkendorfer[61], L. Beresford[48], M. Beretta[53], E. Bergeaas Kuutmann[167], N. Berger[4], B. Bergmann[135], J. Beringer[18a], G. Bernardi[5], C. Bernius[149], F.U. Bernlochner[25], F. Bernon[37], A. Berrocal Guardia[13], T. Berry[97], P. Berta[136], A. Berthold[50], A. Berti[133a], R. Bertrand[104], S. Bethke[112], A. Betti[75a,75b], A.J. Bevan[96], L. Bezio[56], N.K. Bhalla[54], S. Bharthuar[112], S. Bhatta[151], P. Bhattarai[149], Z.M. Bhatti[120], K.D. Bhide[54], V.S. Bhopatkar[124], R.M. Bianchi[132], G. Bianco[24b,24a], O. Biebel[111], M. Biglietti[77a], C.S. Billingsley[45], Y. Bimgdi[36f], M. Bindi[55], A. Bingham[177], A. Bingul[22b], C. Bini[75a,75b], G.A. Bird[33], M. Birman[175], M. Biros[136], S. Biryukov[152], T. Bisanz[49], E. Bisceglie[24b,24a], J.P. Biswal[137], D. Biswas[147], I. Bloch[48], A. Blue[59], U. Blumenschein[96], V.S. Bobrovnikov[39], L. Boccardo[57b,57a], M. Boehler[54], B. Boehm[172], D. Bogavac[13], A.G. Bogdanchikov[38], L.S. Boggia[130], V. Boisvert[97], P. Bokan[37], T. Bold[87a], M. Bomben[5], M. Bona[96], M. Boonekamp[138], A.G. Borbély[59], I.S. Bordulev[38], G. Borissov[93], D. Bortoletto[129], D. Boscherini[24b], M. Bosman[13], K. Bouaouda[36a], N. Bouchhar[169], L. Boudet[4], J. Boudreau[132], E.V. Bouhova-Thacker[93], D. Boumediene[41], R. Bouquet[57b,57a], A. Boveia[122], J. Boyd[37], D. Boye[30], I.R. Boyko[39], L. Bozianu[56], J. Bracinik[21], N. Brahimi[4], G. Brandt[177], O. Brandt[33], B. Brau[105], J.E. Brau[126], R. Brener[175], L. Brenner[117], R. Brenner[167], S. Bressler[175], G. Brianti[78a,78b], D. Britton[59], D. Britzger[112], I. Brock[25], R. Brock[109], G. Brooijmans[42], A.J. Brooks[68], E.M. Brooks[162b], E. Brost[30], L.M. Brown[171,162a], L.E. Bruce[61], T.L. Bruckler[129], P.A. Bruckman de Renstrom[88], B. Brüers[48], A. Bruni[24b], G. Bruni[24b], D. Brunner[47a,47b], M. Bruschi[24b], N. Bruscino[75a,75b], T. Buanes[17], Q. Buat[142], D. Buchin[112], A.G. Buckley[59], O. Bulekov[82], B.A. Bullard[149], S. Burdin[94], C.D. Burgard[49], A.M. Burger[91], B. Burghgrave[8], O. Burlayenko[54], J. Burleson[168], J.C. Burzynski[148], E.L. Busch[42], V. Büscher[102], P.J. Bussey[59], J.M. Butler[26], C.M. Buttar[59], J.M. Butterworth[98], W. Buttinger[137], C.J. Buxo Vazquez[109], A.R. Buzykaev[39], S. Cabrera Urbán[169], L. Cadamuro[66], H. Cai[37], Y. Cai[24b,114c,24a], Y. Cai[114a], V.M.M. Cairo[37], O. Cakir[3a], N. Calace[37], P. Calafiura[18a], G. Calderini[130], P. Calfayan[35], L. Calic[100], G. Callea[59], L.P. Caloba[83b], D. Calvet[41], S. Calvet[41], R. Camacho Toro[130], S. Camarda[37], D. Camarero Munoz[27], P. Camarri[76a,76b], C. Camincher[171], M. Campanelli[98], A. Camplani[43], V. Canale[72a,72b], A.C. Canbay[3a], E. Canonero[97], J. Cantero[169], Y. Cao[168], F. Capocasa[27], M. Capua[44b,44a], A. Carbone[71a,71b], R. Cardarelli[76a], J.C.J. Cardenas[8], M.P. Cardiff[27], G. Carducci[44b,44a], T. Carli[37], G. Carlino[72a], J.I. Carlotto[13], B.T. Carlson[132,g], E.M. Carlson[171], J. Carmignani[94], L. Carminati[71a,71b], A. Carnelli[4], M. Carnesale[37], S. Caron[116], E. Carquin[140g], I.B. Carr[107], S. Carrá[73a,73b], G. Carratta[24b,24a], C. Carrion Martinez[169], A.M. Carroll[126], M.P. Casado[13,h], P. Casolaro[72a,72b], M. Caspar[48], W.R. Castiglioni[40], F.L. Castillo[4], L. Castillo Garcia[13], V. Castillo Gimenez[169], N.F. Castro[133a,133e], A. Catinaccio[37], J.R. Catmore[128], T. Cavaliere[4], V. Cavaliere[30], L.J. Caviedes Betancourt[23b], E. Celebi[82], S. Cella[37], V. Cepaitis[56], K. Cerny[125], A.S. Cerqueira[83a], A. Cerri[74a,i], L. Cerrito[76a,76b], F. Cerutti[18a], B. Cervato[71a,71b],

JHEP06(2026)094

A. Cervelli[24b], G. Cesarini[53], S.A. Cetin[82], P.M. Chabrillat[130], R. Chakkappai[66], S. Chakraborty[173], A. Chambers[61], J. Chan[18a], W.Y. Chan[159], J.D. Chapman[33], E. Chapon[138], B. Chargeishvili[155b], D.G. Charlton[21], C. Chauhan[136], Y. Che[114a], S. Chekanov[6], S.V. Chekulaev[162a], G.A. Chelkov[39,j], B. Chen[157], B. Chen[171], H. Chen[114a], H. Chen[30], J. Chen[144a], J. Chen[148], M. Chen[129], S. Chen[89], S.J. Chen[114a], X. Chen[144a], X. Chen[15,k], Z. Chen[62], C.L. Cheng[176], H.C. Cheng[64a], S. Cheong[149], A. Cheplakov[39], E. Cherepanova[117], R. Cherkaoui El Moursli[36e], E. Cheu[7], K. Cheung[65], L. Chevalier[138], V. Chiarella[53], G. Chiarelli[74a], G. Chiodini[70a], A.S. Chisholm[21], A. Chitan[28b], M. Chitishvili[169], M.V. Chizhov[39,l], K. Choi[11], Y. Chou[142], E.Y.S. Chow[116], K.L. Chu[175], M.C. Chu[64a], X. Chu[14,114c], Z. Chubinidze[53], J. Chudoba[134], J.J. Chwastowski[88], D. Cieri[112], K.M. Ciesla[87a], V. Cindro[95], A. Ciocio[18a], F. Cirotto[72a,72b], Z.H. Citron[175], M. Citterio[71a], D.A. Ciubotaru[28b], A. Clark[56], P.J. Clark[52], N. Clarke Hall[98], C. Clarry[161], S.E. Clawson[48], C. Clement[47a,47b], Y. Coadou[104], M. Cobal[69a,69c], A. Coccaro[57b], R.F. Coelho Barrue[133a], R. Coelho Lopes De Sa[105], S. Coelli[71a], L.S. Colangeli[161], B. Cole[42], P. Collado Soto[101], J. Collot[60], M.R. Coluccia[70a], P. Conde Muiño[133a,133g], M.P. Connell[34c], S.H. Connell[34c], E.I. Conroy[129], M. Contreras Cossio[11], F. Conventi[72a,m], A.M. Cooper-Sarkar[129], L. Corazzina[75a,75b], F.A. Corchia[24b,24a], A. Cordeiro Oudot Choi[142], L.D. Corpe[41], M. Corradi[75a,75b], F. Corriveau[106,n], A. Cortes-Gonzalez[159], M.J. Costa[169], F. Costanza[4], D. Costanzo[145], B.M. Cote[122], J. Couthures[4], G. Cowan[97], K. Cranmer[176], L. Cremer[49], D. Cremonini[24b,24a], S. Crépé-Renaudin[60], F. Crescioli[130], T. Cresta[73a,73b], M. Cristinziani[147], M. Cristoforetti[78a,78b], V. Croft[117], G. Crosetti[44b,44a], A. Cueto[101], H. Cui[98], Z. Cui[7], B.M. Cunnett[152], W.R. Cunningham[59], F. Curcio[169], J.R. Curran[52], G. D'amen[30], V. D'Amico[111], M. D'Andrea[57b,57a], G. D'anniballe[74a,74b], S. D'Auria[71a,71b], A. D'Avanzo[72a,72b], L. D'Eramo[41], A. D'Onofrio[72a,72b], M. D'Onofrio[94], M. D'uffizi[103], M.J. Da Cunha Sargedas De Sousa[57b,57a], J.V. Da Fonseca Pinto[83b], C. Da Via[103], W. Dabrowski[87a], T. Dado[37], S. Dahbi[154], T. Dai[108], D. Dal Santo[20], C. Dallapiccola[105], M. Dam[43], J. Damp[102], J.R. Dandoy[35], D. Dannheim[37], M. Danninger[148], V. Dao[151], G. Darbo[57b], S.J. Das[30], F. Dattola[48], T. Davidek[136], J. Davidson[173], I. Dawson[96], K. De[8], C. De Almeida Rossi[161], R. De Asmundis[72a], N. De Biase[48], S. De Castro[24b,24a], N. De Groot[116], P. de Jong[117], H. De la Torre[118], A. De Maria[114a], A. De Salvo[75a], U. De Sanctis[76a,76b], F. De Santis[70a,70b], A. De Santo[152], J.B. De Vivie De Regie[60], J. Debevc[95], D.V. Dedovich[39], J. Degens[94], A.M. Deiana[45], J. Del Peso[101], L. Delagrange[130], F. Deliot[138], C.M. Delitzsch[49], A. Dell'Acqua[37], L. Dell'Asta[71a,71b], M. Della Pietra[72a,72b], D. Della Volpe[56], M. Delmastro[4], C.C. Delogu[102], P.A. Delsart[60], S. Demers[178], M. Demichev[39], S.P. Denisov[38], H. Denizli[22a,o], D. Derendarz[88], F. Derue[130], P. Dervan[94,†], A.M. Desai[1], K. Desch[25], F.A. Di Bello[57b,57a], A. Di Ciaccio[76a,76b], L. Di Ciaccio[4], A. Di Domenico[75a,75b], C. Di Donato[72a,72b], A. Di Girolamo[37], G. Di Gregorio[37], A. Di Luca[78a,78b], B. Di Micco[77a,77b], R. Di Nardo[77a,77b], K.F. Di Petrillo[40], M. Diamantopoulou[35], F.A. Dias[117], M.A. Diaz[140a,140b], A.R. Didenko[39], M. Didenko[169], S.D. Diefenbacher[18a], E.B. Diehl[108], S. Díez Cornell[48], C. Diez Pardos[147], C. Dimitriadi[150], A. Dimitrievska[21], A. Dimri[151], Y. Ding[62], J. Dingfelder[25], T. Dingley[129], I-M. Dinu[28b], S.J. Dittmeier[63b], F. Dittus[37],

JHEP06(2026)094

M. Divisek[136], B. Dixit[94], F. Djama[104], T. Djobava[155b], C. Doglioni[103,100], A. Dohnalova[29a], Z. Dolezal[136], K. Domijan[87a], K.M. Dona[40], M. Donadelli[83d], B. Dong[109], J. Donini[41], J. Dopke[137], A. Doria[72a], N. Dos Santos Fernandes[133a], I.A. Dos Santos Luz[83e], P. Dougan[103], M.T. Dova[92], A.T. Doyle[59], M.P. Drescher[55], E. Dreyer[175], I. Drivas-koulouris[10], M. Drnevich[120], D. Du[62], T.A. du Pree[117], Z. Duan[114a], M. Dubau[4], F. Dubinin[39], M. Dubovsky[29a], E. Duchovni[175], G. Duckeck[111], P.K. Duckett[98], O.A. Ducu[28b], D. Duda[52], A. Dudarev[37], M.M. Dudek[88], E.R. Duden[27], L. Duflot[66], M. Dührssen[37], I. Duminica[28g], A.E. Dumitriu[28b], M. Dunford[63a], K. Dunne[47a,47b], A. Duperrin[104], H. Duran Yildiz[3a], A. Durglishvili[155b], G.I. Dyckes[18a], M. Dyndal[87a], B.S. Dziedzic[37], Z.O. Earnshaw[152], G.H. Eberwein[129], B. Eckerova[29a], S. Eggebrecht[55], E. Egidio Purcino De Souza[83e], G. Eigen[17], K. Einsweiler[18a], T. Ekelof[167], P.A. Ekman[100], S. El Farkh[36b], Y. El Ghazali[62], H. El Jarrari[37], A. El Moussaouy[36a], D. Elitez[37], M. Ellert[167], F. Ellinghaus[177], T.A. Elliot[97], N. Ellis[37], J. Elmsheuser[30], M. Elsawy[119a], M. Elsing[37], D. Emeliyanov[137], Y. Enari[84], I. Ene[18a], S. Epari[110], D. Ernani Martins Neto[88], F. Ernst[37], M. Errenst[177], M. Escalier[66], C. Escobar[169], E. Etzion[157], G. Evans[133a,133b], H. Evans[68], L.S. Evans[48], A. Ezhilov[38], S. Ezzarqtouni[36a], F. Fabbri[24b,24a], L. Fabbri[24b,24a], G. Facini[98], V. Fadeyev[139], R.M. Fakhrutdinov[38], D. Fakoudis[102], S. Falciano[75a], L.F. Falda Ulhoa Coelho[133a], F. Fallavollita[112], G. Falsetti[44b,44a], J. Faltova[136], C. Fan[168], K.Y. Fan[64b], Y. Fan[14], Y. Fang[14,114c], M. Fanti[71a,71b], M. Faraj[69a,69b], Z. Farazpay[99], A. Farbin[8], A. Farilla[77a], K. Farman[154], T. Farooque[109], J.N. Farr[178], S.M. Farrington[137,52], F. Fassi[36e], D. Fassouliotis[9], L. Fayard[66], P. Federic[136], P. Federicova[134], O.L. Fedin[38,j], M. Feickert[176], L. Feligioni[104], D.E. Fellers[18a], C. Feng[143a], Y. Feng[14], Z. Feng[117], M.J. Fenton[165], L. Ferencz[48], B. Fernandez Barbadillo[93], P. Fernandez Martinez[67], M.J.V. Fernoux[104], J. Ferrando[93], A. Ferrari[167], P. Ferrari[117,116], R. Ferrari[73a], D. Ferrere[56], C. Ferretti[108], M.P. Fewell[1], D. Fiacco[75a,75b], F. Fiedler[102], P. Fiedler[135], S. Filimonov[39], M.S. Filip[28b,p], A. Filipčič[95], E.K. Filmer[162a], F. Filthaut[116], M.C.N. Fiolhais[133a,133c,q], L. Fiorini[169], W.C. Fisher[109], T. Fitschen[103], P.M. Fitzhugh[138], I. Fleck[147], P. Fleischmann[108], T. Flick[177], M. Flores[34d,r], L.R. Flores Castillo[64a], L. Flores Sanz De Acedo[37], F.M. Follega[78a,78b], N. Fomin[33], J.H. Foo[161], A. Formica[138], A.C. Forti[103], E. Fortin[37], A.W. Fortman[18a], L. Foster[18a], L. Fountas[9,s], D. Fournier[66], H. Fox[93], P. Francavilla[74a,74b], S. Francescato[61], S. Franchellucci[56], M. Franchini[24b,24a], S. Franchino[63a], D. Francis[37], L. Franco[116], L. Franconi[48], M. Franklin[61], G. Frattari[27], Y.Y. Frid[157], J. Friend[59], N. Fritzsche[37], A. Froch[56], D. Froidevaux[37], J.A. Frost[129], Y. Fu[109], S. Fuenzalida Garrido[140g], M. Fujimoto[104], K.Y. Fung[64a], E. Furtado De Simas Filho[83e], M. Furukawa[159], J. Fuster[169], A. Gaa[55], A. Gabrielli[24b,24a], A. Gabrielli[161], P. Gadow[37], G. Gagliardi[57b,57a], L.G. Gagnon[18a], S. Gaid[85b], S. Galantzan[157], J. Gallagher[1], E.J. Gallas[129], A.L. Gallen[167], B.J. Gallop[137], K.K. Gan[122], S. Ganguly[159], Y. Gao[52], A. Garabaglu[142], F.M. Garay Walls[140a,140b], C. García[169], A. Garcia Alonso[117], A.G. Garcia Caffaro[178], J.E. García Navarro[169], M.A. Garcia Ruiz[23b], M. Garcia-Sciveres[18a], G.L. Gardner[131], R.W. Gardner[40], N. Garelli[164], R.B. Garg[149], J.M. Gargan[52], C.A. Garner[161], C.M. Garvey[34a], V.K. Gassmann[164], G. Gaudio[73a], V. Gautam[13], P. Gauzzi[75a,75b], J. Gavranovic[95], I.L. Gavrilenko[133a], A. Gavrilyuk[38], C. Gay[170], G. Gaycken[126], E.N. Gazis[10], A. Gekow[122], C. Gemme[57b], M.H. Genest[60], A.D. Gentry[115], S. George[97], T. Geralis[46], A.A. Gerwin[123], P. Gessinger-Befurt[37], M.E. Geyik[177], M. Ghani[173], K. Ghorbanian[96], A. Ghosal[147], A. Ghosh[165], A. Ghosh[7], B. Giacobbe[24b], S. Giagu[75a,75b], T. Giani[117], A. Giannini[62], S.M. Gibson[97], M. Gignac[139], D.T. Gil[87b], A.K. Gilbert[87a], B.J. Gilbert[42], D. Gillberg[35], G. Gilles[117], D.M. Gingrich[2,t], M.P. Giordani[69a,69c], P.F. Giraud[138], G. Giugliarelli[69a,69c], D. Giugni[71a], F. Giuli[76a,76b], I. Gkialas[9,s], L.K. Gladilin[38], C. Glasman[101], M. Glazewska[20], R.M. Gleason[165], G. Glemža[48], M. Glisic[126], I. Gnesi[44b], Y. Go[30], M. Goblirsch-Kolb[37], B. Gocke[49], D. Godin[110], B. Gokturk[22a], S. Goldfarb[107], T. Golling[56], M.G.D. Gololo[34c], D. Golubkov[38], J.P. Gombas[109], A. Gomes[133a,133b], G. Gomes Da Silva[147], A.J. Gomez Delegido[37], R. Gonçalo[133a], L. Gonella[21], A. Gongadze[155c], F. Gonnella[21], J.L. Gonski[149], R.Y. González Andana[52], S. González de la Hoz[169], M.V. Gonzalez Rodrigues[48], R. Gonzalez Suarez[167], S. Gonzalez-Sevilla[56], L. Goossens[37], B. Gorini[37], E. Gorini[70a,70b], A. Gorišek[95], T.C. Gosart[131], A.T. Goshaw[51], M.I. Gostkin[39], S. Goswami[124], C.A. Gottardo[37], S.A. Gotz[111], M. Gouighri[36b], A.G. Goussiou[142], N. Govender[34c], R.P. Grabarczyk[129], I. Grabowska-Bold[87a], K. Graham[35], E. Gramstad[128], S. Grancagnolo[70a,70b], C.M. Grant[1], P.M. Gravila[28f], F.G. Gravili[70a,70b], H.M. Gray[18a], M. Greco[112], M.J. Green[1], C. Grefe[25], A.S. Grefsrud[17], I.M. Gregor[48], K.T. Greif[165], P. Grenier[149], S.G. Grewe[112], A.A. Grillo[139], K. Grimm[32], S. Grinstein[13,u], J.-F. Grivaz[66], E. Gross[175], J. Grosse-Knetter[55], L. Guan[108], G. Guerrieri[37], R. Guevara[128], R. Gugel[102], J.A.M. Guhit[108], A. Guida[19], E. Guilloton[173], S. Guindon[37], F. Guo[14,114c], J. Guo[144a], L. Guo[48], L. Guo[114b,v], Y. Guo[108], A. Gupta[49], R. Gupta[132], S. Gupta[27], S. Gurbuz[25], S.S. Gurdasani[48], G. Gustavino[75a,75b], P. Gutierrez[123], L.F. Gutierrez Zagazeta[131], M. Gutsche[50], C. Gutschow[98], C. Gwenlan[129], C.B. Gwilliam[94], E.S. Haaland[128], A. Haas[120], M. Habedank[59], C. Haber[18a], H.K. Hadavand[8], A. Haddad[41], A. Hadef[50], A.I. Hagan[93], J.J. Hahn[147], E.H. Haines[98], M. Haleem[172], J. Haley[124], G.D. Hallewell[104], K. Hamano[171], H. Hamdaoui[167], M. Hamer[25], S.E. D. Hammoud[66], E.J. Hampshire[97], J. Han[143a], L. Han[114a], L. Han[62], S. Han[14], K. Hanagaki[84], M. Hance[139], D.A. Hangal[42], H. Hanif[148], M.D. Hank[131], J.B. Hansen[43], P.H. Hansen[43], D. Harada[56], T. Harenberg[177], S. Harkusha[179], M.L. Harris[105], Y.T. Harris[25], J. Harrison[13], N.M. Harrison[122], P.F. Harrison[173], M.L. E. Hart[98], N.M. Hartman[112], N.M. Hartmann[111], R.Z. Hasan[97,137], Y. Hasegawa[146], F. Haslbeck[129], S. Hassan[17], R. Hauser[109], M. Haviernik[136], C.M. Hawkes[21], R.J. Hawkings[37], Y. Hayashi[159], D. Hayden[109], C. Hayes[108], R.L. Hayes[117], C.P. Hays[129], J.M. Hays[96], H.S. Hayward[94], M. He[14,114c], Y. He[48], Y. He[98], N.B. Heatley[96], V. Hedberg[100], C. Heidegger[54], K.K. Heidegger[54], J. Heilman[35], S. Heim[48], T. Heim[18a], J.G. Heinlein[131], J.J. Heinrich[126], L. Heinrich[112], J. Hejbal[134], M. Helbig[50], A. Held[176], S. Hellesund[17], C.M. Helling[170], S. Hellman[47a,47b], A.M. Henriques Correia[37], H. Herde[100], Y. Hernández Jiménez[151], L.M. Herrmann[25], T. Herrmann[50], G. Herten[54], R. Hertenberger[111], L. Hervas[37], M.E. Hesping[102], N.P. Hessey[162a], J. Hessler[112], M. Hidaoui[36b], N. Hidic[136], E. Hill[161], T.S. Hillersoy[17], S.J. Hillier[21], J.R. Hinds[109], F. Hinterkeuser[25], M. Hirose[127], S. Hirose[163],

D. Hirschbuehl[177], T.G. Hitchings[103], B. Hiti[95], J. Hobbs[151], R. Hobincu[28e], N. Hod[175], A.M. Hodges[168], M.C. Hodgkinson[145], B.H. Hodkinson[129], A. Hoecker[37], D.D. Hofer[108], J. Hofer[169], M. Holzbock[37], L.B.A.H. Hommels[33], V. Homsak[129], B.P. Honan[103], J.J. Hong[68], T.M. Hong[132], B.H. Hooberman[168], W.H. Hopkins[6], M.C. Hoppesch[168], Y. Horii[113], M.E. Horstmann[112], S. Hou[154], M.R. Housenga[168], J. Howarth[59], J. Hoya[6], M. Hrabovsky[125], T. Hryn'ova[4], P.J. Hsu[65], S.-C. Hsu[142], T. Hsu[66], M. Hu[18a], Q. Hu[62], S. Huang[33], X. Huang[14,114c], Y. Huang[136], Y. Huang[114b], Y. Huang[14], Z. Huang[66], Z. Hubacek[135], F. Huegging[25], T.B. Huffman[129], M. Hufnagel Maranha De Faria[83a], C.A. Hugli[48], M. Huhtinen[37], S.K. Huiberts[17], R. Hulsken[106], C.E. Hultquist[18a], D.L. Humphreys[105], N. Huseynov[12], J. Huston[109], J. Huth[61], L. Huth[48], R. Hyneman[7], G. Iacobucci[56], G. Iakovidis[30], L. Iconomidou-Fayard[66], J.P. Iddon[37], P. Iengo[72a,72b], R. Iguchi[159], Y. Iiyama[159], T. Iizawa[159], Y. Ikegami[84], D. Iliadis[158], N. Ilic[161], H. Imam[36a], G. Inacio Goncalves[83d], S.A. Infante Cabanas[140c], T. Ingebretsen Carlson[47a,47b], J.M. Inglis[96], G. Introzzi[73a,73b], M. Iodice[77a], V. Ippolito[75a,75b], R.K. Irwin[94], M. Ishino[159], W. Islam[176], C. Issever[19], S. Istin[22a,w], K. Itabashi[84], H. Ito[174], R. Iuppa[78a,78b], A. Ivina[175], V. Izzo[72a], P. Jacka[135], P. Jackson[1], P. Jain[48], K. Jakobs[54], T. Jakoubek[175], J. Jamieson[59], W. Jang[159], S. Jankovych[136], M. Javurkova[105], P. Jawahar[103], L. Jeanty[126], J. Jejelava[155a,x], P. Jenni[54,y], C.E. Jessiman[35], C. Jia[143a], H. Jia[170], J. Jia[151], X. Jia[112,114c], Z. Jia[114a], C. Jiang[52], Q. Jiang[64b], S. Jiggins[48], M. Jimenez Ortega[169], J. Jimenez Pena[13], S. Jin[114a], A. Jinaru[28b], O. Jinnouchi[141], P. Johansson[145], K.A. Johns[7], J.W. Johnson[139], F.A. Jolly[48], D.M. Jones[152], E. Jones[48], K.S. Jones[8], P. Jones[33], R.W.L. Jones[93], T.J. Jones[94], H.L. Joos[55], R. Joshi[122], J. Jovicevic[16], X. Ju[18a], J.J. Junggeburth[37], T. Junkermann[63a], A. Juste Rozas[13,u], M.K. Juzek[88], S. Kabana[140f], A. Kaczmarska[88], S.A. Kadir[149], M. Kado[112], H. Kagan[122], M. Kagan[149], A. Kahn[131], C. Kahra[102], T. Kaji[159], E. Kajomovitz[156], N. Kakati[175], N. Kakoty[13], I. Kalaitzidou[54], S. Kandel[8], N. Kanellos[10], N.J. Kang[139], D. Kar[34h,†], E. Karentzos[25], K. Karki[8], O. Karkout[117], S.N. Karpov[39], Z.M. Karpova[39], V. Kartvelishvili[93], A.N. Karyukhin[38], E. Kasimi[158], J. Katzy[48], S. Kaur[35], K. Kawade[146], M.P. Kawale[123], C. Kawamoto[89], T. Kawamoto[62], E.F. Kay[37], F.I. Kaya[164], S. Kazakos[109], V.F. Kazanin[38], J.M. Keaveney[34a], R. Keeler[171], G.V. Kehris[61], J.S. Keller[35], J.M. Kelly[171], J.J. Kempster[152], O. Kepka[134], J. Kerr[162b], B.P. Kerridge[137], B.P. Kerševan[95], L. Keszeghova[29a], R.A. Khan[132], A. Khanov[124], A.G. Kharlamov[38], T. Kharlamova[38], E.E. Khoda[142], M. Kholodenko[133a], T.J. Khoo[19], G. Khoriauli[172], Y. Khoulaki[36a], J. Khubua[155b,†], Y.A.R. Khwaira[130], B. Kibirige[34h], D. Kim[6], D.W. Kim[47a,47b], Y.K. Kim[40], N. Kimura[98], M.K. Kingston[55], A. Kirchhoff[55], C. Kirfel[25], F. Kirfel[25], J. Kirk[137], A.E. Kiryunin[112], S. Kita[163], O. Kivernyk[25], M. Klassen[164], C. Klein[35], L. Klein[172], M.H. Klein[45], S.B. Klein[56], U. Klein[94], A. Klimentov[30], T. Klioutchnikova[37], P. Kluit[117], S. Kluth[112], E. Kneringer[79], T.M. Knight[161], A. Knue[49], M. Kobel[50], D. Kobylianskii[175], S.F. Koch[129], M. Kocian[149], P. Kodyš[136], D.M. Koeck[126], T. Koffas[35], O. Kolay[50], I. Koletsou[4], T. Komarek[88], K. Köneke[55], A.X.Y. Kong[1], T. Kono[121], N. Konstantinidis[98], P. Kontaxakis[56], B. Konya[100], R. Kopeliansky[42], S. Koperny[87a], K. Korcyl[88], K. Kordas[158,z], A. Korn[98],

JHEP06(2026)094

S. Korn[55], I. Korolkov[13], N. Korotkova[38], B. Kortman[117], O. Kortner[112], S. Kortner[112], W.H. Kostecka[118], M. Kostov[29a], V.V. Kostyukhin[147], A. Kotsokechagia[37], A. Kotwal[51], A. Koulouris[37], A. Kourkoumeli-Charalampidi[73a,73b], C. Kourkoumelis[9], E. Kourlitis[112], O. Kovanda[126], R. Kowalewski[171], W. Kozanecki[126], A.S. Kozhin[38], V.A. Kramarenko[38], G. Kramberger[95], P. Kramer[25], M.W. Krasny[130], A. Krasznahorkay[105], A.C. Kraus[118], J.W. Kraus[177], J.A. Kremer[48], N.B. Krengel[147], T. Kresse[50], L. Kretschmann[177], J. Kretzschmar[94], P. Krieger[161], K. Krizka[21], K. Kroeninger[49], H. Kroha[112], J. Kroll[134], J. Kroll[131], K.S. Krowpman[109], U. Kruchonak[39], H. Krüger[25], N. Krumnack[81], M.C. Kruse[51], O. Kuchinskaia[39], S. Kuday[3a], S. Kuehn[37], R. Kuesters[54], T. Kuhl[48], V. Kukhtin[39], Y. Kulchitsky[39], S. Kuleshov[140d,140b], J. Kull[1], E.V. Kumar[111], M. Kumar[34h], N. Kumari[48], P. Kumari[162b], A. Kupco[134], A. Kupich[38], O. Kuprash[54], H. Kurashige[86], L.L. Kurchaninov[162a], O. Kurdysh[4], Y.A. Kurochkin[38], A. Kurova[38], M. Kuze[141], A.K. Kvam[105], J. Kvita[125], N.G. Kyriacou[142], C. Lacasta[169], F. Lacava[75a,75b], H. Lacker[19], D. Lacour[130], N.N. Lad[98], E. Ladygin[39], A. Lafarge[41], B. Laforge[130], T. Lagouri[178], F.Z. Lahbabi[36a], S. Lai[55,37], W.S. Lai[98], J.E. Lambert[171], S. Lammers[68], W. Lampl[7], C. Lampoudis[158,z], G. Lamprinoudis[102], A.N. Lancaster[118], E. Lançon[30], U. Landgraf[54], M.P.J. Landon[96], V.S. Lang[54], O.K. B. Langrekken[128], A.J. Lankford[165], F. Lanni[37], K. Lantzsch[25], A. Lanza[73a], M. Lanzac Berrocal[169], J.F. Laporte[138], T. Lari[71a], D. Larsen[17], L. Larson[11], F. Lasagni Manghi[24b], M. Lassnig[37], S.D. Lawlor[145], R. Lazaridou[165], M. Lazzaroni[71a,71b], E.T. T. Le[165], H.D. M. Le[109], E.M. Le Boulicaut[178], L.T. Le Pottier[18a], B. Leban[24b,24a], F. Ledroit-Guillon[60], T.F. Lee[162b], L.L. Leeuw[34c], M. Lefebvre[171], C. Leggett[18a], G. Lehmann Miotto[37], M. Leigh[56], W.A. Leight[105], W. Leinonen[116], A. Leisos[158,aa], M.A.L. Leite[83c], C.E. Leitgeb[19], R. Leitner[136], K.J.C. Leney[45], T. Lenz[25], S. Leone[74a], C. Leonidopoulos[52], A. Leopold[150], J. LePage-Bourbonnais[35], R. Les[109], C.G. Lester[33], M. Levchenko[38], J. Levêque[4], L.J. Levinson[175], G. Levrini[24b,24a], M.P. Lewicki[88], C. Lewis[142], D.J. Lewis[4], L. Lewitt[145], A. Li[30], B. Li[143a], C-Q. Li[112], C. Li[108], H. Li[143a], H. Li[103], H. Li[15], H. Li[62], H. Li[143a], J. Li[144a], K. Li[14], L. Li[144a], R. Li[178], S. Li[14,114c], S. Li[144b,144a], T. Li[5], X. Li[106], Y. Li[14], Z. Li[159], Z. Li[14,114c], Z. Li[62], S. Liang[14,114c], Z. Liang[14], M. Liberatore[138], B. Liberti[76a], G.B. Libotte[83d], K. Lie[64c], J. Lieber Marin[83e], H. Lien[68], H. Lin[108], S.F. Lin[151], L. Linden[111], R.E. Lindley[7], J.H. Lindon[37], J. Ling[61], E. Lipeles[131], A. Lipniacka[17], A. Lister[170], J.D. Little[68], B. Liu[14], B.X. Liu[114b], D. Liu[144b,144a], D. Liu[139], E.H. L. Liu[21], J.K.K. Liu[120], K. Liu[144b], K. Liu[144b,144a], M. Liu[62], M.Y. Liu[62], P. Liu[14], Q. Liu[144b,142,144a], S. Liu[151], X. Liu[62], X. Liu[143a], Y. Liu[114b,114c], Y.L. Liu[143a], Y.W. Liu[62], Z. Liu[66,ab], S.L. Lloyd[96], E.M. Lobodzinska[48], P. Loch[7], E. Lodhi[161], K. Lohwasser[145], E. Loiacono[48], J.D. Lomas[21], J.D. Long[42], I. Longarini[165], R. Longo[168], A. Lopez Solis[13], N.A. Lopez-canelas[7], N. Lorenzo Martinez[4], A.M. Lory[111], M. Losada[119a], G. Löschcke Centeno[4], X. Lou[47a,47b], X. Lou[14,114c], A. Lounis[66], P.A. Love[93], M. Lu[66], S. Lu[131], Y.J. Lu[154], H.J. Lubatti[142], C. Luci[75a,75b], F.L. Lucio Alves[114a], F. Luehring[68], B.S. Lunday[131], O. Lundberg[150], J. Lunde[37], N.A. Luongo[6], M.S. Lutz[37], A.B. Lux[26], D. Lynn[30], R. Lysak[134], V. Lysenko[135], E. Lytken[100], V. Lyubushkin[39], T. Lyubushkina[39], M.M. Lyukova[151], H. Ma[30], K. Ma[62],

JHEP06(2026)094

L.L. Ma[143a], W. Ma[62], Y. Ma[124], J.C. MacDonald[102], B. Maček[95],
P.C. Machado De Abreu Farias[83e], D. Macina[37], R. Madar[41], T. Madula[98], J. Maeda[86],
T. Maeno[30], P.T. Mafa[34c,ac], H. Maguire[145], M. Maheshwari[33], V. Maiboroda[66],
A. Maio[133a,133b,133d], K. Maj[87a], O. Majersky[48], S. Majewski[126], R. Makhmanazarov[38],
N. Makovec[66], V. Maksimovic[16], B. Malaescu[130], J. Malamant[128], Pa. Malecki[88],
V.P. Maleev[38], F. Malek[60,ad], M. Mali[95], D. Malito[97], U. Mallik[80,†], A. Maloizel[5],
S. Maltezos[10], A. Malvezzi Lopes[83d], S. Malyukov[39], J. Mamuzic[95], G. Mancini[53],
M.N. Mancini[27], G. Manco[73a,73b], J.P. Mandalia[96], S.S. Mandarry[152], I. Mandić[95],
L. Manhaes de Andrade Filho[83a], I.M. Maniatis[175], J. Manjarres Ramos[91], D.C. Mankad[175],
A. Mann[111], T. Manoussos[37], M.N. Mantinan[40], S. Manzoni[37], L. Mao[144a],
X. Mapekula[34c], A. Marantis[158], R.R. Marcelo Gregorio[96], G. Marchiori[5], C. Marcon[71a],
E. Maricic[16], M. Marinescu[48], S. Marium[48], M. Marjanovic[123], A. Markhoos[54],
M. Markovitch[66], M.K. Maroun[105], M.C. Marr[148], G.T. Marsden[103], E.J. Marshall[93],
Z. Marshall[18a], S. Marti-Garcia[169], J. Martin[98], T.A. Martin[137], V.J. Martin[52],
B. Martin dit Latour[17], S. Martin-Haugh[137], L. Martinelli[75a,75b], M. Martinez[13,u],
P. Martinez Agullo[169], V.I. Martinez Outschoorn[105], P. Martinez Suarez[37],
G. Martinovicova[136], V.S. Martoiu[28b], A.C. Martyniuk[98], A. Marzin[37], D. Mascione[78a,78b],
L. Masetti[102], J. Masik[103], A.L. Maslennikov[39], S.L. Mason[42], P. Massarotti[72a,72b],
P. Mastrandrea[74a,74b], A. Mastroberardino[44b,44a], T. Masubuchi[127], T.T. Mathew[126],
J. Matousek[136], D.M. Mattern[49], J. Maurer[28b], T. Maurin[59], A.J. Maury[66],
C. Mavungu Tsava[104], D.A. Maximov[38], A.E. May[103], E. Mayer[41], R. Mazini[34h],
I. Maznas[118], S.M. Mazza[139], E. Mazzeo[37], J.P. Mc Gowan[171], S.P. Mc Kee[108],
C.A. Mc Lean[6], C.C. McCracken[170], E.F. McDonald[107], A.E. McDougall[117],
L.F. Mcelhinney[93], J.A. Mcfayden[152], R.P. McGovern[131], R.P. Mckenzie[34h],
T.C. Mclachlan[48], D.J. Mclaughlin[98], S.J. McMahon[137], C.M. Mcpartland[94],
R.A. McPherson[171,n], S. Mehlhase[111], A. Mehta[94], D. Melini[169], B.R. Mellado Garcia[34h],
A.H. Melo[55], F. Meloni[48], A.M. Mendes Jacques Da Costa[103], L. Meng[93], S. Menke[112],
M. Mentink[37], E. Meoni[44b,44a], G. Mercado[118], S. Merianos[158], C. Merlassino[69a,69c],
C. Meroni[71a,71b], J. Metcalfe[6], A.S. Mete[6], E. Meuser[102], C. Meyer[68], J-P. Meyer[138],
Y. Miao[114a], R.P. Middleton[137], M. Mihovilovic[66], L. Mijović[52], G. Mikenberg[175],
M. Mikestikova[134], M. Mikuž[95], H. Mildner[102], A. Milic[37], D.W. Miller[40], E.H. Miller[149],
A. Milov[175], D.A. Milstead[47a,47b], T. Min[114a], A.A. Minaenko[38], I.A. Minashvili[155b],
A.I. Mincer[120], B. Mindur[87a], M. Mineev[39], Y. Mino[89], L.M. Mir[13],
M. Miralles Lopez[59], M. Mironova[18a], M. Missio[116], A. Mitra[173], V.A. Mitsou[169],
Y. Mitsumori[113], O. Miu[161], P.S. Miyagawa[96], T. Mkrtchyan[63a], M. Mlinarevic[98],
T. Mlinarevic[98], M. Mlynarikova[136], L. Mlynarska[87a], C. Mo[144a], S. Mobius[20],
M.H. Mohamed Farook[115], S. Mohapatra[42], M.F. Mohd Soberi[52], S. Mohiuddin[124],
G. Mokgatitswane[34h], L. Moleri[175], U. Molinatti[129], L.G. Mollier[20], B. Mondal[134],
S. Mondal[135], K. Mönig[48], E. Monnier[104], L. Monsonis Romero[169], J. Montejo Berlingen[13],
A. Montella[47a,47b], M. Montella[122], F. Montereali[77a,77b], F. Monticelli[92], S. Monzani[69a,69c],
A. Morancho Tarda[43], N. Morange[66], A.L. Moreira De Carvalho[48], M. Moreno Llácer[169],
C. Moreno Martinez[56], J.M. Moreno Perez[23b], P. Morettini[57b], S. Morgenstern[37], M. Morii[61],
M. Morinaga[159], M. Moritsu[90], F. Morodei[75a,75b], P. Moschovakos[37], B. Moser[54],

JHEP06(2026)094

M. Mosidze[155b], T. Moskalets[45], P. Moskvitina[116], J. Moss[32], P. Moszkowicz[87a], A. Moussa[36d], Y. Moyal[175], H. Moyano Gomez[13], E.J.W. Moyse[105], T.G. Mroz[88], O. Mtintsilana[34h], S. Muanza[104], M. Mucha[25], J. Mueller[132], G.A. Mullier[167], A.J. Mullin[33], J.J. Mullin[51], A.C. Mullins[45], A.E. Mulski[61], D.P. Mungo[161], D. Munoz Perez[169], F.J. Munoz Sanchez[103], W.J. Murray[173,137], M. Muškinja[95], C. Mwewa[48], A.G. Myagkov[38,j], A.J. Myers[8], G. Myers[108], M. Myska[135], B.P. Nachman[149], K. Nagai[129], K. Nagano[84], R. Nagasaka[159], J.L. Nagle[30,ae], E. Nagy[104], A.M. Nairz[37], Y. Nakahama[84], K. Nakamura[84], K. Nakkalil[5], A. Nandi[63b], H. Nanjo[127], E.A. Narayanan[45], Y. Narukawa[159], I. Naryshkin[38], L. Nasella[71a,71b], S. Nasri[119b], C. Nass[25], G. Navarro[23a], A. Nayaz[19], P.Y. Nechaeva[38], S. Nechaeva[24b,24a], F. Nechansky[134], L. Nedic[129], T.J. Neep[21], A. Negri[73a,73b], M. Negrini[24b], C. Nellist[117], C. Nelson[106], K. Nelson[108], S. Nemecek[134], M. Nessi[37,af], M.S. Neubauer[168], J. Newell[94], P.R. Newman[21], Y.W.Y. Ng[168], B. Ngair[119a], H.D.N. Nguyen[110], J.D. Nichols[123], R.B. Nickerson[129], R. Nicolaidou[138], J. Nielsen[139], M. Niemeyer[55], J. Niermann[37], N. Nikiforou[37], V. Nikolaenko[38,j], I. Nikolic-Audit[130], P. Nilsson[30], I. Ninca[48], G. Ninio[157], A. Nisati[75a], R. Nisius[112], N. Nitika[69a,69c], J-E. Nitschke[50], E.K. Nkadimeng[34b], T. Nobe[159], D. Noll[18a], T. Nommensen[153], M.B. Norfolk[145], B.J. Norman[35], L.C. Nosler[18a], M. Noury[36a], J. Novak[95], T. Novak[95], R. Novotny[135], L. Nozka[125], K. Ntekas[165], D. Ntounis[149], N.M.J. Nunes De Moura Junior[83b], A.P. O'Neill[20], J. Ocariz[130], I. Ochoa[133a], S. Oerdek[48], J.T. Offermann[40], A. Ogrodnik[136], A. Oh[103], C.C. Ohm[150], H. Oide[84], M.L. Ojeda[37], Y. Okumura[159], L.F. Oleiro Seabra[133a], I. Oleksiyuk[56], G. Oliveira Correa[13], D. Oliveira Damazio[30], J.L. Oliver[1], R. Omar[68], Ö.O. Öncel[54], A. Onofre[133a,133e,ag], P.U.E. Onyisi[11], M.J. Oreglia[40], D. Orestano[77a,77b], R. Orlandini[77a,77b], R.S. Orr[161], L.M. Osojnak[42], Y. Osumi[113], G. Otero y Garzón[31], H. Otono[90], M. Ouchrif[36d], F. Ould-Saada[128], T. Ovsiannikova[142], M. Owen[59], R.E. Owen[137], V.E. Ozcan[22a], F. Ozturk[88], N. Ozturk[8], S. Ozturk[82], H.A. Pacey[129], K. Pachal[162a], A. Pacheco Pages[13], C. Padilla Aranda[13], G. Padovano[75a,75b], S. Pagan Griso[18a], G. Palacino[68], A. Palazzo[70a,70b], J. Pampel[25], J. Pan[178], T. Pan[64a], D.K. Panchal[11], C.E. Pandini[60], J.G. Panduro Vazquez[137], H.D. Pandya[1], H. Pang[138], P. Pani[48], G. Panizzo[69a,69c], L. Panwar[130], L. Paolozzi[56], S. Parajuli[168], A. Paramonov[6], C. Paraskevopoulos[53], D. Paredes Hernandez[64b], A. Pareti[73a,73b], K.R. Park[42], T.H. Park[112], F. Parodi[57b,57a], J.A. Parsons[42], U. Parzefall[54], B. Pascual Dias[41], L. Pascual Dominguez[101], E. Pasqualucci[75a], S. Passaggio[57b], F. Pastore[97], P. Patel[88], U.M. Patel[51], J.R. Pater[103], T. Pauly[37], F. Pauwels[136], C.I. Pazos[164], M. Pedersen[128], R. Pedro[133a], S.V. Peleganchuk[38], O. Penc[134], E.A. Pender[52], S. Peng[15], G.D. Penn[178], K.E. Penski[111], M. Penzin[38], B.S. Peralva[83d], A.P. Pereira Peixoto[142], L. Pereira Sanchez[149], D.V. Perepelitsa[30,ae], G. Perera[105], E. Perez Codina[37], M. Perganti[10], H. Pernegger[37], S. Perrella[75a,75b], K. Peters[48], R.F.Y. Peters[103], B.A. Petersen[37], T.C. Petersen[43], E. Petit[104], V. Petousis[135], A.R. Petri[71a,71b], C. Petridou[158,z], T. Petru[136], A. Petrukhin[147], M. Pettee[18a], A. Petukhov[82], K. Petukhova[37], R. Pezoa[140g], L. Pezzotti[24b,24a], G. Pezzullo[178], L. Pfaffenbichler[37], A.J. Pfleger[79], T. Pham[107], T.M. Pham[176], P.W. Phillips[137], G. Piacquadio[151], E. Pianori[18a], F. Piazza[126], R. Piegaia[31],

D. Pietreanu[28b], A.D. Pilkington[103], M. Pinamonti[69a,69c], J.L. Pinfold[2], B.C. Pinheiro Pereira[133a], J. Pinol Bel[13], A.E. Pinto Pinoargote[130], L. Pintucci[69a,69c], K.M. Piper[152], A. Pirttikoski[56], D.A. Pizzi[35], L. Pizzimento[64b], A. Plebani[33], M.-A. Pleier[30], V. Pleskot[136], E. Plotnikova[39], G. Poddar[96], R. Poettgen[100], L. Poggioli[130], S. Polacek[136], G. Polesello[73a], A. Poley[148], A. Polini[24b], C.S. Pollard[173], Z.B. Pollock[122], E. Pompa Pacchi[123], N.I. Pond[98], D. Ponomarenko[68], L. Pontecorvo[37], S. Popa[28a], G.A. Popeneciu[28d], A. Poreba[37], D.M. Portillo Quintero[162a], S. Pospisil[135], M.A. Postill[145], P. Postolache[28c], K. Potamianos[173], P.A. Potepa[87a], I.N. Potrap[39], C.J. Potter[33], H. Potti[153], J. Poveda[169], M.E. Pozo Astigarraga[37], R. Pozzi[37], A. Prades Ibanez[76a,76b], S.R. Pradhan[145], J. Pretel[171], D. Price[103], M. Primavera[70a], L. Primomo[69a,69c], M.A. Principe Martin[101], R. Privara[125], T. Procter[87b], M.L. Proffitt[142], N. Proklova[131], K. Prokofiev[64c], G. Proto[112], J. Proudfoot[6], M. Przybycien[87a], W.W. Przygoda[87b], A. Psallidas[46], J.E. Puddefoot[145], D. Pudzha[53], H.I. Purnell[1], D. Pyatiizbyantseva[116], J. Qian[108], R. Qian[109], D. Qichen[129], Y. Qin[13], T. Qiu[52], A. Quadt[55], M. Queitsch-Maitland[103], G. Quetant[56], R.P. Quinn[170], G. Rabanal Bolanos[61], D. Rafanoharana[112], F. Raffaeli[76a,76b], F. Ragusa[71a,71b], J.L. Rainbolt[40], S. Rajagopalan[30], E. Ramakoti[39], L. Rambelli[57b,57a], I.A. Ramirez-Berend[35], K. Ran[48,114c], D.S. Rankin[131], N.P. Rapheeha[34h], H. Rasheed[28b], D.F. Rassloff[63a], A. Rastogi[18a], S. Rave[102], S. Ravera[57b,57a], B. Ravina[37], I. Ravinovich[175], M. Raymond[37], A.L. Read[128], N.P. Readioff[145], D.M. Rebuzzi[73a,73b], A.S. Reed[59], K. Reeves[27], J.A. Reidelsturz[177], D. Reikher[37], A. Rej[49], C. Rembser[37], H. Ren[62], M. Renda[28b], F. Renner[48], A.G. Rennie[59], M. Repik[56], A.L. Rescia[57b,57a], S. Resconi[71a], M. Ressegotti[57b], S. Rettie[117], W.F. Rettie[35], M.M. Revering[33], E. Reynolds[18a], O.L. Rezanova[39], P. Reznicek[136], H. Riani[36d], N. Ribaric[51], B. Ricci[69a,69c], E. Ricci[78a,78b], R. Richter[112], S. Richter[47a,47b], E. Richter-Was[87b], M. Ridel[130], S. Ridouani[36d], P. Rieck[120], P. Riedler[37], E.M. Riefel[47a,47b], J.O. Rieger[117], M. Rijssenbeek[151], M. Rimoldi[37], L. Rinaldi[24b,24a], P. Rincke[167,55], G. Ripellino[167], I. Riu[13], J.C. Rivera Vergara[171], F. Rizatdinova[124], E. Rizvi[96], B.R. Roberts[18a], S.S. Roberts[139], D. Robinson[33], M. Robles Manzano[102], A. Robson[59], A. Rocchi[76a,76b], C. Roda[74a,74b], S. Rodriguez Bosca[37], Y. Rodriguez Garcia[23a], A.M. Rodríguez Vera[118], S. Roe[37], J.T. Roemer[37], O. Røhne[128], R.A. Rojas[37], C.P.A. Roland[130], A. Romaniouk[79], E. Romano[73a,73b], M. Romano[24b], A.C. Romero Hernandez[168], N. Rompotis[94], L. Roos[130], S. Rosati[75a], B.J. Rosser[40], E. Rossi[129], E. Rossi[72a,72b], L.P. Rossi[61], L. Rossini[54], R. Rosten[122], M. Rotaru[28b], R. Roth[37], B. Rottler[54], D. Rousseau[66], D. Rousso[48], S. Roy-Garand[161], A. Rozanov[104], Z.M. A. Rozario[59], Y. Rozen[156], A. Rubio Jimenez[169], V.H. Ruelas Rivera[19], T.A. Ruggeri[1], A. Ruggiero[129], A. Ruiz-Martinez[169], A. Rummler[37], Z. Rurikova[54], N.A. Rusakovich[39], S. Ruscelli[49], H.L. Russell[171], G. Russo[75a,75b], J.P. Rutherfoord[7], S. Rutherford Colmenares[33], M. Rybar[136], P. Rybczynski[87a], A. Ryzhov[45], J.A. Sabater Iglesias[56], H.F-W. Sadrozinski[139], F. Safai Tehrani[75a], S. Saha[1], M. Sahinsoy[82], B. Sahoo[175], A. Saibel[169], B.T. Saifuddin[123], M. Saimpert[138], G.T. Saito[83c], M. Saito[159], T. Saito[159], A. Sala[71a,71b], A. Salnikov[149], J. Salt[169], A. Salvador Salas[157], F. Salvatore[152], A. Salzburger[37], D. Sammel[54], E. Sampson[93], D. Sampsonidis[158,z], D. Sampsonidou[126], J. Sánchez[169], V. Sanchez Sebastian[169],

JHEP06(2026)094

H. Sandaker[128], C.O. Sander[48], J.A. Sandesara[176], M. Sandhoff[177], C. Sandoval[23b], L. Sanfilippo[63a], D.P.C. Sankey[137], T. Sano[89], A. Sansoni[53], M. Santana Queiroz[18b], L. Santi[37], C. Santoni[41], H. Santos[133a,133b], A. Santra[175], E. Sanzani[24b,24a], K.A. Saoucha[85b], J.G. Saraiva[133a,133d], J. Sardain[7], O. Sasaki[84], K. Sato[163], C. Sauer[37], E. Sauvan[4], P. Savard[161,t], R. Sawada[159], C. Sawyer[137], L. Sawyer[99], C. Sbarra[24b], A. Sbrizzi[24b,24a], T. Scanlon[98], J. Schaarschmidt[142], U. Schäfer[102], A.C. Schaffer[66,45], D. Schaile[111], R.D. Schamberger[151], C. Scharf[19], M.M. Schefer[20], V.A. Schegelsky[38], D. Scheirich[136], M. Schernau[140f], C. Scheulen[56], C. Schiavi[57b,57a], M. Schioppa[44b,44a], B. Schlag[149], S. Schlenker[37], J. Schmeing[177], E. Schmidt[112], M.A. Schmidt[177], K. Schmieden[102], C. Schmitt[102], N. Schmitt[102], S. Schmitt[48], N.A. Schneider[111], L. Schoeffel[138], A. Schoening[63b], P.G. Scholer[35], E. Schopf[147], M. Schott[25], S. Schramm[56], T. Schroer[56], H-C. Schultz-Coulon[63a], M. Schumacher[54], B.A. Schumm[139], Ph. Schune[138], H.R. Schwartz[7], A. Schwartzman[149], T.A. Schwarz[108], Ph. Schwemling[138], R. Schwienhorst[109], F.G. Sciacca[20], A. Sciandra[30], G. Sciolla[27], F. Scuri[74a], C.D. Sebastiani[37], K. Sedlaczek[118], S.C. Seidel[115], A. Seiden[139], B.D. Seidlitz[42], C. Seitz[48], J.M. Seixas[83b], G. Sekhniaidze[72a], L. Selem[60], N. Semprini-Cesari[24b,24a], A. Semushin[179], D. Sengupta[56], V. Senthilkumar[169], L. Serin[66], M. Sessa[72a,72b], H. Severini[123], F. Sforza[57b,57a], A. Sfyrla[56], Q. Sha[14], E. Shabalina[55], H. Shaddix[118], A.H. Shah[33], R. Shaheen[150], J.D. Shahinian[131], M. Shamim[37], L.Y. Shan[14], M. Shapiro[18a], A. Sharma[37], A.S. Sharma[170], P. Sharma[30], P.B. Shatalov[38], K. Shaw[152], S.M. Shaw[103], Q. Shen[14], D.J. Sheppard[148], P. Sherwood[98], L. Shi[98], X. Shi[14], S. Shimizu[84], C.O. Shimmin[178], I.P.J. Shipsey[129,†], S. Shirabe[90], M. Shiyakova[39,ah], M.J. Shochet[40], D.R. Shope[128], B. Shrestha[123], S. Shrestha[122,ai], I. Shreyber[39], M.J. Shroff[171], P. Sicho[134], A.M. Sickles[168], E. Sideras Haddad[34h,166], A.C. Sidley[117], A. Sidoti[24b], F. Siegert[50], Dj. Sijacki[16], F. Sili[92], J.M. Silva[52], I. Silva Ferreira[83b], M.V. Silva Oliveira[30], S.B. Silverstein[47a], S. Simion[66], R. Simoniello[37], E.L. Simpson[103], H. Simpson[152], L.R. Simpson[6], S. Simsek[82], S. Sindhu[55], P. Sinervo[161], S. Singh[30], S.N. Singh[27], S. Sinha[48], S. Sinha[103], M. Sioli[24b,24a], K. Sioulas[9], I. Siral[37], E. Sitnikova[48], J. Sjölin[47a,47b], A. Skaf[55], E. Skorda[21], P. Skubic[123], M. Slawinska[88], I. Slazyk[17], I. Sliusar[128], V. Smakhtin[175], B.H. Smart[137], S.Yu. Smirnov[140b], Y. Smirnov[82], L.N. Smirnova[38,j], O. Smirnova[100], A.C. Smith[42], D.R. Smith[165], J.L. Smith[103], M.B. Smith[35], R. Smith[149], H. Smitmanns[102], M. Smizanska[93], K. Smolek[135], P. Smolyanskiy[135], A.A. Snesarev[39], H.L. Snoek[117], S. Snyder[30], R. Sobie[171,n], A. Soffer[157], C.A. Solans Sanchez[37], E.Yu. Soldatov[39], U. Soldevila[169], A.A. Solodkov[34h], S. Solomon[27], A. Soloshenko[39], K. Solovieva[54], O.V. Solovyanov[41], P. Sommer[50], A. Sonay[13], A. Sopczak[135], A.L. Sopio[52], F. Sopkova[29b], J.D. Sorenson[115], I.R. Sotarriva Alvarez[141], V. Sothilingam[63a], O.J. Soto Sandoval[140c,140b], S. Sottocornola[68], R. Soualah[85a], Z. Soumaimi[36e], D. South[48], N. Soybelman[175], S. Spagnolo[70a,70b], M. Spalla[112], D. Sperlich[54], B. Spisso[72a,72b], D.P. Spiteri[59], L. Splendori[104], M. Spousta[136], E.J. Staats[35], R. Stamen[63a], E. Stanecka[88], W. Stanek-Maslouska[48], M.V. Stange[50], B. Stanislaus[18a], M.M. Stanitzki[48], B. Stapf[48], E.A. Starchenko[38], G.H. Stark[139], J. Stark[91], P. Staroba[134], P. Starovoitov[85b], R. Staszewski[88], C. Stauch[111], G. Stavropoulos[46], A. Stefl[37], A. Stein[102], P. Steinberg[30],

JHEP06(2026)094

B. Stelzer[148,162a], H.J. Stelzer[132], O. Stelzer[162a], H. Stenzel[58], T.J. Stevenson[152], G.A. Stewart[37], J.R. Stewart[124], G. Stoicea[28b], M. Stolarski[133a], S. Stonjek[112], A. Straessner[50], J. Strandberg[150], S. Strandberg[47a,47b], M. Stratmann[177], M. Strauss[123], T. Strebler[104], P. Strizenec[29b], R. Ströhmer[172], D.M. Strom[126], R. Stroynowski[45], A. Strubig[47a,47b], S.A. Stucci[30], B. Stugu[17], J. Stupak[123], N.A. Styles[48], D. Su[149], S. Su[62], X. Su[62], D. Suchy[29a], A.D. Sudhakar Ponnu[55], K. Sugizaki[131], V.V. Sulin[38], D.M.S. Sultan[129], L. Sultanaliyeva[25], S. Sultansoy[3b], S. Sun[176], W. Sun[14], O. Sunneborn Gudnadottir[167], N. Sur[100], M.R. Sutton[152], M. Svatos[134], P.N. Swallow[33], M. Swiatlowski[162a], T. Swirski[172], A. Swoboda[37], I. Sykora[29a], M. Sykora[136], T. Sykora[136], D. Ta[102], K. Tackmann[48,aj], A. Taffard[165], R. Tafirout[162a], Y. Takubo[84], M. Talby[104], A.A. Talyshev[38], K.C. Tam[64b], N.M. Tamir[157], A. Tanaka[159], J. Tanaka[159], R. Tanaka[66], M. Tanasini[151], Z. Tao[170], S. Tapia Araya[140g], S. Tapprogge[102], A. Tarek Abouelfadl Mohamed[37], S. Tarem[156], K. Tariq[14], G. Tarna[37], G.F. Tartarelli[71a], M.J. Tartarin[91], P. Tas[136], M. Tasevsky[134], E. Tassi[44b,44a], A.C. Tate[168], Y. Tayalati[36e,ak], G.N. Taylor[107], W. Taylor[162b], R.J. Taylor Vara[169], A.S. Tegetmeier[91], P. Teixeira-Dias[97], J.J. Teoh[161], K. Terashi[159], J. Terron[101], S. Terzo[13], M. Testa[53], R.J. Teuscher[161,n], A. Thaler[79], O. Theiner[56], T. Theveneaux-Pelzer[104], D.W. Thomas[97], J.P. Thomas[21], E.A. Thompson[18a], P.D. Thompson[21], E. Thomson[131], R.E. Thornberry[45], C. Tian[62], Y. Tian[56], V. Tikhomirov[82], Yu.A. Tikhonov[39], S. Timoshenko[38], D. Timoshyn[136], E.X.L. Ting[1], P. Tipton[178], A. Tishelman-Charny[30], K. Todome[141], S. Todorova-Nova[136], L. Toffolin[69a,69c], M. Togawa[84], J. Tojo[90], S. Tokár[29a], O. Toldaiev[68], G. Tolkachev[104], M. Tomoto[84], L. Tompkins[149,al], E. Torrence[126], H. Torres[91], D.I. Torres Arza[140g], E. Torró Pastor[169], M. Toscani[31], C. Tosciri[40], M. Tost[11], D.R. Tovey[145], T. Trefzger[172], P.M. Tricarico[13], A. Tricoli[30], I.M. Trigger[162a], S. Trincaz-Duvoid[130], D.A. Trischuk[27], A. Tropina[39], L. Truong[34c], M. Trzebinski[88], A. Trzupek[88], F. Tsai[151], M. Tsai[108], A. Tsiamis[158], P.V. Tsiareshka[39], S. Tsigaridas[162a], A. Tsirigotis[158,aa], V. Tsiskaridze[155a], E.G. Tskhadadze[155a], Y. Tsujikawa[89], I.I. Tsukerman[38], V. Tsulaia[18a], S. Tsuno[84], K. Tsuri[121], D. Tsybychev[151], Y. Tu[64b], A. Tudorache[28b], V. Tudorache[28b], S.B. Tuncay[129], S. Turchikhin[57b,57a], I. Turk Cakir[3a], R. Turra[71a], T. Turtuvshin[39,am], P.M. Tuts[42], S. Tzamarias[158,z], Y. Uematsu[84], F. Ukegawa[163], P.A. Ulloa Poblete[140c,140b], E.N. Umaka[30], G. Unal[37], A. Undrus[30], G. Unel[165], J. Urban[29b], P. Urrejola[140e], G. Usai[8], R. Ushioda[160], M. Usman[110], F. Ustuner[52], Z. Uysal[82], V. Vacek[135], B. Vachon[106], T. Vafeiadis[37], A. Vaitkus[98], C. Valderanis[111], E. Valdes Santurio[47a,47b], M. Valente[37], S. Valentinetti[24b,24a], A. Valero[169], E. Valiente Moreno[169], A. Vallier[91], J.A. Valls Ferrer[169], D.R. Van Arneman[117], A. Van Der Graaf[49], H.Z. Van Der Schyf[34h], P. Van Gemmeren[6], M. Van Rijnbach[37], S. Van Stroud[98], I. Van Vulpen[117], P. Vana[136], M. Vanadia[76a,76b], U.M. Vande Voorde[150], W. Vandelli[37], E.R. Vandewall[124], D. Vannicola[157], L. Vannoli[53], R. Vari[75a], M. Varma[178], E.W. Varnes[7], C. Varni[118], D. Varouchas[66], L. Varriale[169], K.E. Varvell[153], M.E. Vasile[28b], L. Vaslin[84], M.D. Vassilev[149], A. Vasyukov[39], L.M. Vaughan[124], R. Vavricka[136], T. Vazquez Schroeder[13], J. Veatch[32], V. Vecchio[103], M.J. Veen[105], I. Veliscek[30], I. Velkovska[95], L.M. Veloce[161], F. Veloso[133a,133c], S. Veneziano[75a], A. Ventura[70a,70b], A. Verbytskyi[112], M. Verducci[74a,74b],

JHEP06(2026)094

C. Vergis[96], M. Verissimo De Araujo[83b], W. Verkerke[117], J.C. Vermeulen[117], C. Vernieri[149],
M. Vessella[165], M.C. Vetterli[148,t], A. Vgenopoulos[102], N. Viaux Maira[140g,an], T. Vickey[145],
O.E. Vickey Boeriu[145], G.H.A. Viehhauser[129], L. Vigani[63b], M. Vigl[112], M. Villa[24b,24a],
M. Villaplana Perez[169], E.M. Villhauer[40], E. Vilucchi[53], M. Vincent[169], M.G. Vincter[35],
A. Visibile[117], A. Visive[117], C. Vittori[37], I. Vivarelli[24b,24a], M.I. Vivas Albornoz[48],
E. Voevodina[112], F. Vogel[111], J.C. Voigt[50], P. Vokac[135], Yu. Volkotrub[87b],
L. Vomberg[25], E. Von Toerne[25], B. Vormwald[37], K. Vorobev[51], M. Vos[169], K. Voss[147],
M. Vozak[37], L. Vozdecky[123], N. Vranjes[16], M. Vranjes Milosavljevic[16], M. Vreeswijk[117],
N.K. Vu[144b,144a], R. Vuillermet[37], O. Vujinovic[102], I. Vukotic[40], I.K. Vyas[35],
J.F. Wack[33], S. Wada[163], C. Wagner[149], J.M. Wagner[18a], W. Wagner[177], S. Wahdan[177],
H. Wahlberg[92], C.H. Waits[123], J. Walder[137], R. Walker[111], K. Walkingshaw Pass[59],
W. Walkowiak[147], A. Wall[131], E.J. Wallin[100], T. Wamorkar[18a], K. Wandall-Christensen[169],
A. Wang[62], A.Z. Wang[139], C. Wang[102], C. Wang[11], H. Wang[18a], J. Wang[64c],
P. Wang[103], P. Wang[98], R. Wang[61], R. Wang[6], S. Wang[14], S.M. Wang[154], T. Wang[116],
T. Wang[62], W. Wang[14], W.T. Wang[129], X. Wang[168], X. Wang[144a], X. Wang[48],
Y. Wang[114a], Y. Wang[62], Z. Wang[108], Z. Wang[144b], Z. Wang[108], C. Wanotayaroj[84],
A. Warburton[106], A.L. Warnerbring[147], S. Waterhouse[97], A.T. Watson[21], H. Watson[52],
M.F. Watson[21], E. Watton[59], G. Watts[142], B.M. Waugh[98], J.M. Webb[54], C. Weber[30],
H.A. Weber[19], M.S. Weber[20], S.M. Weber[63a], C. Wei[62], Y. Wei[54], A.R. Weidberg[129],
E.J. Weik[120], J. Weingarten[49], C. Weiser[54], C.J. Wells[48], T. Wenaus[30], T. Wengler[37],
N.S. Wenke[112], N. Wermes[25], M. Wessels[63a], A.M. Wharton[93], A. White[8], A.S. White[61],
M.J. White[1], D. Whiteson[165], L. Wickremasinghe[127], W. Wiedenmann[176], M. Wielers[137],
R. Wierda[150], C. Wiglesworth[43], H.G. Wilkens[37], J.J. H. Wilkinson[33], D.M. Williams[42],
H.H. Williams[131], S. Williams[33], S. Willocq[105], B.J. Wilson[103], D.J. Wilson[103],
P.J. Windischhofer[40], F.I. Winkel[31], F. Winklmeier[126], B.T. Winter[54], M. Wittgen[149],
M. Wobisch[99], T. Wojtkowski[60], Z. Wolffs[117], J. Wollrath[37], M.W. Wolter[88],
H. Wolters[133a,133c], M.C. Wong[139], E.L. Woodward[42], S.D. Worm[48], B.K. Wosiek[88],
K.W. Woźniak[88], S. Wozniewski[55], K. Wraight[59], C. Wu[161], C. Wu[21], J. Wu[159],
M. Wu[114b], M. Wu[116], S. Wu[14,ao], S.L. Wu[176], X. Wu[62], Y. Wu[62], Y.Q. Wu[161],
Z. Wu[4], Z. Wu[114a], J. Wuerzinger[112], T.R. Wyatt[103], B.M. Wynne[52], S. Xella[43],
L. Xia[114a], M. Xia[15], M. Xie[62], A. Xiong[126], J. Xiong[18a], D. Xu[14], H. Xu[62],
L. Xu[62], R. Xu[131], T. Xu[108], Y. Xu[142], Z. Xu[52], R. Xue[132], B. Yabsley[153],
S. Yacoob[34a], Y. Yamaguchi[84], E. Yamashita[159], H. Yamauchi[163], T. Yamazaki[18a],
Y. Yamazaki[86], S. Yan[59], Z. Yan[105], H.J. Yang[144a,144b], H.T. Yang[62], S. Yang[62],
T. Yang[64c], X. Yang[37], X. Yang[14], Y. Yang[159], Y. Yang[62], W-M. Yao[18a],
C.L. Yardley[152], J. Ye[14], S. Ye[30], X. Ye[62], Y. Yeh[98], I. Yeletskikh[39], B. Yeo[18b],
M.R. Yexley[98], T.P. Yildirim[129], K. Yorita[174], C. Young[149], C.J.S. Young[37],
N.D. Young[126], Y. Yu[62], J. Yuan[14,114c,ao], M. Yuan[108], R. Yuan[144b,144a], L. Yue[98],
M. Zaazoua[62], B. Zabinski[88], I. Zahir[36a], A. Zaio[57b,57a], Z.K. Zak[88], T. Zakareishvili[169],
S. Zambito[56], J.A. Zamora Saa[140d], J. Zang[159], R. Zanzottera[71a,71b], O. Zaplatilek[135],
C. Zeitnitz[177], H. Zeng[14], J.C. Zeng[168], D.T. Zenger Jr[27], O. Zenin[38], T. Ženiš[29a],
S. Zenz[96], D. Zerwas[66], M. Zhai[14,114c], D.F. Zhang[145], G. Zhang[14,ao], J. Zhang[143a],
J. Zhang[6], K. Zhang[14,114c], L. Zhang[62], L. Zhang[114a], P. Zhang[14,114c], R. Zhang[114a],

JHEP06(2026)094

S. Zhang[91], T. Zhang[159], Y. Zhang[142], Y. Zhang[98], Y. Zhang[62], Y. Zhang[114a], Z. Zhang[18a], Z. Zhang[143a], Z. Zhang[66], H. Zhao[142], T. Zhao[143a], Y. Zhao[35], Z. Zhao[62], Z. Zhao[62], A. Zhemchugov[39], J. Zheng[114a], K. Zheng[168], X. Zheng[62], Z. Zheng[149], D. Zhong[168], B. Zhou[108], H. Zhou[7], N. Zhou[144a], Y. Zhou[15], Y. Zhou[114a], Y. Zhou[7], C.G. Zhu[143a], J. Zhu[108], X. Zhu[144b], Y. Zhu[144a], Y. Zhu[62], X. Zhuang[14], K. Zhukov[68], N.I. Zimine[39], J. Zinsser[63b], M. Ziolkowski[147], L. Živković[16], A. Zoccoli[24b,24a], K. Zoch[61], A. Zografos[37], T.G. Zorbas[145], O. Zormpa[46], L. Zwalinski[37]

[1] *Department of Physics, University of Adelaide, Adelaide, Australia*
[2] *Department of Physics, University of Alberta, Edmonton AB, Canada*
[3a] *Department of Physics, Ankara University, Ankara, Türkiye*
[3b] *Division of Physics, TOBB University of Economics and Technology, Ankara, Türkiye*
[4] *LAPP, Université Savoie Mont Blanc, CNRS/IN2P3, Annecy, France*
[5] *APC, Université Paris Cité, CNRS/IN2P3, Paris, France*
[6] *High Energy Physics Division, Argonne National Laboratory, Argonne IL, U.S.A.*
[7] *Department of Physics, University of Arizona, Tucson AZ, U.S.A.*
[8] *Department of Physics, University of Texas at Arlington, Arlington TX, U.S.A.*
[9] *Physics Department, National and Kapodistrian University of Athens, Athens, Greece*
[10] *Physics Department, National Technical University of Athens, Zografou, Greece*
[11] *Department of Physics, University of Texas at Austin, Austin TX, U.S.A.*
[12] *Institute of Physics, Azerbaijan Academy of Sciences, Baku, Azerbaijan*
[13] *Institut de Física d'Altes Energies (IFAE), Barcelona Institute of Science and Technology, Barcelona, Spain*
[14] *Institute of High Energy Physics, Chinese Academy of Sciences, Beijing, China*
[15] *Physics Department, Tsinghua University, Beijing, China*
[16] *Institute of Physics, University of Belgrade, Belgrade, Serbia*
[17] *Department for Physics and Technology, University of Bergen, Bergen, Norway*
[18a] *Physics Division, Lawrence Berkeley National Laboratory, Berkeley CA, U.S.A.*
[18b] *University of California, Berkeley CA, U.S.A.*
[19] *Institut für Physik, Humboldt Universität zu Berlin, Berlin, Germany*
[20] *Albert Einstein Center for Fundamental Physics and Laboratory for High Energy Physics, University of Bern, Bern, Switzerland*
[21] *School of Physics and Astronomy, University of Birmingham, Birmingham, U.K.*
[22a] *Department of Physics, Bogazici University, Istanbul, Türkiye*
[22b] *Department of Physics Engineering, Gaziantep University, Gaziantep, Türkiye*
[22c] *Department of Physics, Istanbul University, Istanbul, Türkiye*
[23a] *Facultad de Ciencias y Centro de Investigaciónes, Universidad Antonio Nariño, Bogotá, Colombia*
[23b] *Departamento de Física, Universidad Nacional de Colombia, Bogotá, Colombia*
[24a] *Dipartimento di Fisica e Astronomia A. Righi, Università di Bologna, Bologna, Italy*
[24b] *INFN Sezione di Bologna, Italy*
[25] *Physikalisches Institut, Universität Bonn, Bonn, Germany*
[26] *Department of Physics, Boston University, Boston MA, U.S.A.*
[27] *Department of Physics, Brandeis University, Waltham MA, U.S.A.*
[28a] *Transilvania University of Brasov, Brasov, Romania*
[28b] *Horia Hulubei National Institute of Physics and Nuclear Engineering, Bucharest, Romania*
[28c] *Department of Physics, Alexandru Ioan Cuza University of Iasi, Iasi, Romania*
[28d] *National Institute for Research and Development of Isotopic and Molecular Technologies, Physics Department, Cluj-Napoca, Romania*
[28e] *National University of Science and Technology Politechnica, Bucharest, Romania*
[28f] *West University in Timisoara, Timisoara, Romania*
[28g] *Faculty of Physics, University of Bucharest, Bucharest, Romania*
[29a] *Faculty of Mathematics, Physics and Informatics, Comenius University, Bratislava, Slovak Republic*

JHEP06(2026)094

[29b] *Department of Subnuclear Physics, Institute of Experimental Physics of the Slovak Academy of Sciences, Kosice, Slovak Republic*
[30] *Physics Department, Brookhaven National Laboratory, Upton NY, U.S.A.*
[31] *Universidad de Buenos Aires, Facultad de Ciencias Exactas y Naturales, Departamento de Física, y CONICET, Instituto de Física de Buenos Aires (IFIBA), Buenos Aires, Argentina*
[32] *California State University, CA, U.S.A.*
[33] *Cavendish Laboratory, University of Cambridge, Cambridge, U.K.*
[34a] *Department of Physics, University of Cape Town, Cape Town, South Africa*
[34b] *iThemba Labs, Western Cape, South Africa*
[34c] *Department of Mechanical Engineering Science, University of Johannesburg, Johannesburg, South Africa*
[34d] *National Institute of Physics, University of the Philippines Diliman (Philippines), Philippines*
[34e] *Department of Physics, Stellenbosch University, Matieland, South Africa*
[34f] *University of South Africa, Department of Physics, Pretoria, South Africa*
[34g] *University of Zululand, KwaDlangezwa, South Africa*
[34h] *School of Physics, University of the Witwatersrand, Johannesburg, South Africa*
[35] *Department of Physics, Carleton University, Ottawa ON, Canada*
[36a] *Faculté des Sciences Ain Chock, Université Hassan II de Casablanca, Morocco*
[36b] *Faculté des Sciences, Université Ibn-Tofail, Kénitra, Morocco*
[36c] *Faculté des Sciences Semlalia, Université Cadi Ayyad, LPHEA-Marrakech, Morocco*
[36d] *LPMR, Faculté des Sciences, Université Mohamed Premier, Oujda, Morocco*
[36e] *Faculté des sciences, Université Mohammed V, Rabat, Morocco*
[36f] *Institute of Applied Physics, Mohammed VI Polytechnic University, Ben Guerir, Morocco*
[37] *CERN, Geneva, Switzerland*
[38] *Affiliated with an institute formerly covered by a cooperation agreement with CERN*
[39] *Affiliated with an international laboratory covered by a cooperation agreement with CERN*
[40] *Enrico Fermi Institute, University of Chicago, Chicago IL, U.S.A.*
[41] *LPC, Université Clermont Auvergne, CNRS/IN2P3, Clermont-Ferrand, France*
[42] *Nevis Laboratory, Columbia University, Irvington NY, U.S.A.*
[43] *Niels Bohr Institute, University of Copenhagen, Copenhagen, Denmark*
[44a] *Dipartimento di Fisica, Università della Calabria, Rende, Italy*
[44b] *INFN Gruppo Collegato di Cosenza, Laboratori Nazionali di Frascati, Italy*
[45] *Physics Department, Southern Methodist University, Dallas TX, U.S.A.*
[46] *National Centre for Scientific Research "Demokritos", Agia Paraskevi, Greece*
[47a] *Department of Physics, Stockholm University, Sweden*
[47b] *Oskar Klein Centre, Stockholm, Sweden*
[48] *Deutsches Elektronen-Synchrotron DESY, Hamburg and Zeuthen, Germany*
[49] *Fakultät Physik, Technische Universität Dortmund, Dortmund, Germany*
[50] *Institut für Kern- und Teilchenphysik, Technische Universität Dresden, Dresden, Germany*
[51] *Department of Physics, Duke University, Durham NC, U.S.A.*
[52] *SUPA – School of Physics and Astronomy, University of Edinburgh, Edinburgh, U.K.*
[53] *INFN e Laboratori Nazionali di Frascati, Frascati, Italy*
[54] *Physikalisches Institut, Albert-Ludwigs-Universität Freiburg, Freiburg, Germany*
[55] *II. Physikalisches Institut, Georg-August-Universität Göttingen, Göttingen, Germany*
[56] *Département de Physique Nucléaire et Corpusculaire, Université de Genève, Genève, Switzerland*
[57a] *Dipartimento di Fisica, Università di Genova, Genova, Italy*
[57b] *INFN Sezione di Genova, Italy*
[58] *II. Physikalisches Institut, Justus-Liebig-Universität Giessen, Giessen, Germany*
[59] *SUPA – School of Physics and Astronomy, University of Glasgow, Glasgow, U.K.*
[60] *LPSC, Université Grenoble Alpes, CNRS/IN2P3, Grenoble INP, Grenoble, France*
[61] *Laboratory for Particle Physics and Cosmology, Harvard University, Cambridge MA, U.S.A.*
[62] *Department of Modern Physics and State Key Laboratory of Particle Detection and Electronics, University of Science and Technology of China, Hefei, China*
[63a] *Kirchhoff-Institut für Physik, Ruprecht-Karls-Universität Heidelberg, Heidelberg, Germany*

[63b] *Physikalisches Institut, Ruprecht-Karls-Universität Heidelberg, Heidelberg, Germany*
[64a] *Department of Physics, Chinese University of Hong Kong, Shatin, N.T., Hong Kong, China*
[64b] *Department of Physics, University of Hong Kong, Hong Kong, China*
[64c] *Department of Physics and Institute for Advanced Study, Hong Kong University of Science and Technology, Clear Water Bay, Kowloon, Hong Kong, China*
[65] *Department of Physics, National Tsing Hua University, Hsinchu, Taiwan*
[66] *IJCLab, Université Paris-Saclay, CNRS/IN2P3, 91405, Orsay, France*
[67] *Centro Nacional de Microelectrónica (IMB-CNM-CSIC), Barcelona, Spain*
[68] *Department of Physics, Indiana University, Bloomington IN, U.S.A.*
[69a] *INFN Gruppo Collegato di Udine, Sezione di Trieste, Udine, Italy*
[69b] *ICTP, Trieste, Italy*
[69c] *Dipartimento Politecnico di Ingegneria e Architettura, Università di Udine, Udine, Italy*
[70a] *INFN Sezione di Lecce, Italy*
[70b] *Dipartimento di Matematica e Fisica, Università del Salento, Lecce, Italy*
[71a] *INFN Sezione di Milano, Italy*
[71b] *Dipartimento di Fisica, Università di Milano, Milano, Italy*
[72a] *INFN Sezione di Napoli, Italy*
[72b] *Dipartimento di Fisica, Università di Napoli, Napoli, Italy*
[73a] *INFN Sezione di Pavia, Italy*
[73b] *Dipartimento di Fisica, Università di Pavia, Pavia, Italy*
[74a] *INFN Sezione di Pisa, Italy*
[74b] *Dipartimento di Fisica E. Fermi, Università di Pisa, Pisa, Italy*
[75a] *INFN Sezione di Roma, Italy*
[75b] *Dipartimento di Fisica, Sapienza Università di Roma, Roma, Italy*
[76a] *INFN Sezione di Roma Tor Vergata, Italy*
[76b] *Dipartimento di Fisica, Università di Roma Tor Vergata, Roma, Italy*
[77a] *INFN Sezione di Roma Tre, Italy*
[77b] *Dipartimento di Matematica e Fisica, Università Roma Tre, Roma, Italy*
[78a] *INFN-TIFPA, Italy*
[78b] *Università degli Studi di Trento, Trento, Italy*
[79] *Universität Innsbruck, Department of Astro and Particle Physics, Innsbruck, Austria*
[80] *University of Iowa, Iowa City IA, U.S.A.*
[81] *Department of Physics and Astronomy, Iowa State University, Ames IA, U.S.A.*
[82] *Istinye University, Sariyer, Istanbul, Türkiye*
[83a] *Departamento de Engenharia Elétrica, Universidade Federal de Juiz de Fora (UFJF), Juiz de Fora, Brazil*
[83b] *Universidade Federal do Rio De Janeiro COPPE/EE/IF, Rio de Janeiro, Brazil*
[83c] *Instituto de Física, Universidade de São Paulo, São Paulo, Brazil*
[83d] *Rio de Janeiro State University, Rio de Janeiro, Brazil*
[83e] *Federal University of Bahia, Bahia, Brazil*
[84] *KEK, High Energy Accelerator Research Organization, Tsukuba, Japan*
[85a] *Khalifa University of Science and Technology, Abu Dhabi, United Arab Emirates*
[85b] *University of Sharjah, Sharjah, United Arab Emirates*
[86] *Graduate School of Science, Kobe University, Kobe, Japan*
[87a] *AGH University of Krakow, Faculty of Physics and Applied Computer Science, Krakow, Poland*
[87b] *Marian Smoluchowski Institute of Physics, Jagiellonian University, Krakow, Poland*
[88] *Institute of Nuclear Physics Polish Academy of Sciences, Krakow, Poland*
[89] *Faculty of Science, Kyoto University, Kyoto, Japan*
[90] *Research Center for Advanced Particle Physics and Department of Physics, Kyushu University, Fukuoka, Japan*
[91] *L2IT, Université de Toulouse, CNRS/IN2P3, UPS, Toulouse, France*
[92] *Instituto de Física La Plata, Universidad Nacional de La Plata and CONICET, La Plata, Argentina*
[93] *Physics Department, Lancaster University, Lancaster, U.K.*
[94] *Oliver Lodge Laboratory, University of Liverpool, Liverpool, U.K.*

[95] Department of Experimental Particle Physics, Jožef Stefan Institute and Department of Physics, University of Ljubljana, Ljubljana, Slovenia
[96] Department of Physics and Astronomy, Queen Mary University of London, London, U.K.
[97] Department of Physics, Royal Holloway University of London, Egham, U.K.
[98] Department of Physics and Astronomy, University College London, London, U.K.
[99] Louisiana Tech University, Ruston LA, U.S.A.
[100] Fysiska institutionen, Lunds universitet, Lund, Sweden
[101] Departamento de Física Teorica C-15 and CIAFF, Universidad Autónoma de Madrid, Madrid, Spain
[102] Institut für Physik, Universität Mainz, Mainz, Germany
[103] School of Physics and Astronomy, University of Manchester, Manchester, U.K.
[104] CPPM, Aix-Marseille Université, CNRS/IN2P3, Marseille, France
[105] Department of Physics, University of Massachusetts, Amherst MA, U.S.A.
[106] Department of Physics, McGill University, Montreal QC, Canada
[107] School of Physics, University of Melbourne, Victoria, Australia
[108] Department of Physics, University of Michigan, Ann Arbor MI, U.S.A.
[109] Department of Physics and Astronomy, Michigan State University, East Lansing MI, U.S.A.
[110] Group of Particle Physics, University of Montreal, Montreal QC, Canada
[111] Fakultät für Physik, Ludwig-Maximilians-Universität München, München, Germany
[112] Max-Planck-Institut für Physik (Werner-Heisenberg-Institut), München, Germany
[113] Graduate School of Science and Kobayashi-Maskawa Institute, Nagoya University, Nagoya, Japan
[114a] Department of Physics, Nanjing University, Nanjing, China
[114b] School of Science, Shenzhen Campus of Sun Yat-sen University, China
[114c] University of Chinese Academy of Science (UCAS), Beijing, China
[115] Department of Physics and Astronomy, University of New Mexico, Albuquerque NM, U.S.A.
[116] Institute for Mathematics, Astrophysics and Particle Physics, Radboud University/Nikhef, Nijmegen, Netherlands
[117] Nikhef National Institute for Subatomic Physics and University of Amsterdam, Amsterdam, Netherlands
[118] Department of Physics, Northern Illinois University, DeKalb IL, U.S.A.
[119a] New York University Abu Dhabi, Abu Dhabi, United Arab Emirates
[119b] United Arab Emirates University, Al Ain, United Arab Emirates
[120] Department of Physics, New York University, New York NY, U.S.A.
[121] Ochanomizu University, Otsuka, Bunkyo-ku, Tokyo, Japan
[122] Ohio State University, Columbus OH, U.S.A.
[123] Homer L. Dodge Department of Physics and Astronomy, University of Oklahoma, Norman OK, U.S.A.
[124] Department of Physics, Oklahoma State University, Stillwater OK, U.S.A.
[125] Palacký University, Joint Laboratory of Optics, Olomouc, Czech Republic
[126] Institute for Fundamental Science, University of Oregon, Eugene, OR, U.S.A.
[127] Graduate School of Science, University of Osaka, Osaka, Japan
[128] Department of Physics, University of Oslo, Oslo, Norway
[129] Department of Physics, Oxford University, Oxford, U.K.
[130] LPNHE, Sorbonne Université, Université Paris Cité, CNRS/IN2P3, Paris, France
[131] Department of Physics, University of Pennsylvania, Philadelphia PA, U.S.A.
[132] Department of Physics and Astronomy, University of Pittsburgh, Pittsburgh PA, U.S.A.
[133a] Laboratório de Instrumentação e Física Experimental de Partículas – LIP, Lisboa, Portugal
[133b] Departamento de Física, Faculdade de Ciências, Universidade de Lisboa, Lisboa, Portugal
[133c] Departamento de Física, Universidade de Coimbra, Coimbra, Portugal
[133d] Centro de Física Nuclear da Universidade de Lisboa, Lisboa, Portugal
[133e] Departamento de Física, Escola de Ciências, Universidade do Minho, Braga, Portugal
[133f] Departamento de Física Teórica y del Cosmos, Universidad de Granada, Granada (Spain), Spain
[133g] Departamento de Física, Instituto Superior Técnico, Universidade de Lisboa, Lisboa, Portugal
[134] Institute of Physics of the Czech Academy of Sciences, Prague, Czech Republic
[135] Czech Technical University in Prague, Prague, Czech Republic
[136] Charles University, Faculty of Mathematics and Physics, Prague, Czech Republic

JHEP06(2026)094

[137] *Particle Physics Department, Rutherford Appleton Laboratory, Didcot, U.K.*
[138] *IRFU, CEA, Université Paris-Saclay, Gif-sur-Yvette, France*
[139] *Santa Cruz Institute for Particle Physics, University of California Santa Cruz, Santa Cruz CA, U.S.A.*
[140a] *Departamento de Física, Pontificia Universidad Católica de Chile, Santiago, Chile*
[140b] *Millennium Institute for Subatomic physics at high energy frontier (SAPHIR), Santiago, Chile*
[140c] *Instituto de Investigación Multidisciplinario en Ciencia y Tecnología, y Departamento de Física, Universidad de La Serena, Chile*
[140d] *Universidad Andres Bello, Department of Physics, Santiago, Chile*
[140e] *Universidad San Sebastian, Recoleta, Chile*
[140f] *Instituto de Alta Investigación, Universidad de Tarapacá, Arica, Chile*
[140g] *Departamento de Física, Universidad Técnica Federico Santa María, Valparaíso, Chile*
[141] *Department of Physics, Institute of Science, Tokyo, Japan*
[142] *Department of Physics, University of Washington, Seattle WA, U.S.A.*
[143a] *Institute of Frontier and Interdisciplinary Science and Key Laboratory of Particle Physics and Particle Irradiation (MOE), Shandong University, Qingdao, China*
[143b] *School of Physics, Zhengzhou University, China*
[144a] *State Key Laboratory of Dark Matter Physics, School of Physics and Astronomy, Shanghai Jiao Tong University, Key Laboratory for Particle Astrophysics and Cosmology (MOE), SKLPPC, Shanghai, China*
[144b] *State Key Laboratory of Dark Matter Physics, Tsung-Dao Lee Institute, Shanghai Jiao Tong University, Shanghai, China*
[145] *Department of Physics and Astronomy, University of Sheffield, Sheffield, U.K.*
[146] *Department of Physics, Shinshu University, Nagano, Japan*
[147] *Department Physik, Universität Siegen, Siegen, Germany*
[148] *Department of Physics, Simon Fraser University, Burnaby BC, Canada*
[149] *SLAC National Accelerator Laboratory, Stanford CA, U.S.A.*
[150] *Department of Physics, Royal Institute of Technology, Stockholm, Sweden*
[151] *Departments of Physics and Astronomy, Stony Brook University, Stony Brook NY, U.S.A.*
[152] *Department of Physics and Astronomy, University of Sussex, Brighton, U.K.*
[153] *School of Physics, University of Sydney, Sydney, Australia*
[154] *Institute of Physics, Academia Sinica, Taipei, Taiwan*
[155a] *E. Andronikashvili Institute of Physics, Iv. Javakhishvili Tbilisi State University, Tbilisi, Georgia*
[155b] *High Energy Physics Institute, Tbilisi State University, Tbilisi, Georgia*
[155c] *University of Georgia, Tbilisi, Georgia*
[156] *Department of Physics, Technion, Israel Institute of Technology, Haifa, Israel*
[157] *Raymond and Beverly Sackler School of Physics and Astronomy, Tel Aviv University, Tel Aviv, Israel*
[158] *Department of Physics, Aristotle University of Thessaloniki, Thessaloniki, Greece*
[159] *International Center for Elementary Particle Physics and Department of Physics, University of Tokyo, Tokyo, Japan*
[160] *Graduate School of Science and Technology, Tokyo Metropolitan University, Tokyo, Japan*
[161] *Department of Physics, University of Toronto, Toronto ON, Canada*
[162a] *TRIUMF, Vancouver BC, Canada*
[162b] *Department of Physics and Astronomy, York University, Toronto ON, Canada*
[163] *Division of Physics and Tomonaga Center for the History of the Universe, Faculty of Pure and Applied Sciences, University of Tsukuba, Tsukuba, Japan*
[164] *Department of Physics and Astronomy, Tufts University, Medford MA, U.S.A.*
[165] *Department of Physics and Astronomy, University of California Irvine, Irvine CA, U.S.A.*
[166] *University of West Attica, Athens, Greece*
[167] *Department of Physics and Astronomy, University of Uppsala, Uppsala, Sweden*
[168] *Department of Physics, University of Illinois, Urbana IL, U.S.A.*
[169] *Instituto de Física Corpuscular (IFIC), Centro Mixto Universidad de Valencia – CSIC, Valencia, Spain*
[170] *Department of Physics, University of British Columbia, Vancouver BC, Canada*
[171] *Department of Physics and Astronomy, University of Victoria, Victoria BC, Canada*
[172] *Fakultät für Physik und Astronomie, Julius-Maximilians-Universität Würzburg, Würzburg, Germany*

JHEP06(2026)094

[173] Department of Physics, University of Warwick, Coventry, U.K.
[174] Waseda University, Tokyo, Japan
[175] Department of Particle Physics and Astrophysics, Weizmann Institute of Science, Rehovot, Israel
[176] Department of Physics, University of Wisconsin, Madison WI, U.S.A.
[177] Fakultät für Mathematik und Naturwissenschaften, Fachgruppe Physik, Bergische Universität Wuppertal, Wuppertal, Germany
[178] Department of Physics, Yale University, New Haven CT, U.S.A.
[179] Yerevan Physics Institute, Yerevan, Armenia

[a] Also at Department of Physics, King's College London, London, U.K.
[b] Also at Institute of Physics, Azerbaijan Academy of Sciences, Baku, Azerbaijan
[c] Also at Imam Mohammad Ibn Saud Islamic University, Saudi Arabia
[d] Also at Department of Physics, University of Thessaly, Greece
[e] Also at An-Najah National University, Nablus, Palestine
[f] Also at Department of Physics, University of Fribourg, Fribourg, Switzerland
[g] Also at Department of Physics, Westmont College, Santa Barbara, U.S.A.
[h] Also at Departament de Fisica de la Universitat Autonoma de Barcelona, Barcelona, Spain
[i] Also at University of Siena, Italy
[j] Also at Affiliated with an institute formerly covered by a cooperation agreement with CERN
[k] Also at The Collaborative Innovation Center of Quantum Matter (CICQM), Beijing, China
[l] Also at Faculty of Physics, Sofia University, 'St. Kliment Ohridski', Sofia, Bulgaria
[m] Also at Università di Napoli Parthenope, Napoli, Italy
[n] Also at Institute of Particle Physics (IPP), Canada
[o] Also at Department of Physics, Bolu Abant Izzet Baysal University, Bolu, Türkiye
[p] Also at Faculty of Physics, University of Bucharest, Romania
[q] Also at Borough of Manhattan Community College, City University of New York, New York NY, U.S.A.
[r] Also at National Institute of Physics, University of the Philippines Diliman (Philippines), Philippines
[s] Also at Department of Financial and Management Engineering, University of the Aegean, Chios, Greece
[t] Also at TRIUMF, Vancouver BC, Canada
[u] Also at Institucio Catalana de Recerca i Estudis Avancats, ICREA, Barcelona, Spain
[v] Also at Henan University, China
[w] Also at Yeditepe University, Physics Department, Istanbul, Türkiye
[x] Also at Institute of Theoretical Physics, Ilia State University, Tbilisi, Georgia
[y] Also at CERN, Geneva, Switzerland
[z] Also at Center for Interdisciplinary Research and Innovation (CIRI-AUTH), Thessaloniki, Greece
[aa] Also at Hellenic Open University, Patras, Greece
[ab] Also at Department of Modern Physics and State Key Laboratory of Particle Detection and Electronics, University of Science and Technology of China, Hefei, China
[ac] Also at Department of Mathematical Sciences, University of South Africa, Johannesburg, South Africa
[ad] Also at Department of Physics, Stellenbosch University, South Africa
[ae] Also at University of Colorado Boulder, Department of Physics, Colorado, U.S.A.
[af] Also at Département de Physique Nucléaire et Corpusculaire, Université de Genève, Genève, Switzerland
[ag] Also at Centre of Physics of the Universities of Minho and Porto (CF-UM-UP), Portugal
[ah] Also at Institute for Nuclear Research and Nuclear Energy (INRNE) of the Bulgarian Academy of Sciences, Sofia, Bulgaria
[ai] Also at Washington College, Chestertown, MD, U.S.A.
[aj] Also at Institut für Experimentalphysik, Universität Hamburg, Hamburg, Germany
[ak] Also at Institute of Applied Physics, Mohammed VI Polytechnic University, Ben Guerir, Morocco
[al] Also at Department of Physics, Stanford University, Stanford CA, U.S.A.
[am] Also at Institute of Physics and Technology, Mongolian Academy of Sciences, Ulaanbaatar, Mongolia
[an] Also at Millennium Institute for Subatomic physics at high energy frontier (SAPHIR), Santiago, Chile
[ao] Also at University of Chinese Academy of Sciences (UCAS), Beijing, China
[†] Deceased

JHEP06(2026)094